FORMING PARAMETERS AND QUANTIFICATION OF CONTINOUS AND STRETCH BROKEN CARBON FIBERS

By

Joseph Charles Janicki

A thesis submitted in partial fulfillment
of the requirements for the degree

of

Master of Science

in

Mechanical Engineering

MONTANA STATE UNIVERSITY
Bozeman, Montana

December 2021

©COPYRIGHT

by

Joseph Charles Janicki

2021

All Rights Reserved

ACKNOWLEDGEMENTS

This work would not have been possible without the support and constant encouragement from an incredible group of people.

First off, I would like to thank by family and friends for supporting my educational endeavors over the years and helping me to always look at the positives in life even when some tasks seem overwhelming.

A sincere gratitude of thanks goes to my advisor Dr. Dilpreet Bajwa and his ability to guide me through this process over the last few years. Any student would count themselves fortunate to be his advisee. The incredible work ethic, intelligence, and optimism he displays every day was pivotal to my success. I would also like to thank my committee members Dr. Douglas Cairns and Dr. Cecily Ryan for supporting my research with countless helpful recommendations and access to various labs and equipment.

Furthermore, I would like to thank all graduate, undergraduate and professional researchers in the MSU Stretch Broken Carbon Fiber lab for assisting me in a multitude of different ways. All of which put me on the path to successfully undergo the following work.

Finally, I would like to give thanks to Kathy Campbell and Dagny Mest for always being willing to help me with last minute administrative issues and guiding me through the MSU degree program.

This work was conducted in partnership with the MSU Stretch Broken Carbon Fiber research group with funding support from the US ARMY Combat Capabilities Development Command Aviation & Missile Center Technology Development Directorate (Contract number: W911W6-18-0050).

TABLE OF CONTENTS

1. INTRODUCTION 1

Advantages of CFRP's over Conventional Aerospace Materials 4
Disadvantages of CFRP's 6
Introduction of Stretch Broken Carbon Fiber 7
Hypothesis and Objectives 8
Thesis Goal 8
Sub-Objectives 8
Thesis Hypothesis 8
Structure of Thesis 9

2. BACKGROUND & LITERATURE REVIEW 11

Mechanics of Carbon Fiber 11
Discontinuous Carbon Fiber 16

3. GAUGE LENGTH AND TEMPERATURE INFLUENCE ON THE TENSILE PROPERTIES OF STRETCH BROKEN CARBON FIBER TOWS 21

Introduction 23
Materials and Methods 25
Materials 25
Sizing 26
Cross-sectional Area of Carbon Fiber Tows 27
SBCF Filament Lengths 28
Sample Preparation 29
Test Method 30
Results and Discussion 31
Cross Sectional Area of Carbon Fiber Tows 31
Continuous Carbon Fiber Tows 34
Stretch Broken Carbon Fibers 36
Stretch Broken Carbon Fibers Peak Stress vs. Continuous Carbon Fiber Tows 37
Conclusion 41

4. FORMABILITY CHARACTERIZATION OF FIBER REINFORCED POLYMER COMPOSITES USING A NOVEL TEST METHOD 42

Introduction 44
Research Significance 47
Proposed Test Method 48
Test Method Implementation 58
Test Matrix 58
Specimen Fabrication 59

TABLE OF CONTENTS CONTINUED

Results and Discussion 60
Design Recommendation 65
Conclusions 66

5. DESIGN OF EXPERIEMENT TO DETERMINE THE EFFECT OF FORMING FIXTURE VARIABLES 67

Introduction 67
Materials 69
Material Properties 69
Characteristics of RDM2019-053 69
Mechanical Properties of IM7 Carbon Fiber 70
Sizing Treatment on CF 71
Fiber Volume Content of Impregnated Tow Samples 72
Testing Methods and Design of Experiments 74
Sample Preparation 74
Methods 74
Design of Experiment 76
Results and Discussion 77
Recommendations for Complex Part Creation 85
Conclusion 87

6. CONCLUSIONS AND RECOMMENDATIONS FOR FUTURE WORK 89

REFERENCES CITED 92

APPENDICES 101

APPENDIX A: Residual Plots From ANOVA Analysis 102

LIST OF TABLES

Table Page

1.1 Material properties of common aerospace materials 4

3.1 C.A. Measurements of carbon fiber tows using areal weight 32

3.2 Yield stress comparison of IM7-G and SBCF tows at room temperature 37

4.1 Biot numbers of the heated components of the forming fixture and the specimen 56

4.2 Experimental test matrix 58

4.3 Huntsman (The Woodlands, TX) RDM 2019-053 resin viscosity at selected temperatures 60

5.1 Huntsman RDM 2019-053 resin viscosity at selected temperatures 69

5.2 Mechanical properties of Hexcel 12K IM7 [42] 70

5.3 Fiber volume ratio of various uncured pre-preg tows 73

5.4 Design of experiment for CFRP single tow samples 77

5.5 Average max force (F_{max}), max yield displacement (Δ_{max}), for various CFRP tows 78

5.6 Results of analysis of variance (ANOVA) for average max force (F_{max}) for IM7-GP 78

5.7 Results of analysis of variance (ANOVA) for max yield displacement (Δ_{max}) for IM7-GP 79

5.8 Results of analysis of variance (ANOVA) for average max force (F_{max}) for Hexcel SBCF 79

5.9 Results of analysis of variance (ANOVA) max yield displacement (Δ_{max}) for Hexcel SBCF 79

5.10 Results of analysis of variance (ANOVA) for average max force (F_{max}) for MSU SBCF 79

5.11 Results of analysis of variance (ANOVA) max yield displacement (Δ_{max}) for MSU SBCF 80

5.12 Results of analysis of variance (ANOVA) for average max force (F_{max}) for IM7-GP 83

LIST OF TABLES - CONTINUED

5.13 Results of analysis of variance (ANOVA) for max yield displacement (Δ_{max}) for IM7-GP 83

5.14 Results of analysis of variance (ANOVA) for average max force (F_{max}) for Hexcel SBCF 83

5.15 Results of analysis of variance (ANOVA) for max yield displacement (Δ_{max}) for Hexcel SBCF 83

5.16 Results of analysis of variance (ANOVA) for average max force (F_{max}) for MSU SBCF 84

5.17 Results of analysis of variance (ANOVA) for max yield displacement (Δ_{max}) for MSU SBCF 84

5.18 Regression equations predicting maximum forming load at high temperature of continuous and stretch broken carbon fibers 86

5.19 Results for predicting maximum forming load at HT 86

LIST OF FIGURES

Figure		Page
1.1	Material evolution in aerospace over time	1
1.2	Material makeup of Airbus A350 XWB [2]	2
1.3	Composition of CFRP's [3]	3
1.4	Visualization of unidirectional and quasi-isotropic laminates [5]	3
1.5	Thesis overview and organization of the chapters	10
2.1	Manufacturing process of PAN based CF [17]	12
2.2	Ideal crystalline structure of graphite, basal planes [20]	12
2.3	Visual of manufacturing flaws in carbon fiber [15]	13
2.4	SEM Image showing surface striations on CF [22]	14
2.5	Weibull shapes based on scale factor [23]	15
2.6	Visualization of tensile strength decreasing as gauge length increases [22]	15
2.7	(A) Effect of Shear Lagging on CFRP [26] (B) Damage stages of CFRP failure [25]	16
2.8	Overview of SB method [28]	17
2.9	Effect of bridging on CFRP laminates	18
2.10	Frequency distribution of filament lengths for different SB generations and break lengths [16, 31]	20
3.1	A) Overview of Hexcel SB2 stretch breaking machine B) Breaking zones on stretch breaking machine C) Sizing application station on stretch breaking machine	24
3.2	SEM images of stretch broken carbon fiber tow	25
3.3	Fiber-matrix distribution of stretch broken carbon fibers [15]	26
3.4	Carbon fiber tow test sample preparation fixture	29
3.5	Elevated temperature carbon fiber tow test set-up	30
3.6	SEM image of continuous carbon fiber tow	33
3.7	SEM image of SBCF tow	33

LIST OF FIGURES - CONTINUED

3.8 Load and displacement values of IM7-G continuous fiber at A) Room temperature and B) Elevated temperature 35

3.9 Maximum load and displacement values of SBCF A) Room temperature B) Elevated temperature 36

3.10 Maximum stress values and gauge length of carbon fiber tows at (A) Continuous IM7-G fibers at room temperature (B) SBCF at room temperature (C) Continuous IM7-G fibers at elevated temperature (D) SBCF at elevated temperature 38

3.11 Maximum load comparison of IM7-G and SBCF at room (RT) and elevated temperatures (HT) 39

3.12 Comparison of SBCF-HT and SBCF frequency of continuity based on gauge length 40

4.1 Forming fixture test design concept (A) forming blocks, (B) forming blocks radius of curvature, (C) forming tool, (D) forming tool radius of curvature, (E) tow sample and (F) deep drawing depth 50

4.2 Overview of the forming fixture assembly when mounted on a Mark-10 ESM303 (Mark-10 Corp. Copiague, NY) universal testing stand. (A) Universal testing stand, (B) force gauge, (C) forming tool adapter, (D) removable forming tool, (E) sample holding assemb 51

4.3 Forming tools with different curvature radii and adapters for Mark-10 ESM303 (Mark-10 Corp. Copiague, NY) universal testing stand 52

4.4 Forming fixture sample holding assembly (A) alignment plate, (B) tightening screw, (C) translation bridge, (D) self-leveling clamp, (E) tab holding block, (F) tab holding block front stop, (G) tow sample, (H) sample holding assembly base and (I) forming 53

4.5 Heating system installed in the forming fixture (A) forming tool, (B) forming blocks and (C) electrically resistive cartridge heater and thermocouple probes 55

4.6 Complete assembly of the forming fixture equipped with temperature control (A) Mark-10 ESM303 (Mark-10 Corp. Copiague, NY) universal testing stand, (B) forming fixture and (C) temperature control unit 55

4.7 Schematic of the fiber reinforced polymer composite tow sample fabrication showing the cardstock tabs adhered to each end of the carbon fiber tows. 59

LIST OF FIGURES - CONTINUED

4.8 Hexcel (Stamford, CT) continuous IM7-G carbon fiber impregnated with Huntsman (The Woodlands, TX) RDM 2019-053 resin tow samples after the forming test at different temperatures, The lowest temperature, (A) RT, shows complete failure, while at elevated te 61

4.9 Load-displacement curves of Hexcel (Stamford, CT) continuous IM7-G carbon fiber impregnated with Huntsman (The Woodlands, TX) RDM 2019-053 resin. Tow samples during deep drawing at room temperature show failure as: (A) rapid drop in the post-peak force 62

4.10 Load-displacement curves of Hexcel (Stamford, CT) continuous IM7-G carbon fiber impregnated with Huntsman (The Woodlands, TX) RDM 2019-053 resin tow samples during deep drawing at elevated temperature; (A) 57 °C, (B) 82 °C, (C) 107 °C and (D) 121 °C 63

4.11 Average maximum forming load of Hexcel (Stamford, CT) continuous IM7-G carbon fiber impregnated with Huntsman (The Woodlands, TX) RDM 2019-053 resin tow samples during deep drawing with increasing forming temperatures. 64

5.1 FE-SEM microscopy image of sizing connection between carbon fiber filaments 71

5.2 Solvent washed CFRP samples 73

5.3 Overview of major forming fixture factors 76

5.4 Interaction plots of max load (F_{max}) for different factors 81

5.5 Interaction plots of yield displacement (Δ_{max}) for different factors 82

5.6 Interaction plot of F_{max} plunger nose & gap combined (A) Interaction plot of Δ_{max} plunger nose & gap combined 85

A.1 Residual plots for IM7-GP ANOVA for max load (F_{max}) 103

A.2 Residual plots for IM7-GP ANOVA for max yield disp. (Δ_{max}) 103

A.3 Residual plots for Hexcel SBCF ANOVA for max load (F_{max}) 104

A.4 Residual plots for Hexcel SBCF ANOVA for max yield disp. (Δ_{max}) 104

A.5 Residual plots for MSU SBCF ANOVA for max load (F_{max}) 105

A.6 Residual plots for MSU SBCF ANOVA for max yield disp. (Δ_{max}) 105

LIST OF ABBREVIATIONS

AFP .....Automated Fiber Placement

AL .....Aluminum

ANOVA .....Analysis of Variance

ASME .....American Society of Mechanical Engineers

ASTM .....American Society of Testing and Materials

BMI .....Bismaleimide

CA .....Cross-sectional Area

CF.....Carbon Fiber

CFRP.....Carbon Fiber Reinforced Polymer

CNC .....Computer Numerical Control

CT .....Connecticut

CTE.....Coefficient of Thermal Expansion

DE .....Delaware

DOE .....Design of Experiment

DOF.....Degree of Freedom

FEA.....Finite Element Analysis

FE-SEM .....Field Emission Scanning Electron Microscope

FLD.....Forming Limit Diagram

GFRP.....Glass Fiber Reinforced Polymer

GR.....Grade

HT .....High Temperature

ID .....Identification

IEEE.....Institute of Electrical and Electronics Engineers

LLC.....Limited Liability Corporation

MA .....Massachusetts

LIST OF ABBREVIATIONS - CONTINUED

MD .....Maryland

MO .....Missouri

MS.....Mean Squares

MSU.....Montana State University

MT.....Montana

NMP.....N-Methyl-Pyrrolidone

NY.....New York

PAN.....Polyacrylic nitrile

PEEK.....Poly-ether-ether-ketone

PID .....Proportional Integral Derivative

RT .....Room Temperature

SAMPE .....Society for the Advancement of Material and Process Engineering

SB.....Stretch Broken

SBCF.....Stretch Broken Carbon Fiber

SEM .....Scanning Electron Microscope

SMC .....Sheet Molding Compound

SS .....Sum of Squares

SSR .....Solid State Relay

Ti .....Titanium

TMA.....Thermomechanical Analysis

TX .....Texas

USA.....United State of America

XWB .....Extra Wide Body

LIST OF SYMBOLS

µin .....micro inch

C° .....Degrees Celsius

cm3.....cubic centimeter

cm.....centimeter

Bi.....Biot Number

Δmax .....Maximum Yield Displacement

E1 .....Elastic Modulus

F .....Distribution Function

F°.....Degrees Fahrenheit

F1 .....Force

Fmax .....Maximum Force

g.....grams

Gpa.....Giga pascals

in .....inch

in3 .....cubic inch

k.....Thermal Conductivity

kg.....kilo-gram

kN.....kilo-Newton

Ksi.....Kilopound per square inch

lb .....pound

m .....Weibull shape parameter

LIST OF SYMBOLS - CONTINUED

m .....meter

m2 .....square meter

mm .....millimeter

mm2 .....square millimeter

Mpa .....Mega-pascals

Mpsi .....Megapound per square inch

N.....Newton

Nm .....Newton-meter

Pa.....Pascals

Pa-s.....Pascals-second

vc.....Composite Volume

Vf .....Fiber Volume Ratio

vf .....Fiber Volume Ratio

W.....Watt

ε.....Strain

ρ.....Density

σ .....Stress

σ_0 .....Weibull scale parameter

ABSTRACT

Continuous carbon fibers are premium reinforcing material for aerospace composites. Carbon fiber reinforced polymers are five times stronger than steel and twice as stiff, making it an ideal candidate for structural aircraft components where weight is an important factor. The challenge with continuous carbon fibers is their difficulty to form deep drawn parts requiring intricate manufacturing techniques that increase manufacturing time, cost, and material waste.

An alternative to continuous carbon fibers is stretch broken carbon fiber (SBCF). SBCF is a form of aligned discontinuous fiber, it has been proposed as an alternative to overcome this formability challenge. SBCF provides flexibility to form complex shapes while maintaining comparable strength and stiffness. A variety of testing methods have been developed to study both the ability of SBCF to form over traditional continuous carbon fiber and how different iterations of SBCF perform against each other. These include testing carbon fiber tows in tension on a universal test stand as well as designing and creating a forming tool that tests resin impregnated tows under different geometry conditions and temperatures.

Tensile properties of both a continuous tow and a SBCF tow were evaluated at different gauge lengths and temperatures. It shows that SBCF tow maximum load increases as the gauge length decreases as well as elevated temperature has a clear effect on the tensile properties when fiber continuity is considered. Cross-sectional areas of continuous and SBCF tows were calculated using both areal weight and scanning electron microscopy showing that in general continuous fiber tows have a larger cross-section than SBCF. Using a forming fixture to test samples, results were statistically analyzed in order to display the significance of geometry and temperature on the maximum forming load of different fibers.

The suite of testing and results indicate that in general SBCF maintains superior formability to that of continuous fibers. Overall lower maximum force is required for SBCF to form into deep drawn shapes. This supports their ability to be used more readily in complex aircraft structure while minimizing the disadvantages posed by traditional carbon composites.

CHAPTER ONE

INTRODUCTION

The continual pursuit of high-performance materials in the aerospace industry since the inception of air flight has led to a major increase in the use of carbon fiber reinforced polymers (CFRP) in recent years in both structural components and parts exposed to extreme environments. Historically aerospace has been on the fore front of materials development, because of the diverse conditions in which airplanes are subjected. Airplanes experience high loads and rapidly changing weather conditions when in service but must still be light enough to address the aerodynamic challenges of flight. This leads to the search for lightweight materials with exceptional mechanical properties. The overall material progress in aerospace has followed the outline in figure 1.1. It should be stated that even now there are various parts made of metal and other non-composite materials, but most next generation airplanes have transitioned to a primarily composite structure.

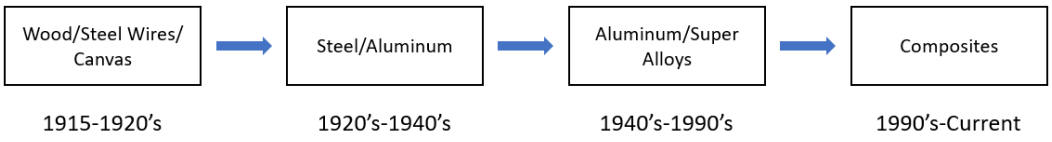


Figure 1.1: Material evolution in the aerospace industry

Weight savings derived from the mechanical strength of CFRP's are important factors to commercial airplane manufacturers as fuel costs continue to increase and environmental concerns have become more pronounced. A study conducted by the Federal Aviation Administration Advanced Materials Research Program reported a $100-$300 costs savings per

pound of weight saved over the life of the aircraft [1]. Airbus and Boeing, the two clear leaders in commercial aircraft manufacturing have invested heavily in CFRP adoption in aircraft since the early 1990's. When the Airbus A310 was introduced in the 1982 less than 5% of the airframe was made of composite material whereas the Airbus A380 (2005) increased composite usage to 25%. Continuing this trend, when the Airbus A350XWB was first flown in 2013 it was comprised of 53% composites [2].

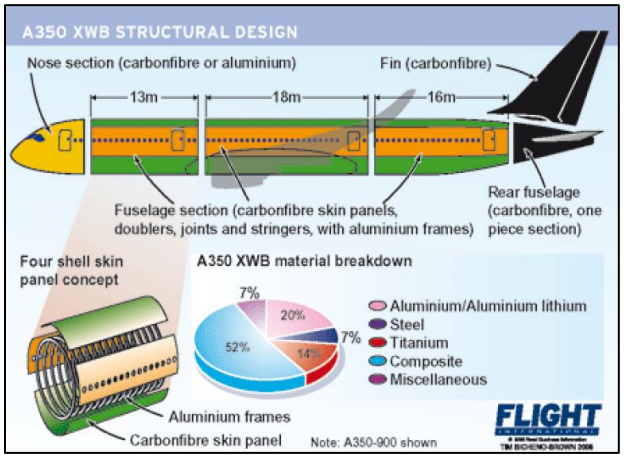


Figure 1.2: Material makeup of Airbus A350 XWB [2]

Composites are defined by two or more materials that are combined to create a singular material that uses the desired material properties of each constituent to produce the final component. Specifically, for CFRP's there are two main components, the carbon fiber (CF) and the matrix. The CF provides the strength and low density to CFRP's while the matrix encapsulates the CF maintaining the final shape and protects the CF from external impacts and damage.

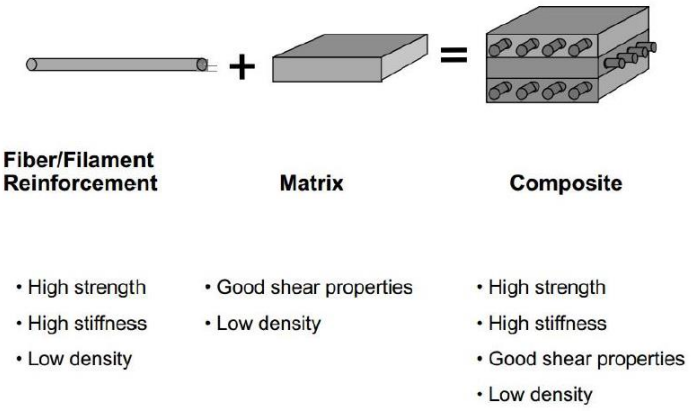


Figure 1.3: Composition of CFRP's [3]

CFRP's are an anisotropic material because the strength of the CF is directionally dependent along the axis of the fiber. Because of this dependency CFRP's are often laminated in layers to produce a quasi-isotropic material where direction is less important, similar to the truly isotropic nature of metallics. To create a quasi-isotropic laminate, technicians are given a ply sequence to layer the material before curing of the matrix. A common quasi-isotropic layup scheme is $[0/90\ +45/-45\text{-}45/+45/90/0]_s$, which can be continuously repeated until the desired thickness is obtained [3].

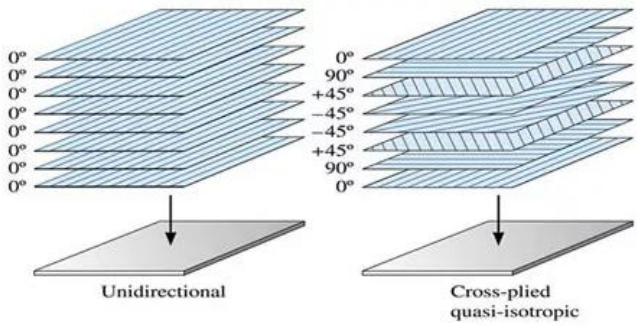


Figure 1.4: Visualization of unidirectional and quasi-isotropic laminates [5]

Advantages of CFRP's over Conventional Aerospace Materials

When compared to steel, aluminum, and super alloys such as titanium; CFRP's have several distinct mechanical advantages. CFRP's are both lighter than standard metallics and show superior mechanical strength. Table 1 shows the comparison of mechanical properties between different metals and a common aerospace grade CFRP termed IM7/8552 produced by Hexcel Corporation (Stamford, Connecticut).

Table 1.1: Material properties of common aerospace materials

Material	**E_1 (ksi)**	**F_1 (ksi)**	**ρ (lb/in^3)**	**E_1/ρ**	**F_1/ρ**
Hexcel IM7/8552 [4]	23.7	373	.057 [5]	415.8	6543.9
AL 7075-T6 [6]	10.4	83	.101	103	821.8
Steel A572 GR50 [7]	29.7	65.3	.282	105.3	231.6
Ti 6AI-4V (GR 5) [6]	16.5	138	.16	103.1	862.5

The specific modulus (E_1/ρ) for the CFRP laminate is roughly 4 times that of the conventional metal alloys and the specific ultimate tensile strength (F_1/ρ) is almost 10 times as strong AL 7075-T6 and Ti 6AI-4V, while close to 30 times that of steel. For aerospace design the use of specific values for mechanical properties is preferred because it details how strong a material is based on the density of the material. Using an incredibly strong material with a high density is of minimal use to designers when weight is a primary concern. Because of the directional strength advantages of the CFRP's this also allows tailoring of the laminate to achieve desired mechanical performance based on the loading direction that the part will see. For example, a wing stringer for a commercial aircraft will primarily see a cantilevered load from the tip of the wing to where it is anchored to the fuselage. This means with proper

forethought; designers can modify the laminate to increase the mechanical strength in the out of plane direction [8].

Several other factors contribute to the increased use of CFRP's in aerospace. When operating at high temperature, aircraft must balance the varying coefficients of thermal expansion (CTE) of different materials so that expansion does not have adverse effects on the structure and pressurization of the fuselage. In most cases a low CTE is desirable because it limits dimensional changes over long distances. Kappel and Pruzzak employed thermomechanical analysis (TMA) to determine the CTE for a closely balanced ([4 x 0°, 10 x ±45°, 4 x 90°]) M21E/IMA CFRP laminate and observed a CTE of 1.94-2.17 µin/in-F° in varying directions [9]. AL 7075-T6, Steel A572 GR50, Ti 6AI-4V (GR 5) have CTE's of 12-14 µin/in-F°, 6.7 µin/in-F°, and 4.78-5.39 µin/in-F° respectively. Thus, CFRP's have superior CTE properties when the laminate is balanced, though when layered in a completely unidirectional laminate, CTE's in directions perpendicular to the axis of fiber can reach close to 30 µin/in-F° [10]. CFRP's also have high damage tolerance and fatigue resistance, when CFRP's undergo impacts the damage is dispersed throughout the matrix reducing the crack propagation that is prevalent in metallics [11]. The high stiffness of CFRP's also allows the laminate to recover from concentrated impacts and fatigue be recovering elastically to its original shape more readily than ductile materials. Kwon et al, investigated this effect by comparing impact resistance of a CFRP and steel car fender, and found that the steel deformed easily due to the impact of a 97.7 kg weight while the CFRP showed a stable impact response, and no fracture was identified after five repeated impacts [12].

CFRP's also possess increased corrosion resistance over metallics, this property of CFRP's lends itself to be used in industries outside of aerospace including marine and civil

construction. Some estimates have shown that corrosion of metals cost the U.S economy $300 billion per year in maintenance, repair, and replacement costs [13]. Epoxy resin systems have high resistance to saltwater and water in general because they are structured in a long molecular chain with reactive sites at both ends [14]. These reactive sites are formed by epoxy groups without the presence of ester groups resulting in excellent water resistance [14]. This has led to widescale adoption of epoxy resin composites in pressure vessels, naval ship components, and offshore wind farms.

Disadvantages of CFRP's

With the distinct material advantages of CFRP's it is often wondered why high performance CFRP's are not more widely adopted outside of specialized applications. Several minor factors are attributed to constraining the use of CFRP's, including difficulty in structural analysis of tailored CFRP parts and relative recency of standard CF and matrix formulations, but the most limiting factor is the manufacturing cost of producing the laminate. The individual constitutes of CFRP's (CF and matrix) are competitive with high performance metallics on a cost basis. The true cost for the final structural shape is dominated by the processing costs. Expensive and complex equipment, experienced layup technicians, and stringent environmental controls can quickly increase the cost by 10-100 times that of the raw material [15]. These processing bottlenecks also lead to low throughput of parts. The downsides in manufacturing have led to an increased interest in alternative material forms of CFRP's to reduce processing costs. Sheet molding compounds (SMC's) and chopped CF are commonly used in low-risk applications but do not encompass the required strength for structural aerospace parts. One CF

form, termed stretch broken carbon fiber (SBCF), has been studied intermittently since the 1980's has seen renewed interest because of the increased use of CFRP's in many industries.

Introduction of Stretch Broken Carbon Fiber

SBCF is produced from conventional continuous CF feed stock. The CF is feed through a specialized stretch breaking machine similar to those used in conventional textile industries. The fiber is then broken at set break lengths to produce an aligned discontinuous fiber tow. This is differentiated from other discontinuous CF because, in theory, breaks in the SBCF are occurring at natural flaws in the CF itself (see chapter 2). These breaks in the fiber are specifically spaced so that the fiber can hold itself in tension enough to be handled and impregnated with a resin system but small enough to allow the fibers to slide past each other when elevated temperature and pressure is applied. Promising results have been introduced by Hexcel Corporation in the mid 2000's but inadequate machine technology and fiber length distributions led to a phase out of their research [16]. Montana State University (MSU, Bozeman, MT) has recently (2018) restarted the work where Hexcel left off with new innovative ways to produce SBCF. Aside from the manufacturing and mechanical strength studies of SBCF a pivotal factor for the successful use of SBCF is formability. Since SBCF is a little understood material, there are few ways to test the formability behavior. MSU researchers have conducted novel test methods to study formability of SBCF that will be presented in this paper.

Hypothesis and Objectives

Thesis Goal

The goal of this thesis is to provide insight into the formability characteristics of both continuous CF and SBCF. Three major objectives are presented: 1) gauge length study of CF tows, 2) design and validation of a novel stretch-bending forming fixture, and 3) statistical ANOVA modeling of CFRP tows in the stretch-bending formability test. Several sub-objectives are also present in this study:

Sub-Objectives

(1) Create repeatable gauge length samples of continuous and SB CF tows to be tested on a universal test stand at various temperatures

(2) Develop sample preparation technique for analysis of tow cross-sections in Field Emission Scanning Electron Microscope (FE-SEM)

(3) Compare tow strength of SBCF and continuous tows based on cross-sectional area

(4) Verify holding force on test fixture and temperature control to ensure confidence in testing.

(5) Conduct design of experiments to produce ANOVA model that provides information on formability of different CFRP tows.

Thesis Hypothesis

The research presented hypothesizes the following:

(1) SBCF tows have superior formability to that of continuous CF because of the discontinuous nature of the fibers

(2) Fiber length distribution and continuity of SBCF contributes to formability

Structure of thesis

The structure of this thesis paper is divided into seven chapters; Chapter one is a general introduction and purpose of research, a background and literature review is detailed in Chapter two, Chapters three and four are major findings of the research that have been published or under review in peer reviewed journals, Chapter five presents research that helps to address the formability hypothesis explained earlier, and Chapter six is an overview of the conclusions of the paper and recommendations for future work. Figure 1.5 presents a schematic of the general organization of the thesis.

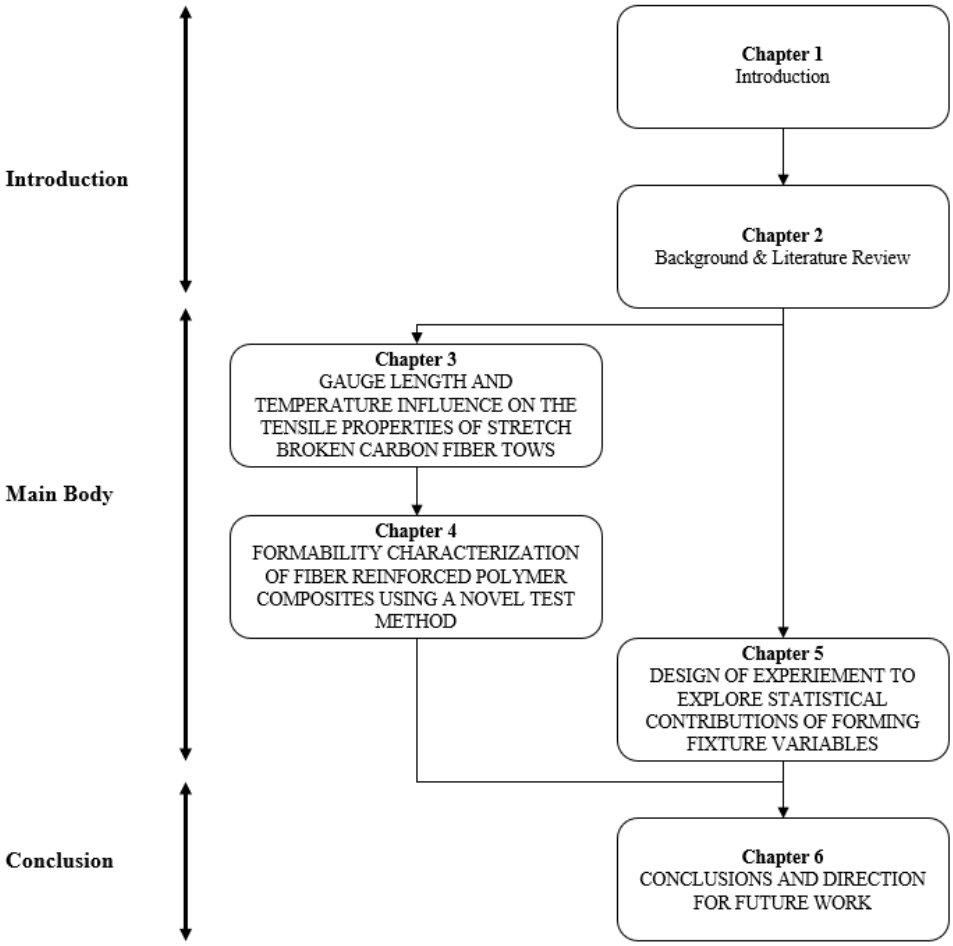


Figure 1.5: Thesis overview and organization of the chapters

CHAPTER TWO

BACKGROUND & LITERATURE REVIEW

Mechanics of Carbon Fiber

The prevalence of carbon fiber reinforced polymer composites in aerospace applications has steadily increased since there use by the U.S. military in the early 1960's [17]. Carbon fiber (CF) has distinct advantages over traditional structural metal alloys such as steel and aluminum because CF has a superior strength to weight ratio. CF composites also benefit from good dimensional stability, low coefficient of thermal expansion, and both corrosion and fatigue resistance [18]. These features have led CF to be used not only in aerospace but a multitude of different industries including automotive, sports equipment, and marine.

CFs are made from two main precursors, polyacrylonitrile (PAN) and pitch based synthetic fibers. PAN based fibers are most common in military aerospace applications because consistency and cost to manufacture are the most competitive. This dissertation will solely focus on PAN based fiber because of their ubiquity in the structural components of high-end aerospace applications. PAN fibers go through a process of polymerization, spinning, oxidation and then finally carbonization to transition into the final carbon filament form. Figure 2.1 shows the basic process for production of PAN based CF.

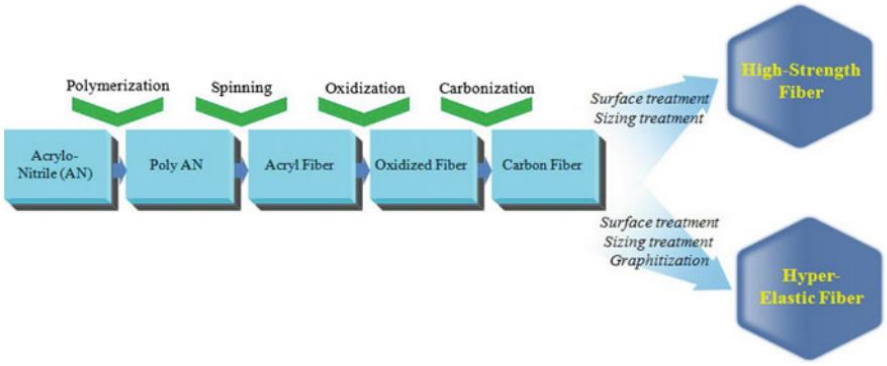


Figure 2.1: Manufacturing process of PAN based CF [17]

CFs are defined by a polycrystalline graphitic structure that exhibits a high modulus because the crystalline layers or basal planes are parallel to the fiber axis, this also means the modulus of the fiber is weaker perpendicular to the fiber axis [19]. Processing parameters of CF in this case are of upmost importance because the better alignment of basal planes to the axis of the fiber the stronger the fiber is mechanically.

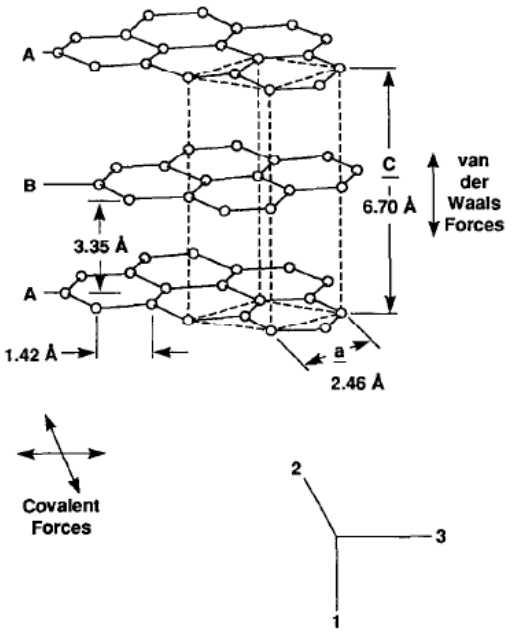


Figure 2.2: Ideal crystalline structure of graphite, basal planes [20]

Even in the most tightly controlled CF manufacturing settings, flaws in carbon fiber are always present. When a fiber fails the culprit is normally a result of these flaws, some of which can originate from the precursor itself. When the PAN precursor is spun to create the final diameter of the CF, it is drawn through a spinneret that can have striations in the tooling of the equipment. These striations and other small manufacturing flaws are imprinted on the fiber itself creating failure zones when the fiber is put under stress. It is known from previous work and work current research that the average strength of a filament will decrease as the gauge length of the fiber increases [20]. The main cause of this is that as the gauge length increases the number of flaws present in the filament increases leading to more opportunities for failure to occur and propagate throughout. Figures 2.3 & 2.4 show the effect that manufacturing flaws can imprint on the fiber surface.

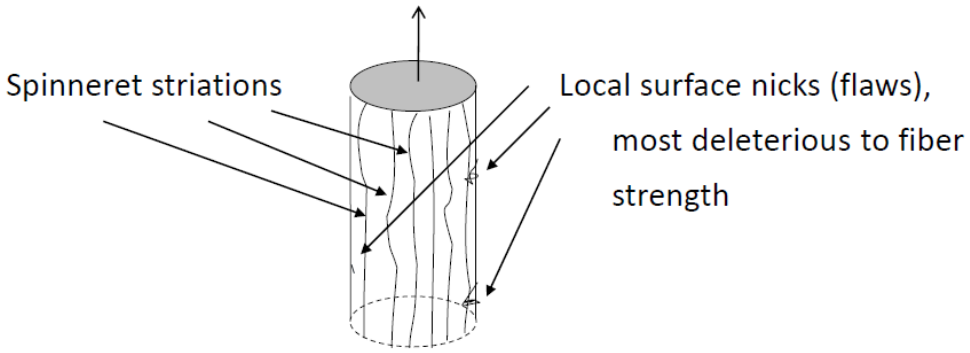


Figure 2.3: Visual of manufacturing flaws in carbon fiber [15]

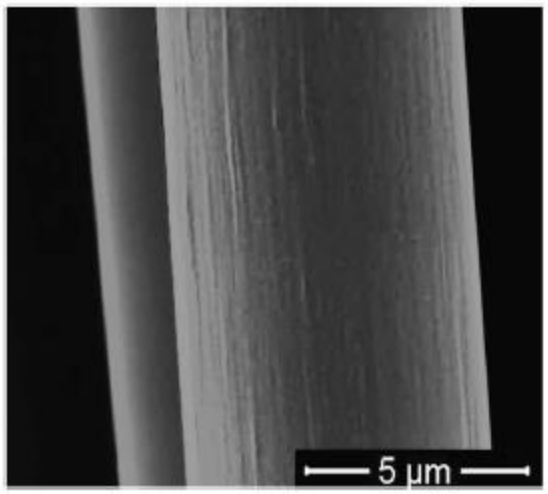


Figure 2.4: SEM Image showing surface striations on CF [22]

Several models from both Stoner and Durham, have been constructed to investigate the flaw distribution throughout a fiber filament. Because tensile strengths of CF filaments vary rather broadly from fiber to fiber, and since flaws are not consistent throughout the length of the fiber, mechanical characteristics of CF filaments can be estimated using a distribution model based on the Weibull cumulative distribution function, F, with parameters σ_0, and m [21].

$$F = 1 - \exp\left[-\left(\frac{\sigma}{\sigma_0}\right)^m\right] \quad (2.1)$$

Where σ_0, and m are Weibull scale and shape parameters, respectively, and σ is the failure stress. The distribution function (F) models the probability that the fiber will fail at a stress less than or equal to σ [21]. Where failure stress illustrates ideal fiber composition and F, factors in the failure due to the realistic flaws in the fiber. The Weibull scale factor, m, is what accounts for the flaw distributions of fiber in longer gauge sections. Figure 2.5 shows the various shapes that Weibull distribution can produce.

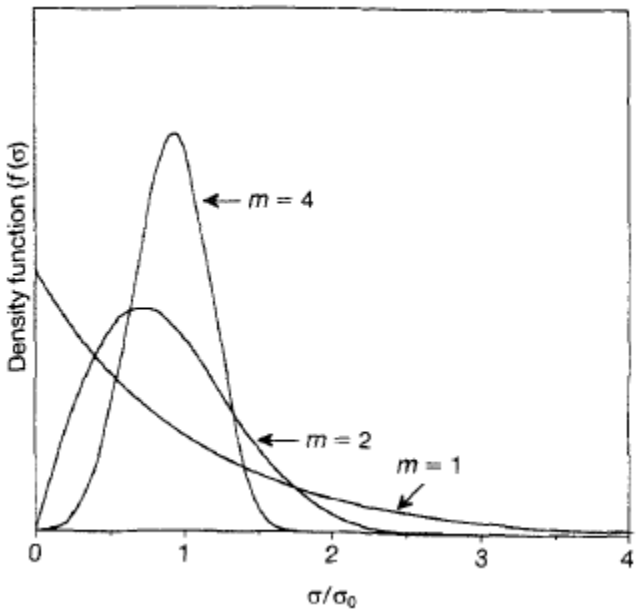


Figure 2.5: Weibull shapes based on scale factor [23]

These models have been corroborated through experimental analysis, Langston and Parra-Venegas have both reported on the effect that surface flaws have on the allowable stress of fibers, although the Parra-Venegas study focused on glass fibers [22, 23]. Langston was able to test various gauge lengths of individual CF filaments and show the predicted decrease in tensile strength as the length increases.

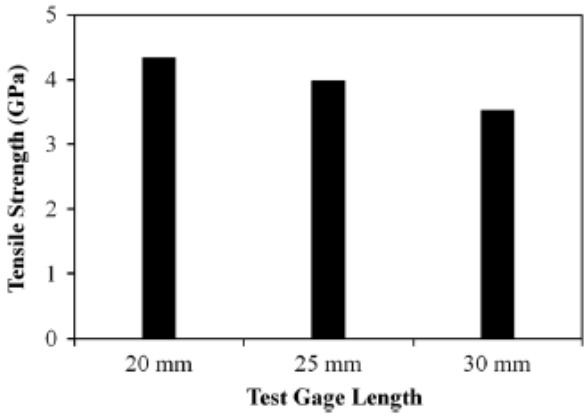


Figure 2.6: Visualization of tensile strength decreasing as gage length increases [22]

When CF is laminated with a resin system the manufacturing flaws in the fiber are still present in the final cured part. Meaning that surface flaws in the initial manufacturing process are carried all the way to the use point and potential failure of the part. When a cured part begins to fail the broken fiber caries no load at the end, after fiber failure there is a secondary interaction that carries the complete structure to its yield stress value known as shear lagging. Shear lagging is a result of the bond between the matrix and surface of fiber filaments, the difference in shear moduli between them contributes to the majority of the total tensile load [24].

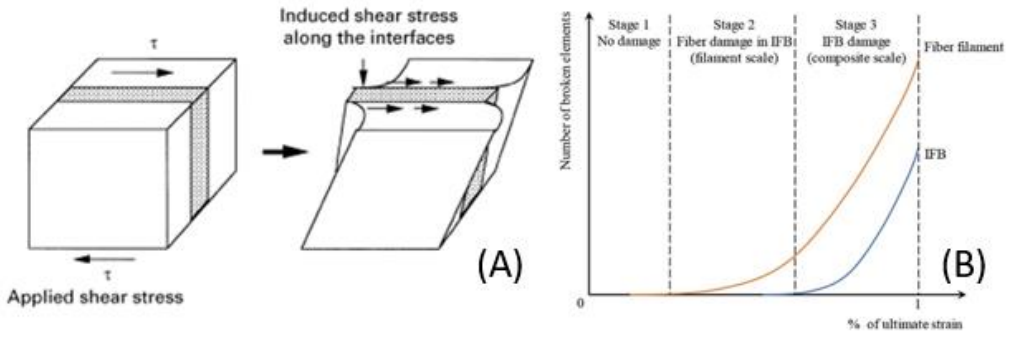


Figure 2.7: (A) Effect of shear lagging on CFRP [26] (B) Damage stages of CFRP failure [25]

Discontinuous Carbon Fiber

Because of the shear lagging effect, it has been hypothesized that there is no significant mechanical advantage to have laminates maintain CF continuity throughout its length. Eliminating this requirement opens the door to a variety of novel manufacturing methods that potentially increase the prevalence of CFRPs in traditionally metallic components. Although discontinuous CFRPs are relatively common in sheet molding compounds (SMC's) and chopped fiber laminates, being misaligned mostly eliminates the shear lag effect. Fiber that is cut and

aligned at a pre-determined length has also seen some development, but this process still consists of the fiber failure flaws discussed earlier [25]. Advances in stretch broken carbon fiber (SBCF), however, have identified it as a possible solution to these drawbacks. SBCF is aligned discontinuous CF that is broken at the natural flaws of continuous CF using differentially driven rollers in order to "stretch" the fiber until failure as shown in figure 2.8.

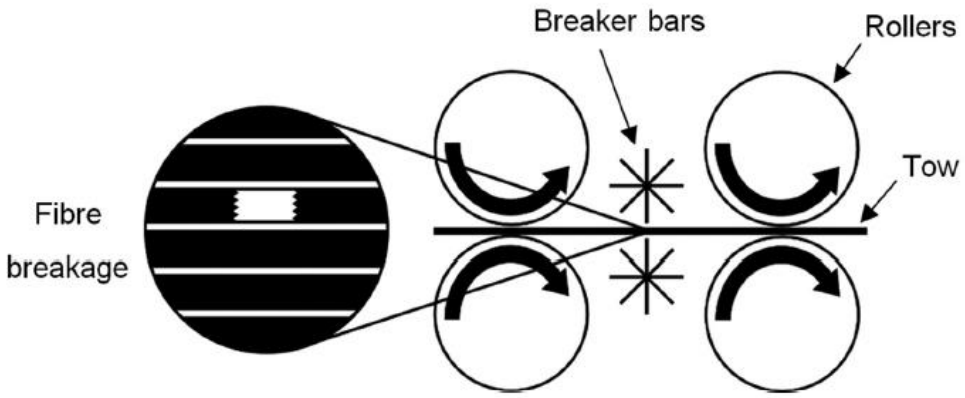


Figure 2.8: Overview of SB method [28]

Another major advantage of SBCF over continuous CF is its potential to be formed into complex shapes more readily. Formability of a material describes the ease in which it takes on the target shape without hindering the mechanical properties of the material [26]. Traditional CF is difficult to form because its strength and brittleness resists out of plane movement. These restrictions have made processing costs for layups of structural CF components to be incredibly high. Complicated and time intensive layup schedules are needed to reduce internal stresses from fiber bridging and specialized equipment such as autoclaves and ply projectors are required to maintain the quality and repeatability of manufactured parts.

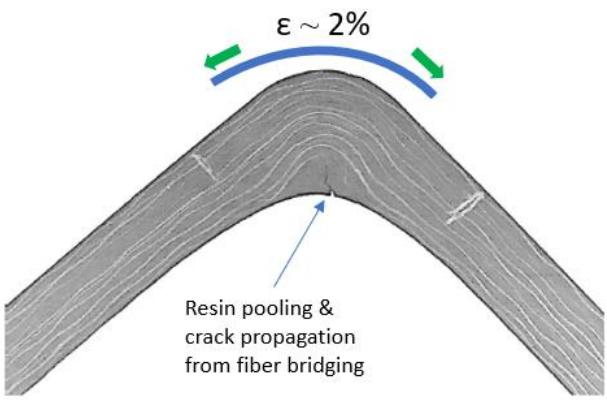


Figure 2.9: Effect of bridging on CFRP laminates

SBCF solves costly and complicated layup procedures by allowing the fibers in the pre-cured laminate to slide past each other in the resin matrix when elevated temperature and pressure are applied. This pseudo plastic effect means that deep drawn shapes and sharp radii are more realistic with SBCF than with continuous CF. Processing costs could be reduced substantially while still maintaining mechanical properties resulting from the shear lag effect discussed earlier. An important factor for the wider spread adoption of SBCF is the fiber break length. The break length of the fiber is set by the distance between the SB rollers. It is imperative that both the fiber break length and break length distribution is relatively small in order to facilitate fiber sliding in complex geometry. Montana State University (MSU, Bozeman, MT)) has identified 38.1 mm (1.5 in) as the target value for the break length because it maintains enough effective length to promote shear lag and break at flaws while still being small enough to form sufficiently.

The first iterations of SBCF were made by DuPont (Wilmington, DE) in the 1980's utilizing a modified textile SB machine, in which they reported break length between 25 mm (1

in) and 100 mm (3.93 in). Okine et al. used a thermoplastic resin matrix for lamination of the plates used in testing and reported a modulus of 129.6 GPa (18.8 mpsi) and strength of 1696.1 MPa (246 kpsi). Compared to the continuous fiber results of 125.5 GPa (18.2 mpsi) and 1674.4 MPa (243 kpsi) it shows that the SBCF laminates maintained similar mechanical properties [27]. It is unclear exactly why the use of this experimental fiber was ended but no significant research was conducted after the conclusion of the aforementioned study. Another major study, aside from current work being conducted by MSU, was development work led by Hexcel (Stamford, CT) from the late 1990's until the early 2010's [28]. The second-generation Hexcel SB machines is shown in figure 3.1. Hexcel's SBCF research study was divided into two different generations of work. Generation one used a modified textile based, Sydel Model 682, SB machine to break AS4 12K carbon fiber tows at a nominal break length at 100 mm (3.93 in). Generation two Hexcel machine was dubbed as SB2. The SB2 machine was able to manufacture IM7-GP 12K CF tows at a nominal break length of 73 mm (2.875 in) [16, 28]. A major goal of the generation two effort was to reduce the filament length of the broken fiber to potentially increase the formability of the fiber. Figure 2.10 shows the comparison between fibers by generation. Frequency of continuity is a measure of how continuous the fiber bundle is from end to end. The Hexcel SB process does not allow for complete breakage of the fiber primarily because of mechanical limitations (i.e. nip roller control and pressure, feed rate control, slippage, ect.). Ideally the plot of fiber continuity vs fiber length would show an almost vertical representation with a small tail at either end. Data was collected using ASTM D 5103 "Standard Test Method for Length and Length Distribution of Manufactured Staple Fibers (Single-Fiber Test)" [29].

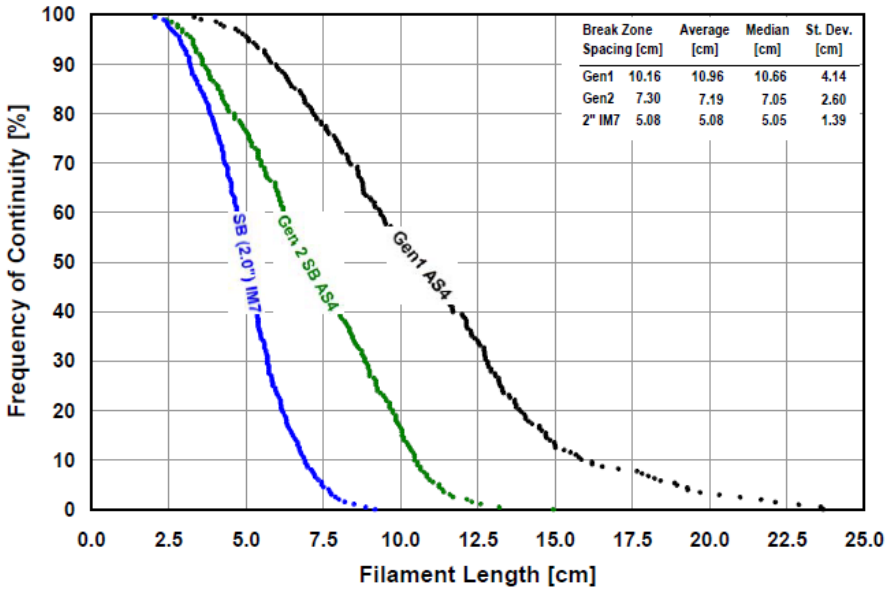


Figure 2.10: Frequency distribution of filament lengths for different SB generations and break lengths [16, 31]

Similar to the work DuPont conducted, Hexcel found that SBCF laminates performed mechanically within the range similar to tradition continuous CF. Testing in this study utilized generation two SB IM7-GP 12K tows laminated by Hexcel with proprietary 8552 toughened epoxy resin in pre-preg form. Even with some promising initial results, Hexcel ended research in SBCF primarily because of limitations in manufacturing technology that made producing consistent SBCF tows very difficult.

CHAPTER THREE

GAUGE LENGTH AND TEMPERATURE INFLUENCE ON THE TENSILE PROPERTIES OF STRETCH BROKEN CARBON FIBER TOWS

Contribution of Authors and Co-Authors

Manuscript in Chapter 3: Gauge length and temperature influence on the tensile properties of stretch broken carbon fiber tows

Co-Author: Joseph Janicki

Contributions: Methodology, Data curation, Formal analysis.

Author: Dilpreet S. Bajwa

Contributions: Conceptualization, Supervision, Visualization.

Co-author: Douglas Cairns

Contributions: Project administration, Conceptualization, Funding acquisition.

Co-author: Roberta Amendola

Contributions: Conceptualization.

Co-author: Cecily Ryan

Contributions: Conceptualization.

Co-author: Alexey Dynkin

Contributions: Methodology, Resources, Validation.

Manuscript Information

Joseph Janicki, Dilpreet S. Bajwa, Douglas Cairns, Roberta Amendola, Cecily Ryan, Alexey Dynkin

Composites Part A: Applied Science and Manufacturing

Status of Manuscript:

- ☐ Prepared for submission to a peer-reviewed journal
- ☐ Officially submitted to a peer-reviewed journal
- ☐ Accepted by a peer-reviewed journal
- ☒ Published in a peer-reviewed journal

Publisher: Elsevier Ltd

Published: July 2021

DOI: https://doi.org/10.1016/j.compositesa.2021.106426

Introduction

Polyacrylonitrile (PAN) derived carbon fibers are premium quality carbon fibers widely used in high value applications such as aerospace and automobile composite manufacturing [17]. The use of PAN based fibers in aerospace industry has been increasing over the years. For example, the Boeing 777 used roughly 12% composites by weight when it was first introduced in 1994, whereas the current Boeing 777X variant with the new composite wing is roughly 30% composite [30]. The benefits from implementing composites range from increased structural performance, to weight reduction and improved fuel efficiency, as well as improved corrosion resistance.

Carbon fiber is widely used in polymer composites for manufacturing high value structural components because it can be processed to form target shapes in complex tools. In advanced composite fly-away parts, carbon fiber is laid into a tool in a resin impregnated sheet form known as prepreg and subsequently pressure and often elevated temperature is applied to cure the resin [17, 31]. This process can be done manually, with an automated fiber placement machine (AFP), or via automated compression molding.

Currently there are several factors that limit the manufacturing of complex shapes using continuous carbon fiber. Because of the inherently low strain to failure of carbon fiber (~ 2%), to making complex shapes with deep drawn profiles is a complicated, costly and time intensive process [32]. These processes also lead to large amounts of waste material, as net-zero blanks are not possible. A potential solution to overcome the processing limitations and high cost is to use carbon fiber that has been pre-broken at natural flaws using a process called stretch breaking [33]. The most common method for producing stretch broken carbon fiber is to use differentially

driven rollers that are set at a specific break distance from each other. The break distance is referred to as the “stretch break zone” and can be adjusted based on the desired mean fiber length. Figure 3.1 shows the Hexcel SB2 machine for producing stretch broken carbon fiber. According to Dillon et al, Stretch Broken Carbon Fiber (SBCF) can provide the benefit of being highly formable at variable temperature and load conditions but maintain comparable material properties to continuous fiber composites when fully cured [34]. Several previous studies have demonstrated the potential of SBCF fibers to manufacture bead panels, box and cross panels and web stiffer frames [35, 36].

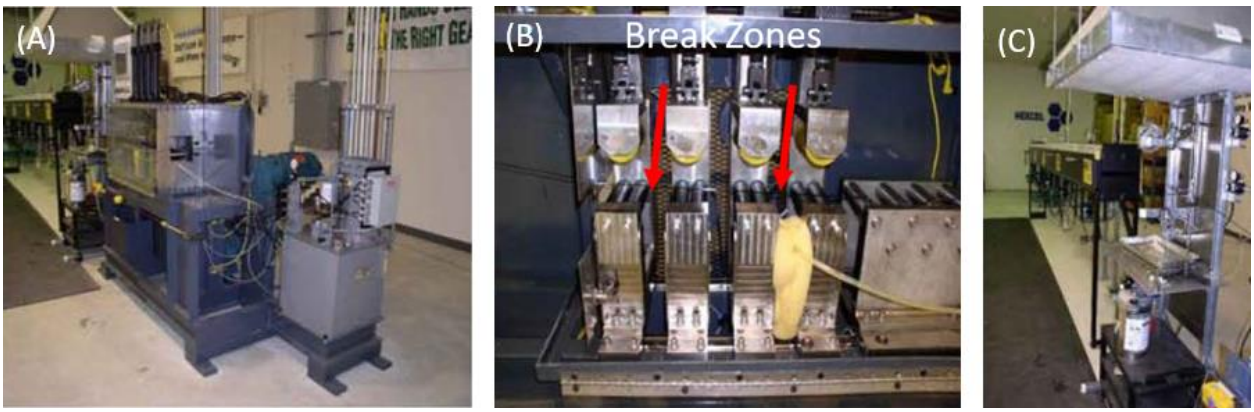


Figure 3.1: A) Overview of Hexcel SB2 stretch breaking machine B) Breaking zones on stretch breaking machine C) Sizing application station on stretch breaking machine

To understand the formability potential of SBCF, tensile testing of sized tows at various gauge lengths was conducted and compared to continuous carbon fiber. Gauge length is an important factor for formability as it can relate how the forming force or applied load varies between continuous and SBCF based on the length of the test sample (carbon fiber tows). It is expected that, for discontinuous fiber tows, longer gauge lengths will result in lower tensile strength due to the higher number of fiber breaks within the gauge section, instead lower gauge lengths should be on par with that of continuous fiber because filaments “bridge” across the

gauge section, thus imparting quasi-continuous behavior [37]. By analyzing the load-displacement data acquired from testing different gauge lengths of SBCF tows of known mean fiber length, this research aims to establish a correlation between fiber length and temperature that can be used to characterize SBCF and compare its attributes to traditional continuous carbon fibers.

Materials and Methods

Materials

The materials used in this testing were acquired from Hexcel Corporation (Stamford, CT, USA). The two types of carbon fiber were continuous 12K IM7-G and 12K Hexcel IM7-GP stretch broken carbon fiber. The SBCF was manufactured by Hexcel using their proprietary Generation 2 stretch breaking machine as shown in figure 1. A SEM image of SBCF is shown in figure 3.2.

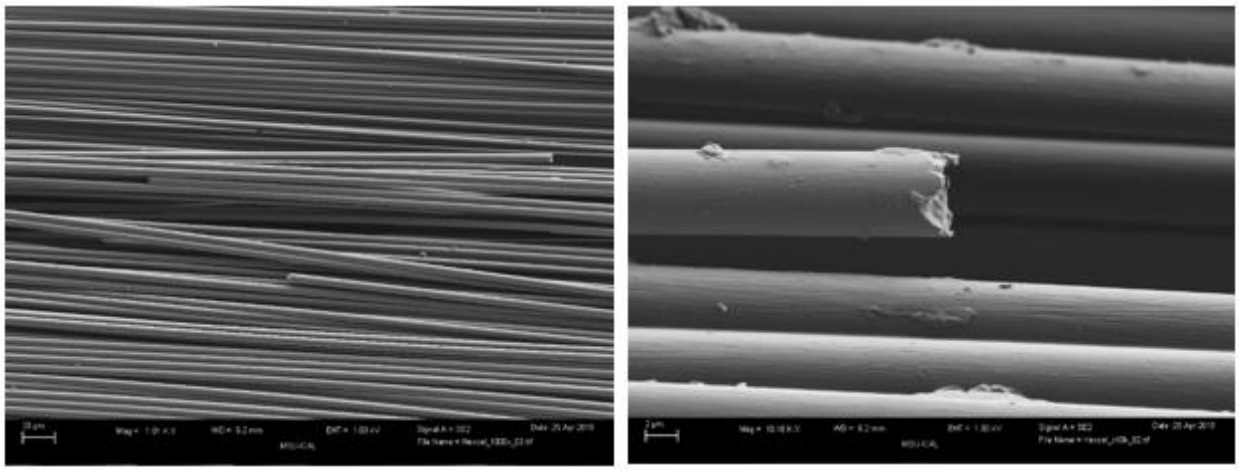


Figure 3.2: SEM images of stretch broken carbon fiber tow

Once the fiber is processed through the stretch breaking machine it is ‘sized’ with Hexcel’s proprietary G-Prime sizing using a spray booth.

Sizing

Sizing is an important component to the material stability of SBCF. At gauge lengths longer than the break zone of the production process, there is little to no continuous fiber across the whole length of the sample. This results in no significant tensile strength contribution from the carbon fibers themselves. For long gauge lengths of unsized SBCF, the tow counteracts tension mainly with friction between fibers. Sizing attempts to reconstitute the tensile strength of carbon fiber tows by creating a physical bond between disconnected fibers. The bond creates strong interfacial shear properties between fibers resulting in a composite like structure where the sizing acts as the matrix. A visualization of fiber matrix distribution is shown in figure 3.3, and data showing the effect of sizing is discussed later in this study. At elevated temperature sizing softens and diminishes fiber-sizing interaction thus weakening the bond between fibers [38].

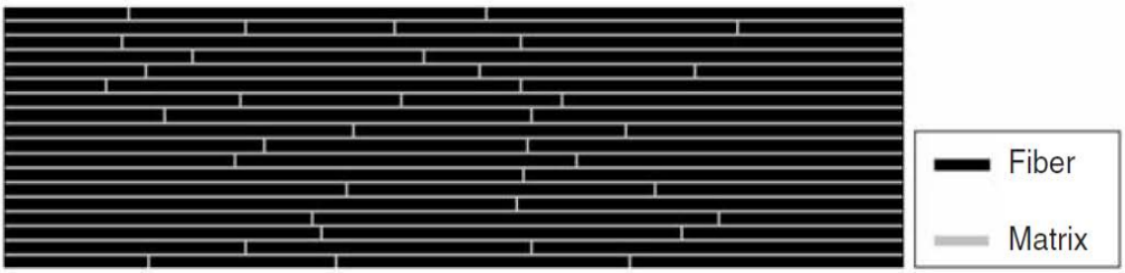


Figure 3.3: Fiber-matrix distribution of stretch broken carbon fibers [15]

Cross-sectional area of carbon fiber tows

According to technical specification data from Hexcel and verified by measurements performed internally at Montana State University, the average fiber length of this SBCF material was 50.8 mm [16, 29]. Although SBCF is made from 12K IM7 fiber, the resulting cross-sectional area (C.A.) is expected to be lower after the stretch-breaking process because the material is altered longitudinally. In the SBCF manufacturing process the fiber is attenuated due to stretching and some fiber is lost due to sticking on the roller surface due to processing. It is therefore expected that the tensile strength will be affected when compared to continuous IM7 fiber.

The C.A. directly affects the yield stress of the fiber tows because it determines the number of fibers that can resist the applied load. Using equation 3.1, the peak forming stress of the tow can be calculated, where σ is peak stress [Pa], P_{max} is the maximum load [N] at failure, and C.A. is cross-sectional area of the tow.

$$\sigma = \frac{P\text{max}}{C.A.of\ tow} \qquad (3.1)$$

Two separate methods were used to calculate the C.A. of tows to ensure the accuracy of data. The first method considered areal weight, number, and fiber diameter and second method used scanning electron microscope imaging technique to calculate the CA of carbon fiber tows.

Method 1: C.A based on carbon fiber specifications. The C.A. of IM7-G continuous fiber tows is 0.25 mm^2 as reported in Hexcel's published data sheet [39]. While the C.A. of Hexcel's SBCF is not published, it can be approximated by multiplying the published individual filament diameter from Hexcel's IM7 data sheet by the fiber count in SBCF. The fiber count can be

estimated by dividing the weight per unit length of the tow in g/m by the weight of the filament in g/m.

Method 2: Scanning electron microscopy (SEM) image analysis. This method provides a more accurate measurement by digitally measuring the C.A. of carbon fibers from SEM images. Specimens for SEM were fabricated by holding a tow vertically in light tension using a Mark-10 ESM303 (Mark-10 Corp. Copiague, NY, USA) motorized test stand. The tow was then encased in heat shrink tubing and heated to create a compacted sample. SBCF samples were heated carefully to counter any effects of fiber sliding, resulting in reduced C.A. The force gauge on the test stand was monitored during heating to verify that no reduction in force was observed while heating. The sample was embedded in clear epoxy resin and cut into imaging samples using a diamond saw. The samples were analyzed using a SUPRA 55VP scanning electron microscope (Carl Zeiss AG, Oberkochen, Germany). Five images were randomly obtained from five different samples at 200X and 2000X magnifications. Images of a continuous tows and a SBCF tows where then outlined using ImageJ software (National Institutes of Health, Bethesda, MD) for determining an overall C.A and to calculate the void percentage in each CA image. Based on the void percentage, the actual C.A. of each tow was calculated.

SBCF filament lengths

The SBCF filament lengths were measured following ASTM D 5103 protocol “Standard Test Method for Length and Length Distribution of Manufactured Staple Fibers (Single-Fiber Test)” [29]. The Montana State University research team conducted its own study to verify the fiber break length distribution. Using a similar method to Hexcel, it was found that the material exhibited fiber break distribution that was in general agreement with Hexcel but there were some

extended fibers to approximately 9 cm. Figure 3.3 shows a visualization of the fiber break distribution of SBCF.

Sample Preparation

Continuous and SBCF tows were used to make the test samples. For better gripping the carbon fiber tows were taped at the end and pulled from a spool at a specified length as shown in figure 3.4. The tabs were adhered to the carbon fiber tow ends using a fast-curing ethyl cyanoacrylate adhesive. Cardstock was used for sample tabs with dimensions 31.75 (mm) x 19.05 (mm). Precautions were taken to ensure that all fibers were aligned correctly with the tabs and no twists were present in the fiber prior to the application of the adhesive. Samples were then clamped and cured at room temperature (24 °C) for at least 30 minutes before testing. Since the SBCF was expected to maintain a consistent break length of 50.8 (mm) average filament length throughout the entire spool, samples with gauge lengths of 127.0, 101.6, 76.2, 50.8, 25.4, 12.7 and 6.35 (mm) were prepared for testing.

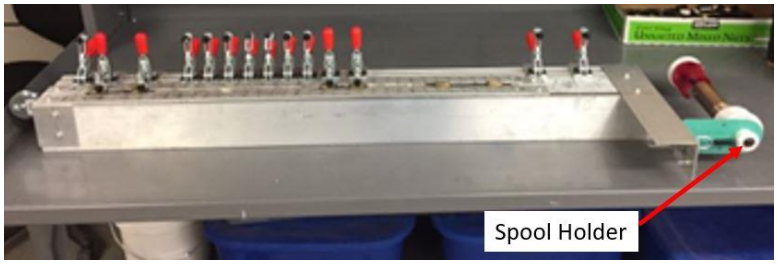


Figure 3.4: Carbon fiber tow test sample preparation fixture

Test method

Tensile testing was performed using a Mark-10 ESM303 motorized test stand. The machine was equipped with 1.5 (kN) load cell with a resolution of 0.445 (N). The crosshead speed was set at 12.7 (mm/min). The test samples were held in position by self-tightening wedge grips for consistent testing and to minimize damage to the sample tabs. The room temperature tests were conducted at 24° C +/- 5° C and elevated temperature tests were conducted at 100° C +/- 5° C at the center of the tow. Heating was accomplished using a precise temperature-controlled heat gun, as shown in figure 3.5. The temperature was measured with a thermocouple at various points along the tow gauge length.

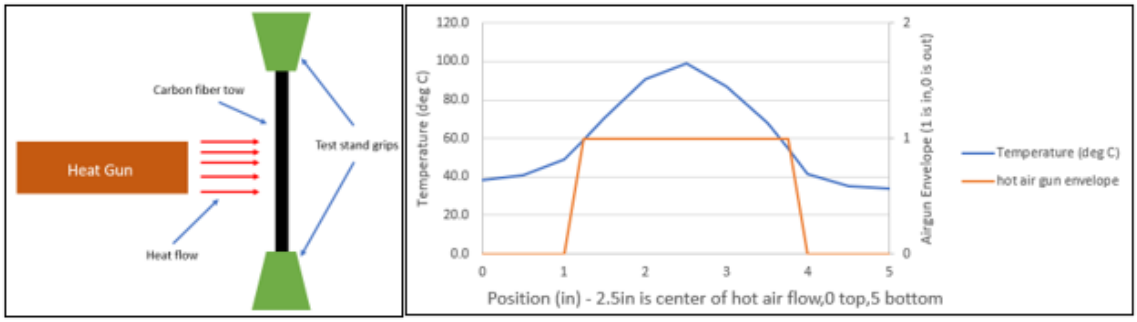


Figure 3.5: Elevated temperature carbon fiber tow test set-up

The heat gun method was selected to direct the heat on the center of the gauge sections of the tow. Concerns about heating the tabs of the tow and reducing the grip strength of the adhesive made using an environmental chamber impractical. The elevated temperature of 100° C +/- 5° C was selected because the center of the tow would see the highest temperature whereas the upper and lower limits of the heat gun nozzles would show lower temperatures. To account for this reduction a higher temperature was needed at the center of the tow. Even though 100° C is

somewhat higher than what would be seen in industrial forming with carbon fiber pre-pregs, and since the fiber tows used in this study are not impregnated this was not determined to be an issue [31, 39]. A total of 140 samples were tested, 35 at room temperature and 35 at the elevated temperature of two fiber type. Load versus displacement curves were plotted using MatLab (MathWorks, Inc. Natick, MA, USA) analysis software.

Results and Discussion

When forming carbon fiber, the axial direction of the fiber can be a limiting factor because its high stiffness creates resistance to out of plane bending. In this paper, 'load' refers directly to feedback from the load cell on the test stand and stress refers to the calculated engineering stress values derived from the cross-sectional area results in Table 3.1. Thus, tensile load contributes directly to forming limit. In forming processes, tensile loads measure the ability of a material to withstand load without complete failure while complying to the desired shape. Hence, comparing the tensile properties of continuous and SBCF would contribute to better understanding of forming processes for the considered fibers. In this instance, higher tensile loads would correspond to lower formability and would be detrimental to forming processes.

Cross sectional area of carbon fiber tows

Carbon fiber tow properties and C.A. analysis results from two methods, areal weight and SEM are presented in table 3.1. The values for IM7-G were supplied by Hexcel's published data and for SBCF the values were calculated based on the physical measurements.

Table 3.1: C.A. Measurements of carbon fiber tows using areal weight

Carbon fiber tow properties [39]		
	IM7-G	**SBCF**
Tow Weight [g/m]	0.446	0.389 (.004)[1]
Estimated Fiber Count	12000	10466
Weight Per Fiber [g/m]	3.71667E-05	3.71667E-05
Filament Diameter [mm]	0.0052	0.0052
Filament Area [mm^2]	2.12264E-05	2.12264E-05
Cross-sectional area		
	IM7-G	**SBCF**
Aerial Weight (Method 1)	0.250	0.222
SEM Images (Method 2)	0.282(0.02)[1]	0.215 (0.01)[1]

[1]Values in parenthesis denote the standard deviation

The figures 3.6 and 3.7 illustrate the SEM images of continuous and SBCF tows respectively. The C.A. was calculated using the scale bar and the threshold of higher magnification images to remove the void areas in the samples.

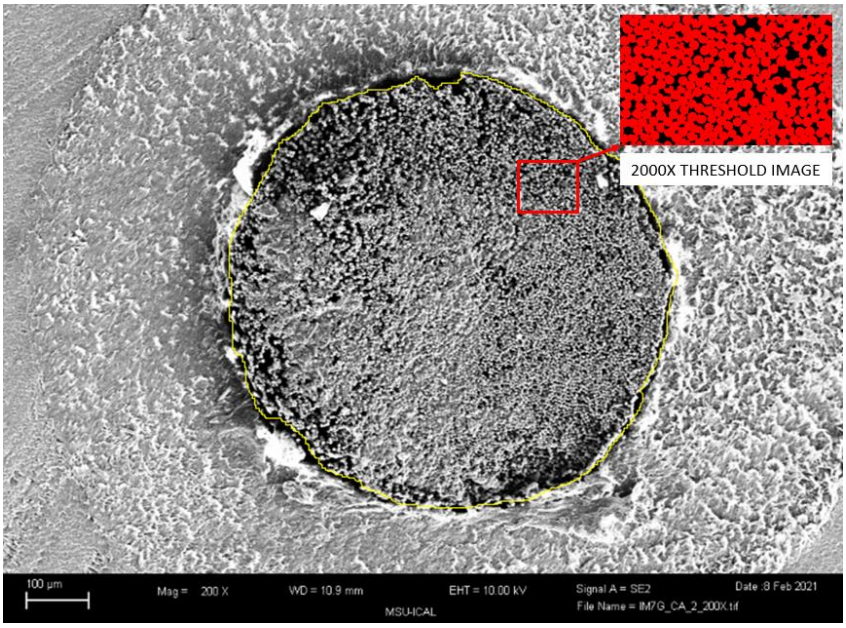


Figure 3.6: SEM image of continuous carbon fiber tow

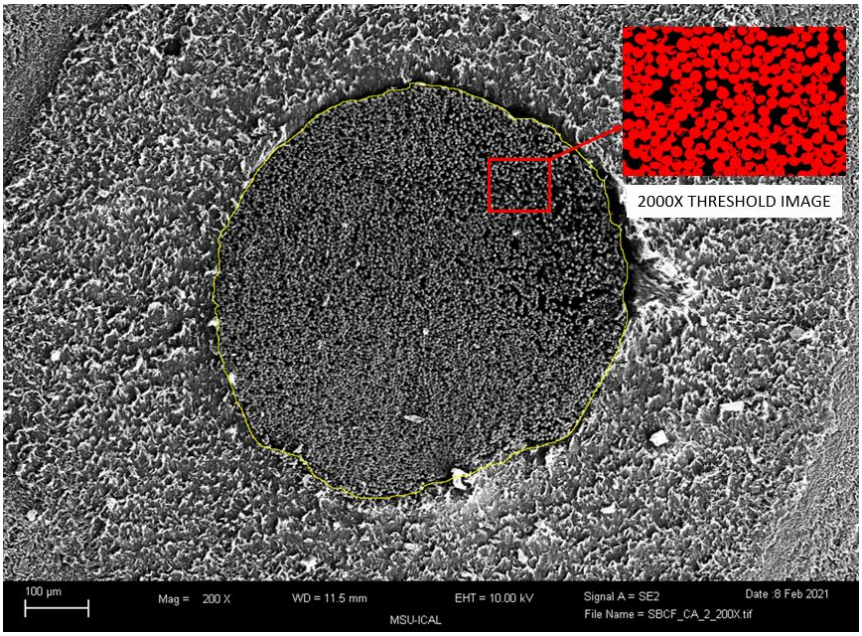


Figure 3.7: SEM image of SBCF tow

The data from areal weight and SEM image analysis methods showed that there was a 11% increase in C.A. of IM7-G and a 3% decrease in C.A. of SBCF based on Hexcel carbon fiber tow

properties described in Table 3.1. This comparison shows that in general the two methods produce similar trends in C.A., supporting the hypothesis that SBCF does have lower C.A. when compared to IM7-G tows. The remainder of this work will use Method 2 results to discuss and present various findings since Method 1 uses Hexcel published data while Method 2 used more accurate data from SEM images. The results also showed that there is a 24% difference between the C.A. of IM7-G and SBCF when analyzed through SEM image technique. Since, the C.A. of SBCF is smaller than that of IM7-G continuous fiber, it is expected to result in a lower load at failure.

Continuous carbon fiber tows

Figure 3.8 shows the peak load values of the continuous fiber for seven-gauge lengths (127, 101.6, 76.2, 50.8, 25.4, 12.7 and 6.35 mm) at room and elevated temperatures. As observed from the maximum load distribution, the overall tensile load of the tow decreases as the gauge length increases. This decrease can be shown to be rather linear for the increase in gauge length. Based on theory for the material characterization of carbon fiber that fibers contain inherent flaws throughout the continuity of the filament, it can be surmised that longer tows will statistically contain more flaws than shorter tows, resulting in lower tensile load [40, 21]. From the limited data acquired, there appears to be no difference in maximum load when tested at room temperature and at elevated temperature, which suggests that sizing does not have a noticeable effect on the tensile load of continuous fiber tows.

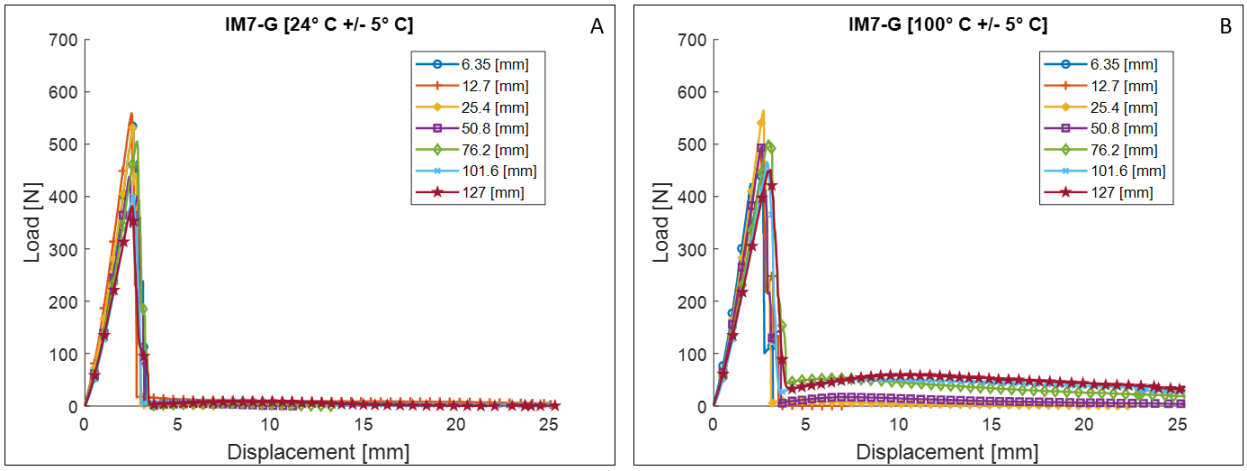


Figure 3.8: Load and displacement values of IM7-G continuous fiber at A) Room temperature and B) Elevated temperature

At room temperature, the fibers fail catastrophically resulting in no post-peak behavior. At elevated temperature, post-peak forces are observed that can be possibly attributed to sized fiber to fiber interactions. This post peak behavior is more pronounced for longer gauge lengths. When the fiber is put in tension, it breaks at flaws randomly along the length of the tow. This allows the fibers to interlock due to frictional forces when individual fiber slide past each other when in tension much like SBCF would in a similar condition at elevated temperature. The absence of this interaction at room temperature could be attributed to the sizing on the tow. At room temperature the sizing is vitrified thus preventing low shear forces between the fibers and thereby resulting in catastrophic failure.

Stretch broken carbon fibers

The test results of SBCF at gauge lengths (127.0, 101.6, 76.2, 50.8, 25.4, 12.7 and 6.4 mm), are shown in Figure 3.9. It was observed that the gauge lengths at room temperature follow the same decreasing maximum load trend observed for continuous fibers.

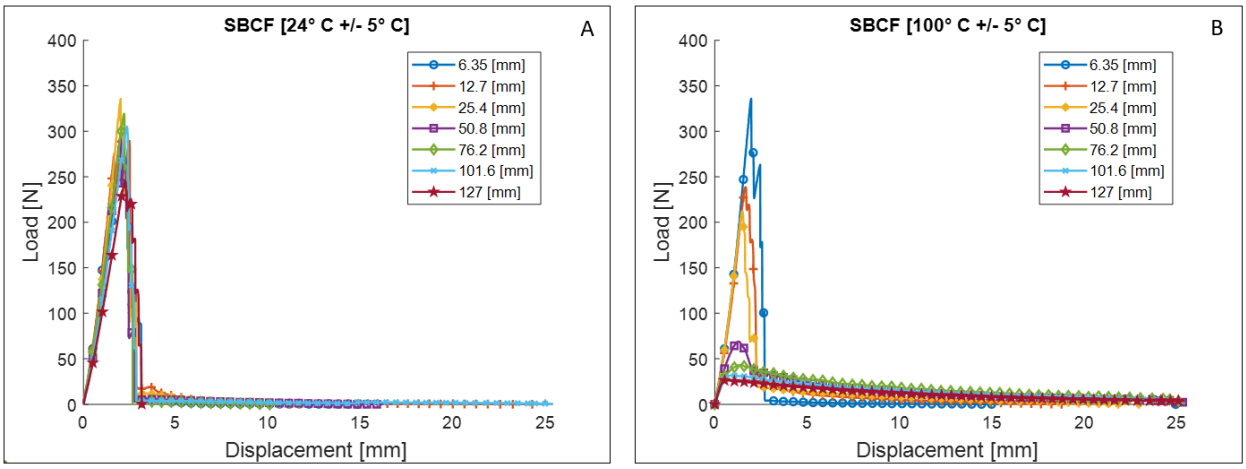


Figure 3.9: Maximum load and displacement values of SBCF A) Room temperature B) Elevated temperature

The lower maximum load at failure or tensile load of SBCF as compared to the continuous fiber can be attributed to several factors including possible lower fiber volume in the tows and the specified fiber breaks. Overall, there is a consistent 30% decrease in maximum load between IM7-G fibers and SBCF at room temperature over all gauge lengths. It is proposed that the cross-sectional area (table 3.1) may contribute to this decrease. Determining the peak load and calculating the peak stress using the cross-section, it can be found that there is an average 8% decrease over all gauge lengths for SBCF at room temperature. As shown in table 3.2, the 8% difference in peak stress when using equation 3.1 and normalized for the decrease in C.A. indicates that a SBCF tow is slightly weaker in tension than IM7-G continuous fiber.

Table 3.2: Yield stress comparison of IM7-G and SBCF tows at room temperature

Carbon fiber tow maximum yield stress	
	IM7-G vs. SBCF
% Decrease in maximum load	30%
% Decrease in cross-sectional area	24%
% Decrease in yield stress	8%

Stretch broken carbon fibers peak stress vs. continuous carbon fiber tows

In general, the data show minimal change in the peak load values for samples tested at room-temperature, but a significant reduction in the peak load from 50.8 (mm) to 76.2 (mm) gauge length in the heated samples (with little change observed between 101.6 (mm) and 127 (mm) gauge lengths) is observed. These results have two implications: (1) at room temperature, the bonding effect of sizing (which provides a binding action between fibers at room temperature) continues to dominate the tensile behavior (i.e., the SBCF tows behave similarly to continuous material), and (2) at elevated temperature, a change in the tensile behavior is observed somewhere between 76.2 (mm) and 101.6 (mm) [41]. The latter result presents an interesting corollary to the fiber length/distribution study performed earlier, which indicated that the long-fiber “tail” of the distribution for Hexcel SBCF extends to approximately 90 (mm). Such length is roughly the same fiber length at which high-temperature tensile behavior begins to change (figure 3.9).

The maximum stress distribution for each gauge length calculated using the cross-sectional area calculated in table 3.2, and the maximum stress distribution for each gauge length is displayed for each fiber type in figure 3.10. Plots A and B illustrate the overall decrease in strength at room temperature for continuous fiber and SBCF. Plots C and D show the effect of temperature on both the continuous fiber and SBCF at different gauge lengths.

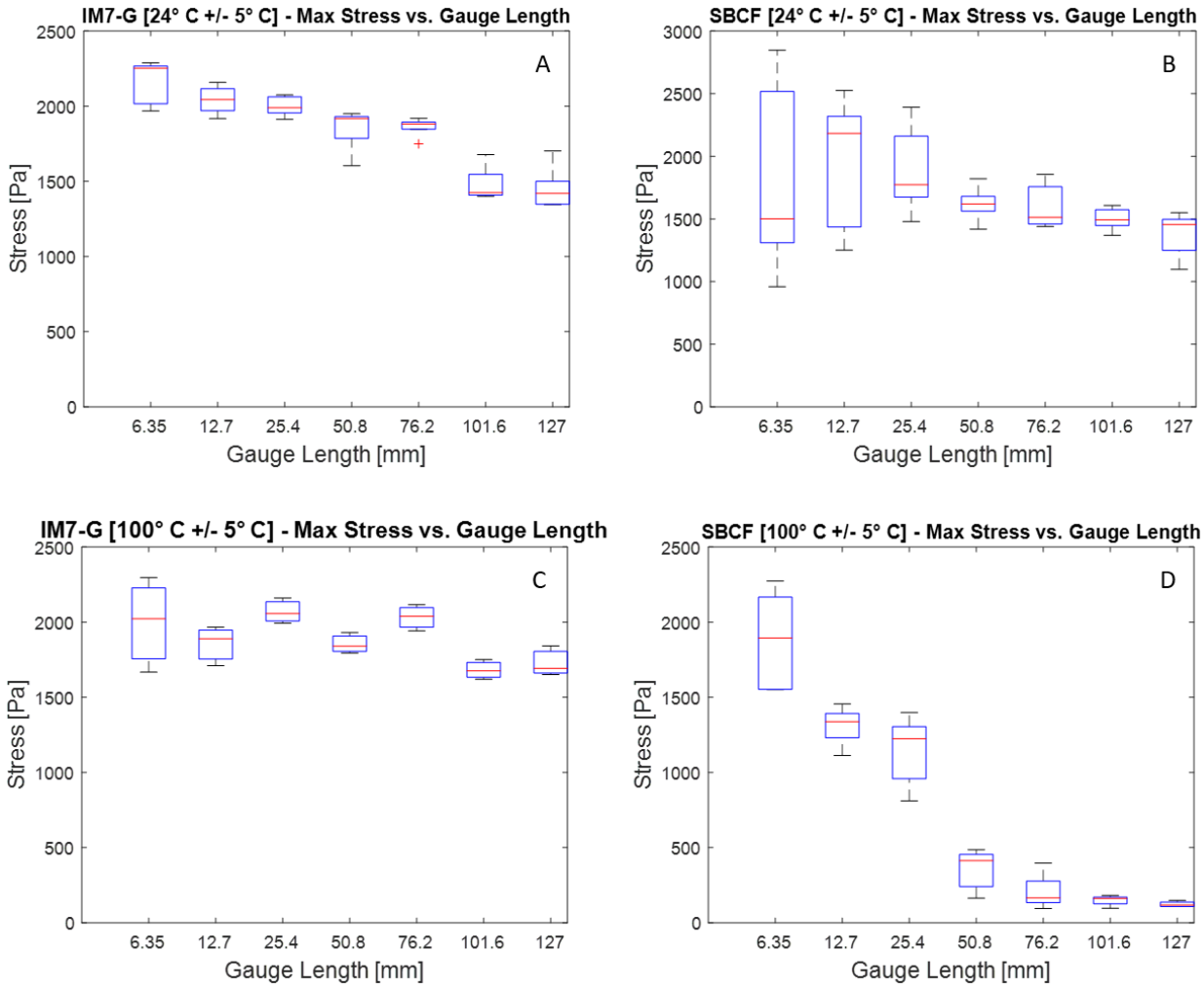


Figure 3.10: Maximum stress values and gauge length of carbon fiber tows at (A) Continuous IM7-G fibers at room temperature (B) SBCF at room temperature (C) Continuous IM7-G fibers at elevated temperature (D) SBCF at elevated temperature

In figure 3.11, is a fit curve used to show the comparison between each fiber at room and elevated temperature. The deviation in maximum load and related tensile strength between room temperature and elevated temperature of continuous fiber is nearly identical. SBCF tensile load at room temperature is consistently around 150 (N) lower than continuous fiber. When heated, the SBCF shows similar tensile behavior to both continuous fiber and room temperature SBCF at smaller gauge lengths with an exponential drop in tensile strength and load when the gauge length increases. From the material characteristics of SBCF, the fiber essentially becomes discontinuous at 50.8 (mm). In figure 3.11 this change is apparent from the plateauing of the maximum load required in tension.

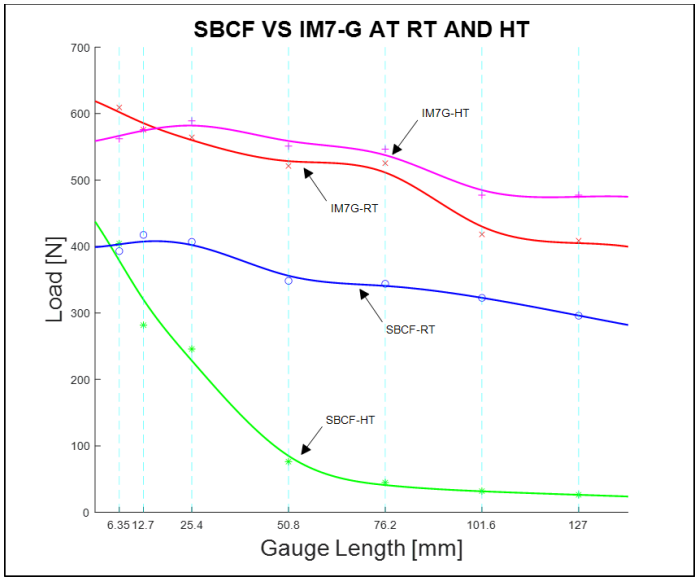


Figure 3.11: Maximum load comparison of IM7-G and SBCF at room (RT) and elevated temperatures (HT)

Figure 3.12 illustrates the relationship between SBCF tow strength, and the fiber continuity based on gauge length. The continuity study mentioned earlier was conducted on the same Hexcel SBCF tows that were tested in tension. A 100% fiber continuity means that throughout

the length of the tow each individual carbon filament is continuous from end to end. The heated SBCF tests show that the frequency of continuity, as a percentage, contributes to the strength of the tow in tension. Once the gauge length of the tow reaches the break zone of approximately 50.8 (mm), the frequency of continuity is < 10%. With nearly no continuous filaments when the frequency of continuity is < 10% it would follow that tensile loads should be relatively low when tested in tension. The plot of SBCF at elevated temperature in figure 3.10 supports this hypothesis by showing that for break lengths over 50.8 (mm) and a frequency of continuity of < 10%, the peak load is under 100 (N) and decreases as the gauge lengths increase.

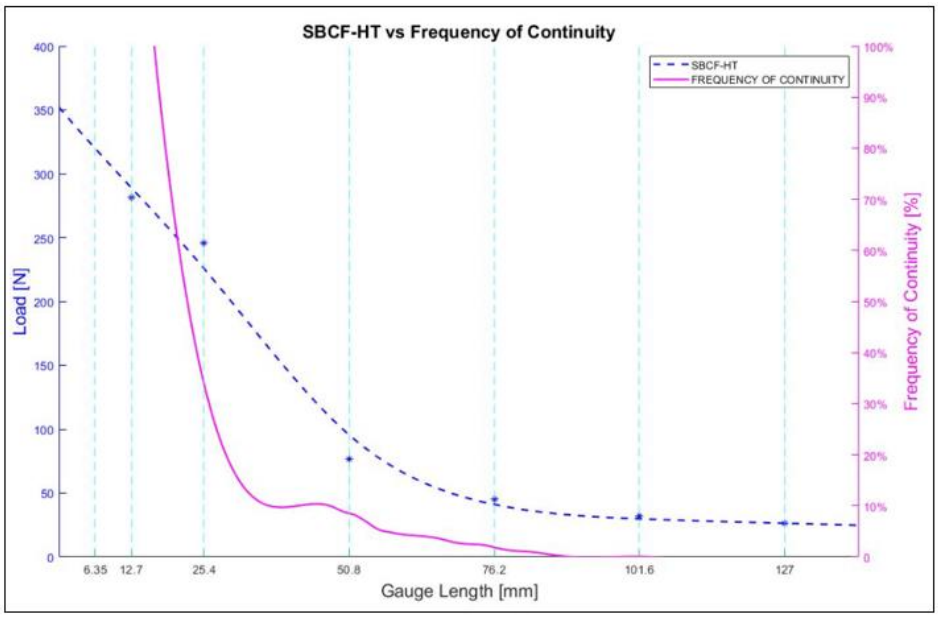


Figure 3.12: Comparison of SBCF-HT and SBCF frequency of continuity based on gauge length

Conclusion

This study compares the tensile properties of stretch broken versus continuous carbon fiber tows at different gauge lengths and temperatures. From the experimental data analysis, it can be shown that gauge length has a discrete effect on the tensile strengths on all types of fiber tows. Temperature particularly affects tensile strength of SBCF because of the loss of the sizing functionality. The nearly linear decrease in tensile strength based on gauge length of SBCF at room temperature supports this observation. The exponential decrease of tensile strength for heated SBCF samples supported the published literature stating that the break length of the SBCF is approximately 50.8 (mm). For shorter gauge lengths below 50.8 (mm) at elevated temperature the tensile strength of SBCF tows increases because the sample contains more continuous fibers. The tensile behavior of stretch broken IM7-GP is differentiated from continuous IM7-G fiber in that there is no discernable difference in tensile behavior between heated and room temperature samples for continuous fibers. The findings of this study provide insight on the ability of SBCF to be used in forming carbon composites. The results show that at high temperatures and longer gauge lengths, SBCF exhibits behavior that allows the fibers to slide past each other with minimal forces (< 100 N when longer than 50.8 mm). This potentially corresponds to increased formability into target shapes than its continuous counterpart. These findings also support the conclusion that SBCF maintains its strength in tension when compared to IM7-G continuous fibers at room temperature when normalized for cross-sectional area of the tow. Additional research on formability and strength properties will further help to corroborate these conclusions. This would include forming pre-impregnated composite plies into a variety of shapes and sizes to measure stresses and strains in multiple directions.

CHAPTER FOUR

FORMABILITY CHARACTERIZATION OF FIBER REINFORCED POLYMER COMPOSITES USING A NOVEL TEST METHOD

Contribution of Authors and Co-Authors

Manuscript in Chapter 4: Formability Characterization of Fiber Reinforced Polymer Composites Using a Novel Test Method

Co-Author: Joseph Janicki

Contributions: Methodology, Data curation, Formal analysis.

Co-author: Matthew Egloff

Contributions: Conceptualization, Supervision, Visualization.

Author: Roberta Amendola

Contributions: Conceptualization, Methodology

Co-author: Cecily Ryan

Contributions: Conceptualization.

Co-author: Dilpreet Bajwa

Contributions: Conceptualization.

Co-author: Alexey Dynkin

Contributions: Methodology, Resources, Validation.

Co-author: Douglas Cairns

Contributions: Project administration, Conceptualization, Funding acquisition.

Manuscript Information

Joseph Janicki, Matthew Egloff, Roberta Amendola, Cecily Ryan, Dilpreet S. Bajwa, Alexey Dynkin, Douglas Cairns

Journal of Testing and Evaluation

Status of Manuscript:

- ☐ Prepared for submission to a peer-reviewed journal
- ☐ Officially submitted to a peer-reviewed journal
- ☒ Accepted by a peer-reviewed journal
- ☐ Published in a peer-reviewed journal

Publisher: ASTM Journal of Testing and Evaluation

Accepted: August 2021

Introduction

Formability is defined as a material's capacity to undergo deformation without being damaged and without compromising the mechanical properties. It is a key factor in composite parts design because it defines the ability to create complex shapes [42]. Continuous fiber reinforced polymer composites are often used as a replacement for metal alloys because of the high strength to weight ratio. However, the major drawback of these composites is the lack of formability due to the low strain to failure ratio of the fibers, which, does not allow the material to follow the contours of the tooling into deep drawn shapes or tight radii [32]. Instead, fibers tend to either bridge, misalign, or fail under forming loads, negatively affecting the behavior and durability of the final products.

Recently, composite technology research and development efforts have focused on discontinuous fiber composites, such as aligned chopped fibers and stretch broken carbon fiber (SBCF) [37, 25, 43]. The main advantages of this material are in the ability of the fibers to move independently in the uncured resin matrix. This mobility enables a pseudo-ductile deformation response, which allows the material to be molded in complex geometries, reducing manufacturing costs, as compared to continuous fiber composites.

Regardless of the selected fiber reinforcement, many composite structures are made of laminates obtained by stacking individual plies with different fiber orientations. This process creates a multiscale hierarchical structure where micro and meso effects (fiber and tow scales) contribute to the macro structural response (laminate scale). The final component characteristics are generally complex because of the intrinsic orthotropic or anisotropic nature of the material. When discontinuous reinforcement is used, this complexity is more pronounced as the material

does not behave like either a conventional composite or an isotropic material [44]. During a forming process, the hierarchical structure becomes relevant as different deformations occur simultaneously at the micro, meso, and macro scales.

Traditional metal formability tests can be divided into three main categories, namely intrinsic tests, simulative tests, and tests to determine Forming Limit Diagrams (FLD) [45]. Intrinsic tests provide information about the basic mechanical properties of the material, which can be related to formability independent of other characteristics like thickness and surface conditions. However, the strain state is simplified and not representative of industrial processes. In addition, intrinsic tests do not account for the effect of the processing variables. The most common example of an intrinsic test is the uniaxial tensile test which is widely used to determine tensile strength and strain at failure. The simulative tests aim to reproduce the stress and strain conditions experienced during specific forming operations, and include the effects of variables, such as friction with the forming tool, that are not taken into account in the intrinsic tests. Simulative tests are identified according to the forming process they aim to replicate, specifically bending, stretching, drawing, and stretch-drawing [45]. Examples of simulative tests are the cupping tests (e.g. Erichsen and Olsen) used to evaluate material stretchability [46]. The major drawback of simulative tests is that they tend to be less reproducible when compared to intrinsic tests and must be performed under carefully controlled testing conditions to minimize variability in the results. Tests to determine FLD are stretch tests producing out-of-plane or in-plane deformation. Sheets of materials are clamped between a die and a sheet holder and stretched by the action of a punch. Examples of FLD tests include the Nakajima test, which uses a hemispherical punch, a circular die, and rectangular sheets, and the Marciniak test that uses punches of different shapes (circular, elliptical, rectangular)

with a central hole and sheets of different widths [47, 48]. Despite being widely employed, the reliability of tests results is affected by the bending effect due to the punch curvature, limitations in sample thickness, and the need for elevated and reproducible clamping force.

In the fiber composites industry, most formability characteristics are determined by a “trial error approach”, along with empirical evaluations of the target shape. In most cases, the tooling and the forming process for the final product are limited by the geometric profile of the part being produced. For example, if continuous fibers are considered and the geometry has deep cavities or tight radii, the ability to use either vacuum forming, or compression molding is very limited [49]. Hand lay-ups are a suitable alternative, but the process is expensive, labor-intensive, less consistent and time-consuming.

During the last decade, the demand for stamp and press forming of composite materials has increased because of its suitability for mass production [50, 51]. Such processes, while being established for thermoplastic composites, are not well suited for thermosetting composites as the material flow is hindered by the chemistry of the resin. Recent studies were conducted on the formability of thermoplastic composites using cupping tests [52, 53, 54, 55]. It was found that forming rate, tool temperature and sample holding force have the strongest effect on the structural behavior and the service life of products. Recently, studies conducted on the formability of thermosetting composites using cupping and stretch bending tests revealed that the composite shows sufficient ductility for press forming at elevated temperature (100°C) [56, 57, 58, 59]. Analytical modeling aided in relating the phenomenon to the resin crosslinking density and the consequent variation of its mechanical properties [57, 58].

Currently, the amount of quantifiable and comparable forming data for both continuous and discontinuous fiber reinforced polymer composites, including a multi-scale understanding of the deformation response, is still limited. The availability of a quantitative, repeatable, and predictive experimental tool is highly desirable to reduce the reliance on "trial and error approach" and highly tooling-specific empirical responses during the forming process.

Research Significance

During the last decade, the application of multi-scale modelling, to investigate the complex mechanical response of heterogeneous materials like composites has increased [60, 61, 62, 63]. The underlying assumption behind multiscale modelling is that, at the structural scale, the material appears to be homogeneous. With this assumption, the properties for the macro scale can be formulated by investigating the behavior of a suitably "small", heterogeneous statistically representative volumes of material at the micro scale. It has been shown that, the representative volume needs to be at least one order of magnitude smaller than the size of the macro domain [64].

Based on the hierarchical multi scale composite structure and the modeling approach, this work presents a novel experimental method to characterize the mesoscale formability of fiber reinforced polymer composites. In the uncured state, the composite exhibits viscoelastic properties which determine the pseudo-ductile deformation response of the material. When a load is applied during forming operations, the fibers move independently in the resin matrix and may bridge, misalign or fail, compromising the quality of the final cured products. The investigation of the forming behavior of the uncured composite therefore becomes important to characterizing the deformation response while optimizing the forming process variables that generated it, thereby preventing the development of defects.

The experimental apparatus was designed to evaluate the composite behavior by measuring forming load versus displacement in a stretch drawing process. Several variables relevant to the forming process (e.g. temperature and load) can be controlled during testing [see "Proposed Test Method", below]. With a sequential approach, the material is first tested at the tow scale and then the results can be used to improve understanding of larger scale problems such as laminate deformation phenomena during dome (hemispherical) forming tests or for validating multiscale modelling results [65, 54, 51]. Better knowledge of composite formability can potentially allow for reduced material waste, cost-effective processing techniques and more complex and advanced structures.

Test results from the forming of Hexcel (Stamford, CT) IM7-G 12K continuous carbon fiber impregnated with Huntsman (The Woodlands, TX) RDM 2019-053 proprietary epoxy based thermosetting resin system are presented in this study to demonstrate the use of the proposed testing apparatus and data collection.

Proposed test method

In this section, a novel method is proposed for testing the formability of fiber reinforced polymer composites at the mesoscale (tow). The simulative testing apparatus detailed in this paper is called the "forming fixture". The test method determines the required load to form a dry or uncured resin impregnated fiber tow (here generally defined as tow sample) into a stretch drawn profile. Limitations of cupping and stretch bending forming tests are related to the sample holding mechanism and to the imposed test geometry [52, 65, 54, 55, 56, 57, 58]. When mechanical clamping is used, insufficient and inconsistent clamping force, during and between experiments, may lead to sample slippage, compromising test repeatability and the reliability of results,

especially when tests are conducted at elevated temperature [56]. Because these tests' geometries do not offer flexibility, if the need to perform experiments using different sizes or shapes of the forming tool arises, a whole new unit must be machined in most cases. The "forming fixture" is equipped with a sample holding assembly that offers high reliability by completely avoiding sample slippage. The clamping force is controlled and a self-leveling system accounts for variation in the sample thickness. In addition, the forming parts (blocks and tool) can be quickly and easily replaced to accommodate the desired testing geometry.

During industrial forming operations, especially when complex shapes are formed, the material must properly follow the contours of the tooling. The amount of material involved in this process is usually much larger than the size of a complex feature (e.g. drawn profile or a tight radius); therefore, the strain response of the material located in its surrounding region becomes relevant to the quality of the final product. A common trait of the previously established forming tests is the sample being clamped at the edges of the die [52, 65, 54, 55, 56, 58, 59]. Excess material is only used for securing the sample in position. This condition is only partially simulative since it does not account for the strain response of the material in the region surrounding the die. In the proposed "forming fixture", the clamping system is placed away from the forming tool. Once the sample is secured in place, part of it lays on the blocks next to the forming region during testing and will generate a strain response related to the selected geometric configuration. This test set-up is novel as it better simulates the complexity of the industrial forming processes and most importantly, allows for the investigation of the synergistic effects of multiple forming variables. Figure 1 shows a schematic of the test set-up.

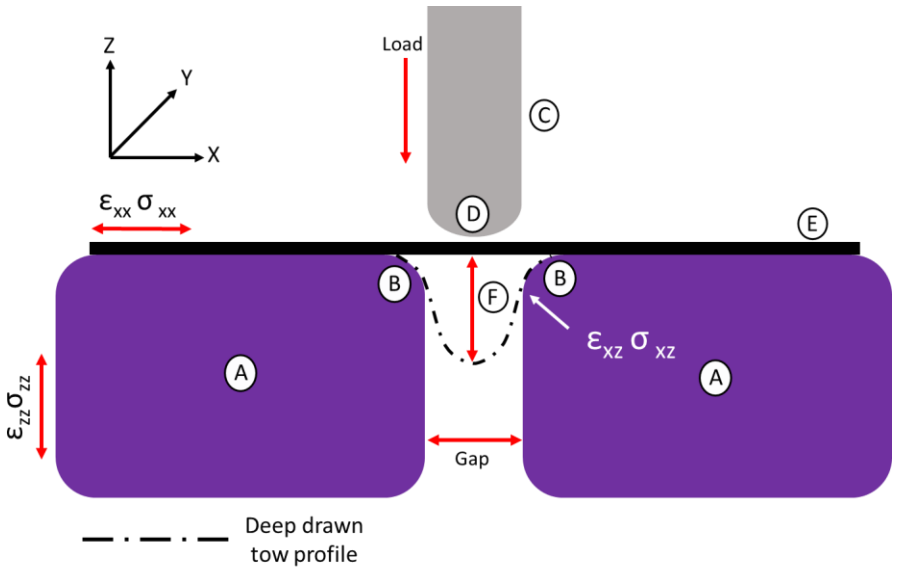


Figure 4.1: Forming fixture test design concept (A) forming blocks, (B) forming blocks radius of curvature, (C) forming tool, (D) forming tool radius of curvature, (E) tow sample and (F) deep drawing depth

During testing, different stress conditions result in the tow sample. The part of the tow sample laying on the top of the forming blocks experiences shear stress. Bending stress (as uniaxial tension/compression) is created around the forming blocks radius of curvature (fig. 1B) and plain strain tension exists on the walls of the stretch drawn tow sample. The stress condition experienced at the bottom of the stretch drawn profile and in contact with the forming tool depends on the nature of the tested sample and on the geometry of the tool. For example, uniaxial stretch is created when a single tow is tested using a semi-cylindrical profile tool, while biaxial stretch (deep drawing) can be achieved when a hemispherical forming tool is used to test laminate tape samples manufactured with different fiber orientations [see “Design Recommendation” section]

The general set up of the forming fixture when mounted on a Mark-10 ESM303 (Mark-10 Corp. Copiague, NY) universal testing stand is shown in figure 4.2.

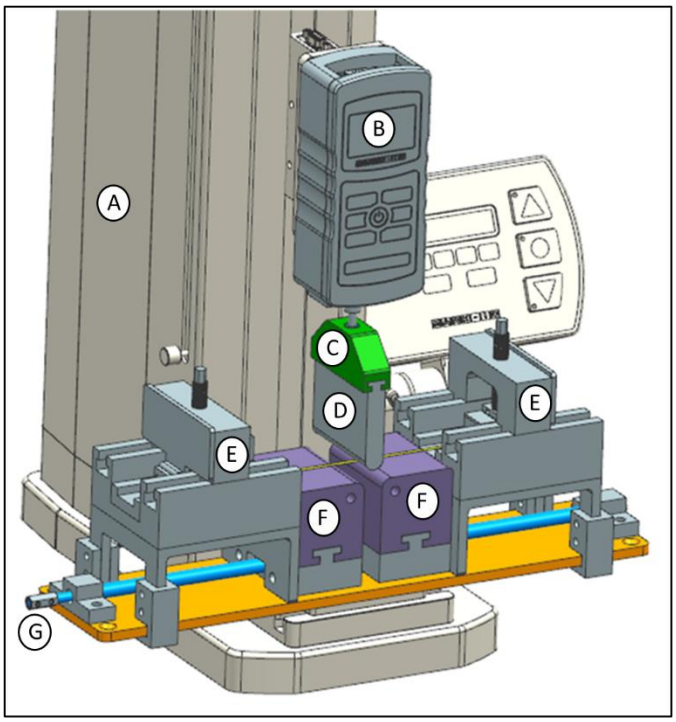


Figure 4.2: Overview of the forming fixture assembly when mounted on a Mark-10 ESM303 (Mark-10 Corp. Copiague, NY) universal testing stand. (A) Universal testing stand, (B) force gauge, (C) forming tool adapter, (D) removable forming tool, (E) sample holding assemb

The tow can be tested dry or resin infused. Any material combination of interest for fiber and resin can be used. The following parameters can be adjusted to accommodate a variety of forming processes:

- Forming blocks and forming tool radius of curvature
- Forming blocks and forming tool profile geometry
- Forming blocks and forming tool temperature
- Forming blocks span distance

- Tow sample gauge length
- Loading rate
- Temperature

The forming blocks and tool are removable and are held in place by T-slots. This design allows for fast forming part replacement to accommodate the desired profile geometry during testing. Figure 2 shows the forming fixture equipped with the forming blocks and the tool having a semi-cylindrical profile (figs. 2D and *2*F). Figure 4.3 shows a set of forming tools with semi-cylindrical profile of different sizes and the tool adapters (fig. 2C).

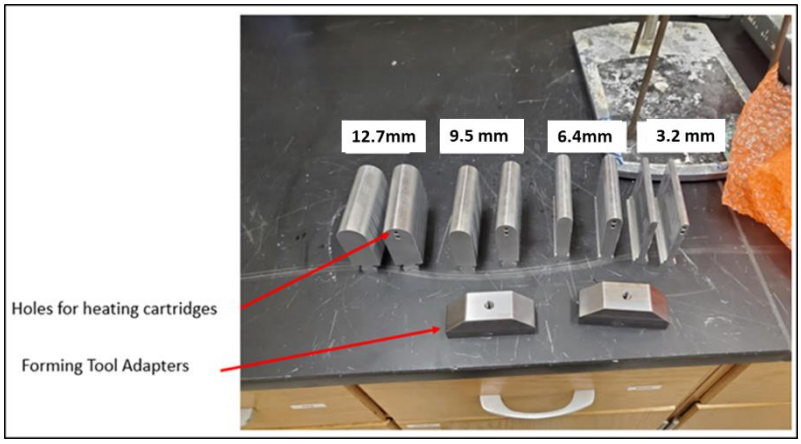


Figure 4.3: Forming tools with different curvature radii and adapters for Mark-10 ESM303 (Mark-10 Corp. Copiague, NY) universal testing stand

The ability to securely hold the tow sample is a major requirement during testing. Slippage of any kind must be avoided to assure test repeatability and data reliability. For this reason, a sample holding assembly has been specifically designed (fig. 2E) to securely hold the tow ends as follows. When prepared for testing, the ends of the tow sample are secured between two cardstock tabs, using a fast curing ethyl cyanoacrylate adhesive [see “Specimen Fabrication” section]. Figure 4.4

shows the sample holding assembly with one of the tabbed ends of the tow sample held in place by a self-leveling clamp mechanism.

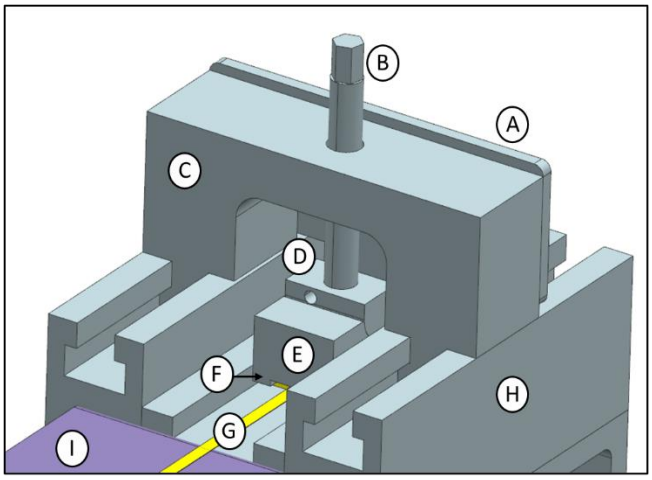


Figure 4.4: Forming fixture sample holding assembly (A) alignment plate, (B) tightening screw, (C) translation bridge, (D) self-leveling clamp, (E) tab holding block, (F) tab holding block front stop, (G) tow sample, (H) sample holding assembly base and (I) forming

The plate (fig. 4A) aligns the parts of the clamping mechanism. The tightening screw (fig. 4B) on the translating bridge (fig. 4C) forces the self-leveling clamp (fig. 4D) into the tab holding block (fig. 4E). The self-leveling clamp accounts for variation in the tab geometry and tow sample thickness. A 20 N·m torque is applied with a wrench to ensure a consistent clamping force of ~ 14,000 N. The tabbed ends of the tow sample are constrained in the horizontal direction by a combination of friction and stop features on the front of the tab holding block (fig. 4F).

At elevated temperatures, the cyanoacrylate bond between the cardstock tab and the tow sample degrades causing slippage and inconsistent test results [66]. To address this issue, the tow sample material protruding from the back side of the cardstock tab is secured over a capstan and

clamped on the back surface of the tab holding block. Testing efficiency and repeatability is further enhanced by the translation bridge which can be quickly adjusted in the horizontal x-direction depending on the sample's gauge lengths. The central channel machined in the sample holding assembly base (fig. 4H) constrains the tab holding block in the horizontal direction. The entire sample holding assembly exerts force only in the vertical direction, eliminating inconsistent and off axis loading of the sample tabs.

Accurate temperature control is another major requirement during testing because it directly relates to the viscosity and curing points of different resins and therefore, to the formability of different fiber and resin combinations. Each forming block and the forming tool are equipped with a 250 W and a 125 W electrically resistive cartridge heater, respectively. The temperature is controlled by a Watlow (St. Louis, MO) proportional-integral-derivative (PID, part number PM6C1CA-EAAAPWP) controller coupled to a solid-state relay (SSR, part number SSR-240-10A-DC1) that can switch the power to the 125 W (part number 2165-1904) and 250 W (part number E2A72-L12) cartridge heaters every three electrical cycles, or every 0.05 seconds. Each heated part is equipped with thermocouple probes (part numbers 20CJFGD036A and 40EJFGB036A) used for feedback and control of the PID system. This system allows for a temperature accuracy of ±1 ºC of the set value. The tow sample temperature is controlled through the contact with the heated top surface of the forming blocks and the heated forming tool (figure 4.1 and figure 4.2). Figure 4.5 shows the cartridge heaters and the thermocouple probes installed in the forming fixture.

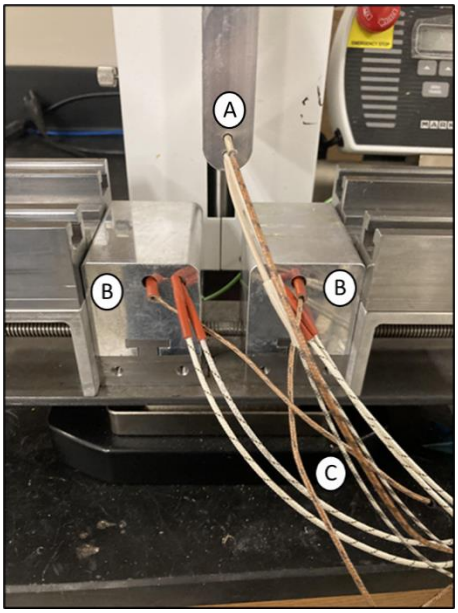


Figure 4.5: Heating system installed in the forming fixture (A) forming tool, (B) forming blocks and (C) electrically resistive cartridge heater and thermocouple probes

Figure 4.6 shows the complete assembly of the forming fixture equipped with the heating control unit.

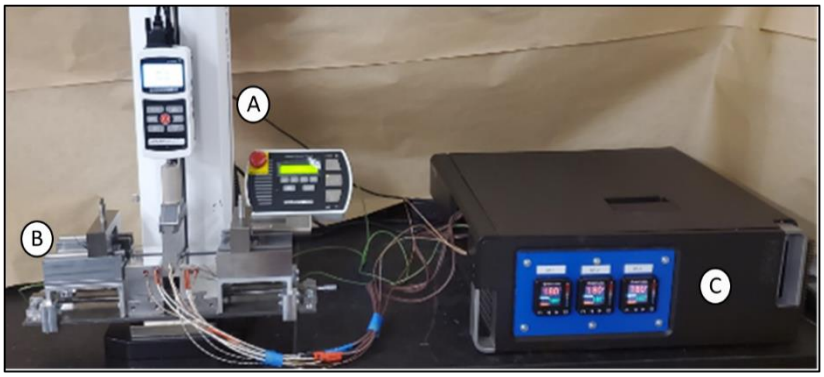


Figure 4.6: Complete assembly of the forming fixture equipped with temperature control (A) Mark-10 ESM303 (Mark-10 Corp. Copiague, NY) universal testing stand, (B) forming fixture and (C) temperature control unit

Uniformity of temperature within the volume of the forming blocks, forming tool and the tow sample are predicted by the Biot number (*Bi*) [67]. *Bi* is the ratio of heat flow resistance within a

body due to thermal conduction, to heat flow resistance at and above the surface of the body by thermal convection. The Biot number is given by:

$$Bi = \frac{\mathrm{h}L_c}{k} \qquad (4.1)$$

Where h is the convective heat transfer coefficient $\left(\frac{W}{m^2K}\right)$, L_c is the characteristic length (m) and *k* is the thermal conductivity of the material ($\frac{W}{mK}$).

In the natural convection condition of the forming fixture, as would be experienced in a laboratory environment, the convective heat transfer coefficient h is 5 W/(m^2·K). The forming blocks and the forming tool are made of 6061-T6 Aluminum alloy with a thermal conductivity *k* of 170 W/(m·K). Carbon fiber reinforced polymer [see "Test Method Implementation" section] was used as the tow sample. The thermal conductivity *k* of resin impregnated carbon fiber is typically 0.8 W/(m·K). Table 4.1 lists *Bi* calculated for the heated blocks, forming tool, and tow sample.

Table 4.1: Biot numbers of the heated components of the forming fixture and the specimen

Component	*Bi* (unitless)
Heated 6061-T6 alloy aluminum block	<0.0005
Heated 6061-T6 alloy aluminum tool	<0.0003
Resin impregnated carbon fiber tow	<0.01

The temperature within the volume of the body is uniform when *Bi* < 0.1. The highest number in Table 4.1 is one order of magnitude smaller than the boundary value (0.1). Therefore, it can be considered that the temperature within the volume of the forming blocks, forming tool and the tow sample is uniform [68]. The forming blocks and the forming tool can be considered as thermal reservoirs because of their thermal mass, (the product of the specific heat and the mass of the

considered component), which is much larger than that of the tow sample. In steady state, the temperature of the tow sample is the same as the contacting component (forming block/tool) temperature. Heat transfer calculations estimated that the tow sample reaches steady state within 60 seconds; this response was also confirmed by thermocouple measurements. The short length (< 50 mm) of the tow sample resting on the surface of the sample holder assembly, is in proximity but not in physical contact with either of the heated forming fixture parts and a very small gradient (< 2 °C) may be observed in these locations. This temperature difference has a nonexistent or negligible effect on the resin viscosity. Therefore, the measured thermal gradient is not deemed sufficient to compromise test results

The test starts with setting the desired span distance between the forming blocks by turning the ball screw. The span can be adjusted from 0 (blocks in contact) to 78 mm. The desired forming tool is then selected and attached to the load cell of the test stand equipped with the appropriate adaptor. To protect the load cell from overheating, a thermally insulative spacer made from polyether ether ketone (PEEK) polymer is used between the heated forming tool and the load cell. This insulation enables operation of the tool at a temperature up to 121^{o}C without damaging the load cell. The prepared tow sample is set evenly across the forming blocks on the forming fixture. The tightening screw is then used to clamp the sample tow tabs; the tow sample material protruding from the back side of each tab is secured on the capstan and clamped on the back surface of the tab holding block. Once the specimen is secured and all other components are ready for testing and the steady state forming temperature is reached, the forming tool can be lowered into the starting position and the forming test can commence. Forming load and displacement data are collected using the Mark-10 MESUR® Gauge Plus software.

Test Method Implementation

To validate the forming fixture set-up performance, an experimental matrix consisting of twenty-five continuous carbon fiber reinforced polymer tows was designed. This section includes the description of the matrix, the tow sample fabrication process, test results and discussion.

Test Matrix

Table 4.2 presents the test matrix for the forming fixture tow samples, categorized in five groups. Each group contains six replicates for a total of 25 samples identified by a code of "Cx-y". "C" stands for "continuous" and "x" identifies the group number while "y" identifies the sample number in each group.

Table 4.2: Experimental test matrix

No.	Group	Fiber Type	Temperature (°C)	Specimen IDs
1	C1	IM7-G	RT[a]	C1-1, C1-2, C1-3, C1-4, C1-5
2	C2	IM7-G	57	C2-1, C2-2, C2-3, C2-4, C2-5
3	C3	IM7-G	82	C3-1, C3-2, C3-3, C3-4, C3-5
4	C4	IM7-G	107	C4-1, C4-2, C4-3, C4-4, C4-5
5	C5	IM7-G	121	C5-1, C5-2, C5-3, C5-4, C5-5

Note: [a]Room temperature (21°C)

Tow samples were tested in the forming fixture under the following conditions:

- 22 mm span distance between forming blocks
- 6.4 mm forming blocks radius of curvature

- 9.5 mm forming tool radius of curvature
- 21-121 °C forming temperature range
- 6.4 mm/min loading rate
- Maximum drawing depth 51 mm

Specimen Fabrication

The fiber reinforced polymer composite tow samples were prepared using Hexcel continuous IM7-G carbon fiber impregnated with Huntsman RDM 2019-053 resin. Prior to resin impregnation, precautions were taken to ensure that all fibers were aligned correctly, and no twists were present. After impregnation, the average volume fraction of the carbon fiber for a tow sample was 50±2%. After the tow was impregnated with the resin, it was prepared for placement on CNC routed cardstock tabs (32 mm x 19 mm). The tabs were adhered to the tow sample ends using a cyanoacrylate adhesive. Samples were clamped and left at room temperature for a minimum of 30 minutes, to allow for complete curing of the adhesive. If the specimen was not tested immediately after preparation, it was stored in a freezer at -18 °C to prevent the resin from cross-linking [69]. Prepared samples measured 203 mm between the inside of the tabs, were 7.6 mm wide and 0.25 mm thick. Figure 4.7 is an illustration of tow sample fabrication.

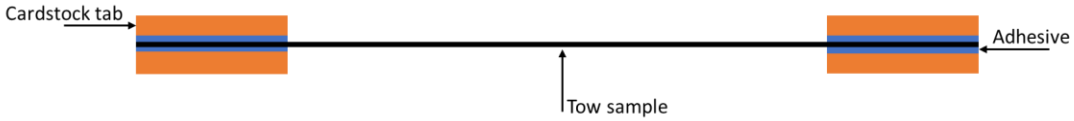


Figure 4.7: Schematic of the fiber reinforced polymer composite tow sample fabrication showing the cardstock tabs adhered to each end of the carbon fiber tows.

Results and Discussion

In this section, data from the test matrix were collected and analyzed to determine testing reliability, tow sample forming behavior and failure mode. All tow samples were prepared using the method proposed in this article and tested according to the conditions stated in the experimental matrix. Because experiments were conducted in the temperature range of 21-121 °C, it is expected that the change in the resin viscosity will relate to the tow sample formability process. Table 4.3 presents the Huntsman RDM 2019-053 resin viscosity values at the selected testing temperatures.

Table 4.3: Huntsman (The Woodlands, TX) RDM 2019-053 resin viscosity at selected temperatures

Temperature (°C)	Viscosity (Pa·s) [70]
21	> 3500
57	791
82	168
107	25
121	11

Figure 4.8 displays tow samples after forming test at each selected temperature.

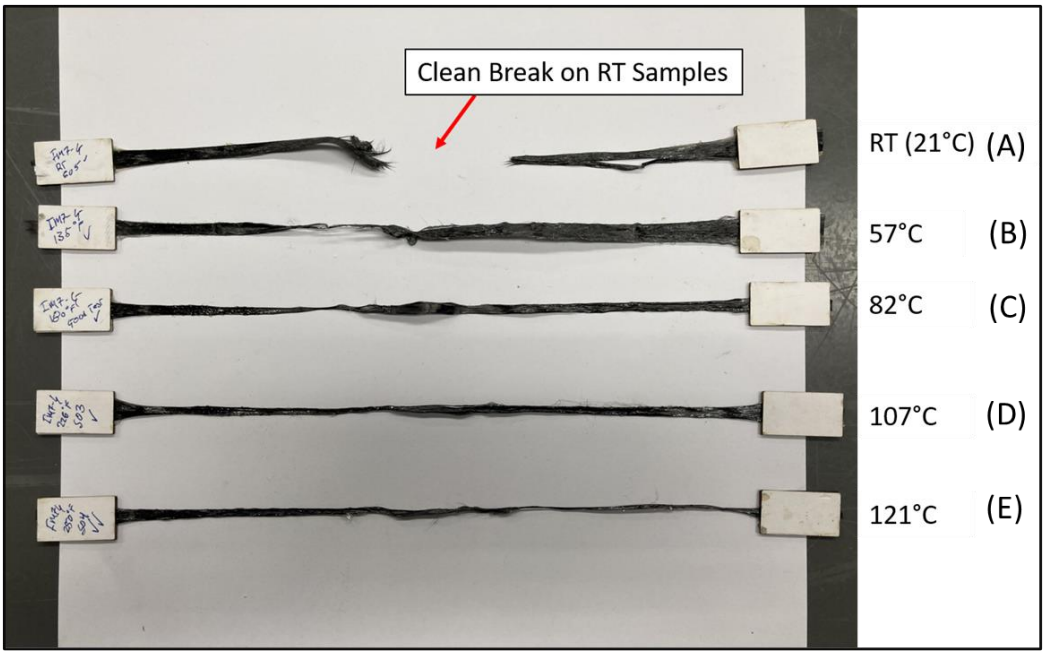


Figure 4.8: Hexcel (Stamford, CT) continuous IM7-G carbon fiber impregnated with Huntsman (The Woodlands, TX) RDM 2019-053 resin tow samples after the forming test at different temperatures, The lowest temperature, (A) RT, shows complete failure, while at elevated te

Complete failure (breakage) is observed only for the samples tested at room temperature (21°C, figure 4.8A). The resin viscosity at room temperature is very high (> 3500 Pa·s) and leads to a composite material with increased shear resistance which, greatly decreases the formability causing a clean break close to the middle region of the sample (figure 4.8A).

All samples tested at elevated temperature show partial failure visible as increased cross-sectional thinning from 57 to 121°C (figs. 8B-E). Because the viscosity decreases as the temperature increases (table 4.3), the fibers can intertwine after failure inside the resin matrix resulting in the observed thinning.

The forming behavior of the tow samples is expressed as load versus displacement curves during the deep drawing process (figures 4.9A and 4.10). For all experiments, no slippage of the samples in the sample holding assembly was observed during testing.

Figure 4.9 shows the forming behavior of the tow samples tested at room temperature. It was observed that the load drops to zero after an average maximum forming of load of 850±29 N (figure 4.9A) indicating rapid and complete failure of the tow.

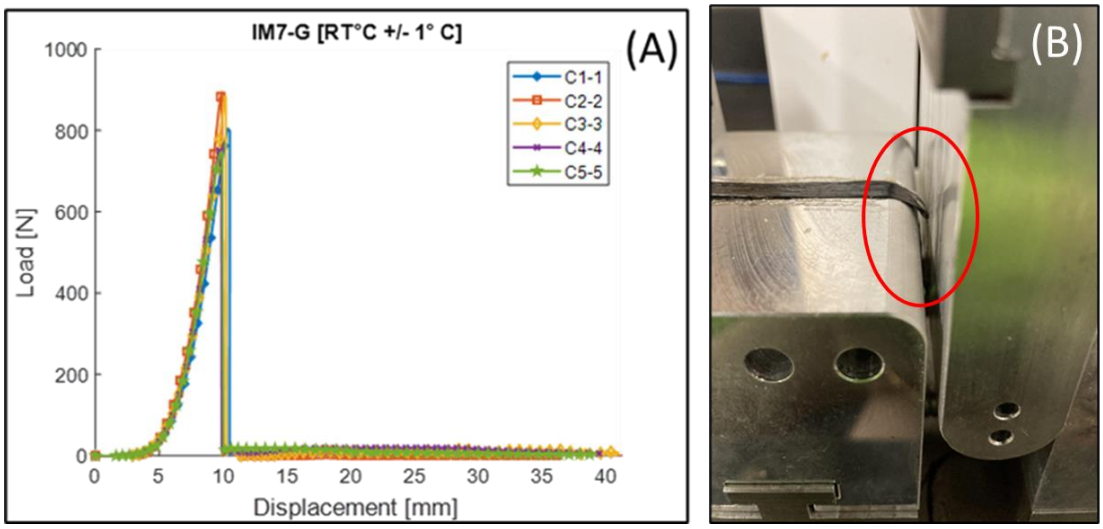


Figure 4.9: Load-displacement curves of Hexcel (Stamford, CT) continuous IM7-G carbon fiber impregnated with Huntsman (The Woodlands, TX) RDM 2019-053 resin. Tow samples during deep drawing at room temperature show failure as: (A) rapid drop in the post-peak force (B) catostrophic failure on curvature of tooling

Figure 4.9B shows how the designed forming fixture allowed for the observation of the sample failure in "real time" confirming the mechanism of failure and the inability of the continuous fiber material to follow the contours of the tooling into deep drawn shapes or tight radii.

Figure 10 shows the forming behavior of the tow samples tested at temperatures of 57 °C (figure 4.10A), 82 °C (figure 4.10B), 107 °C (figure 4.10C) and 121 °C (figure 4.10D). For all elevated temperatures a primary peak, corresponding to the maximum forming load, is observed. It is then followed by a secondary peak related to the partial failure process of the fibers within the

resin matrix. The secondary peak maximum load decreases from 57°C to 121°C proportionally to the resin viscosity (Table 4.3). The highest secondary peak values are observed for the tests conducted at 57°C (resin viscosity 791 Pa·s), while the lowest correspond to the tests conducted at 121°C (resin viscosity 11 Pa·s). The secondary peak load relates to the ability of the fibers to readjust or intertwine after failing, facilitated by lower resin viscosity.

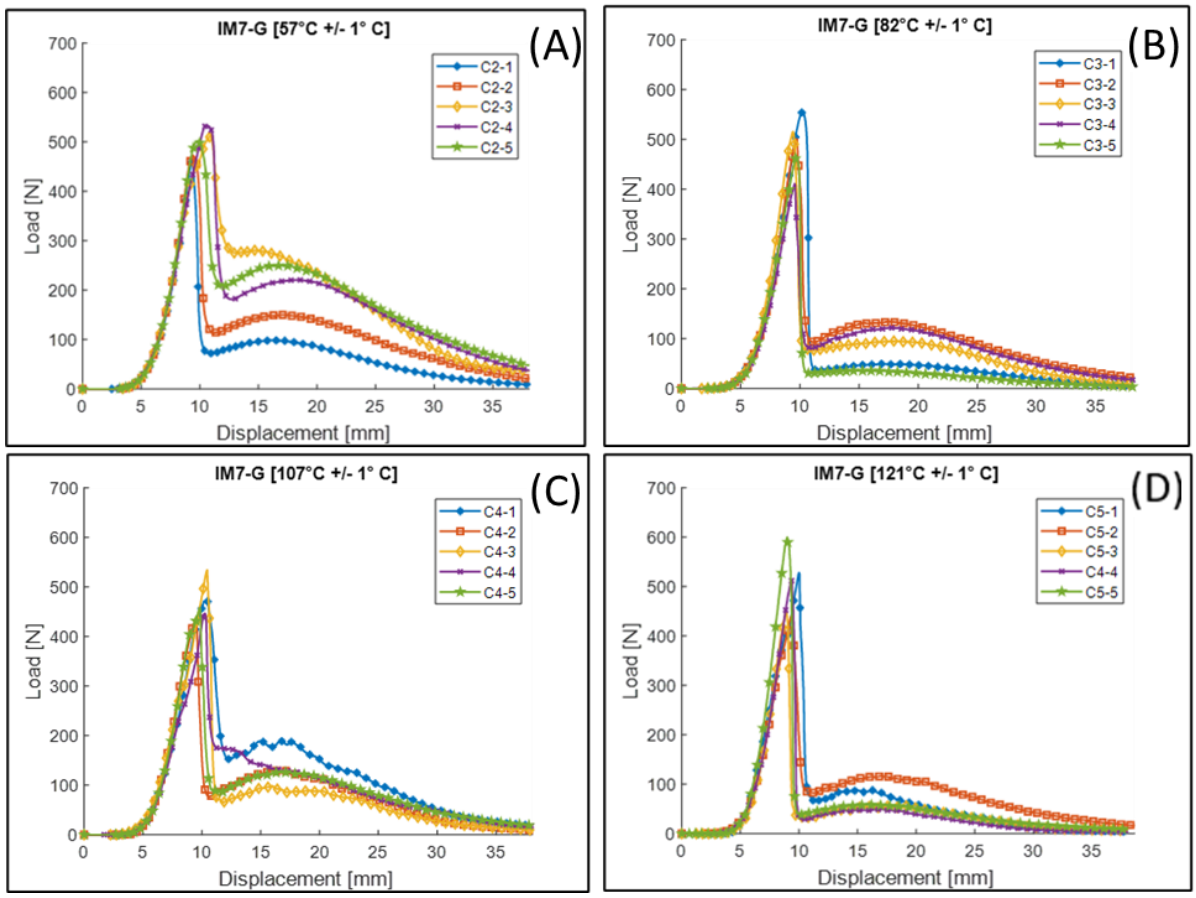


Figure 4.10: Load-displacement curves of Hexcel (Stamford, CT) continuous IM7-G carbon fiber impregnated with Huntsman (The Woodlands, TX) RDM 2019-053 resin tow samples during deep drawing at elevated temperature; (A) 57 °C, (B) 82 °C, (C) 107 °C and (D) 121 °C

Figure 4.11 shows the average maximum forming load for the forming of the tow samples in the 21-121°C temperature range. All tests conducted at elevated temperature resulted in a reduced average maximum forming load when compared to the room temperature tests.

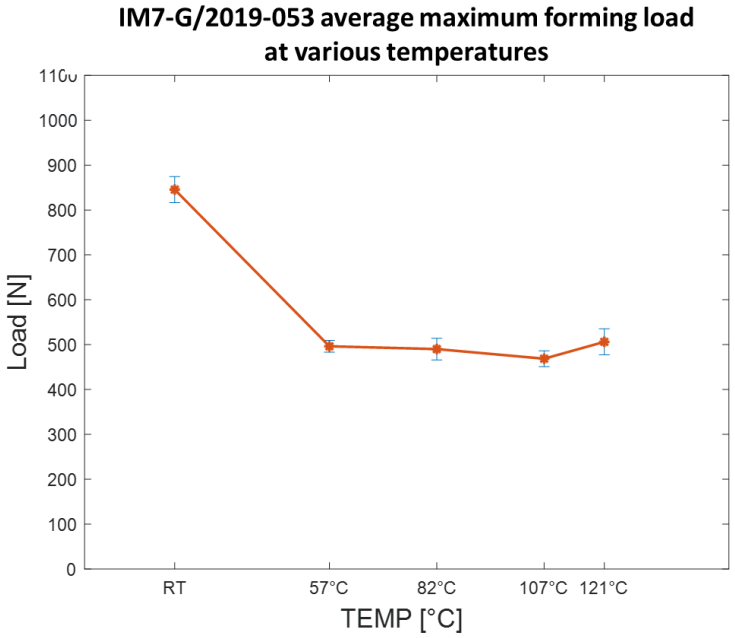


Figure 4.11: Average maximum forming load of Hexcel (Stamford, CT) continuous IM7-G carbon fiber impregnated with Huntsman (The Woodlands, TX) RDM 2019-053 resin tow samples during deep drawing with increasing forming temperatures.

From room temperature to 57°C the forming load decreases of 42% from 850±29 N to 496±13 N. In the range 57-107°C, the forming load plateaus suggesting that the effect of the resin viscosity on formability is reduced. These results well agree with previous findings which determined that the formability of carbon fiber thermosetting composites was increased from room temperature to 100 °C [56, 57, 58, 59]. A 8% increase of the forming load from 468±18 N to 506±29 N is observed between 107°C and 121°C. At 121 °C, the very low resin viscosity (table 4.3), allows the fibers to have an increased mobility within the resin matrix after failing. Under the

applied load, failed fiber can intertwine creating a “yarn effect”. This phenomenon in turn, can increase the overall tow sample strength, thus resulting in a modest increase in the forming load. This mechanism is well supported by figure 4.8E where the smallest cross-sectional area is observed without breakage.

Design Recommendation

The fixture presented in this paper offers extensive flexibility for the mesoscale investigation of the formability of fiber reinforced polymer composites. The data show herein were collected using the interchangeable forming blocks and a forming tool with a semi-cylindrical profile during uniaxial stretch drawing. The tabs used for manufacturing the tow samples were 19 mm wide and were held by a 20 mm channel within the sample holding assembly. However, part of the tailorability of the setup is that the geometry of each piece (forming blocks and forming tool) can be machined to best accommodate and reproduce the forming process of interest. Custom channel inserts were manufactured that to accommodate different sample widths, replacing the one described in detail herein, without the need for any further modification within the holding assembly or the forming fixture. This design allows for clamping larger tabs and enables the testing of multi tow or prepreg samples up to 50 mm (about 6 tows) wide. The sample holding system also self-adjusts to the tow sample thickness. To take advantage of these features, future work will focus on the testing of multi tow and prepreg laminate to investigate the forming behavior of a composite material similar to those used in industrial tape laying machines. In particular, the deep drawing biaxial stretch response of fiber reinforced polymer laminate tape samples, manufactured with different fiber orientations, will be investigated using hemispherical forming tools.

Since the bonding state of the fiber/resin interface and the presence of voids are characteristics of the mesoscale, observations using microscopy will be performed after forming tests to better understand how defect development relates to forming conditions.

Conclusions

The forming fixture discussed in this paper successfully evaluated the stretch drawing forming behavior of composite tow samples made from Hexcel continuous IM7-G carbon fibers impregnated with Huntsman RDM 2019-053 resin at several forming temperatures (21-121°C). Results showed consistency and repeatability as measured by the peak, post-peak, and force vs. displacement curves during forming, demonstrating the viability of the forming fixture to evaluate composite forming at the mesoscale. Catastrophic failure was observed only for tow samples tested at room temperature while samples tested at elevated temperature showed partial failure identified by cross-sectional area thinning. The proposed fixture aided in defining the forming behavior of the material in real time both visually (e.g. room temperature tow samples failure around the forming block) and in terms of forming load versus displacement curves. For elevated temperature testing, a primary peak corresponding to the maximum forming load was identified followed by a secondary peak that is related to the decrease of the resin viscosity when the temperature is increased. These results were used to establish novel forming metrics: such as the maximum drawing depth with no failure, the maximum forming load, and post-peak (secondary) loading behavior. These metrics can be used to compare forming behavior with different tooling geometries and selection of different fiber and resin formulations to match desired part and processing specifications.

CHAPTER FIVE

DESIGN OF EXPERIEMENT TO DETERMINE THE EFFECT OF FORMING FIXTURE VARIABLES

Introduction

Manufacturing costs for processing CFRPs are the main driver for the limited use of carbon fiber in modern mechanical components despite its superior properties when compared to tradition metallics and other fiber composites [71]. Recent advances in the production of CF filaments aim to bridge the gap between the mechanical and environmental advantages of CF, with the relative ease of manufacturing for metallic components. SBCF is a leading candidate in this space because it has proven to be more formable than traditional CF while still maintaining superior mechanical properties compared to that of metallic parts [16]. SBCF is produced by utilizing traditional continuous fiber tows and stretching it at a pre-determined length using differentially driven rollers so that the fiber breaks at the natural flaws in the fiber. This process creates an aligned discontinuous tow that can then be sized and impregnated by resin into a ply similar to that of traditional CF pre-preg. The primary benefit of the discontinuous fiber is that, at elevated temperatures under the cross-linking temperature of the resin system, the fibers can slide past each other when pressure is applied. As a result of this phenomenon, when a laminate is laid into a complex mold the fibers are free to follow the contours of the part shape more effectively than continuous fibers that resist out of plane movement because of their low strain to failure rate (~ 2%).

To successfully supplant metallics as the premier material of choice for numerous industries SBCF must be proven to be easily formable so that manufacturing costs are reduced sufficiently enough to make the final product cost effective. Formability is defined by the ease with which a material can be formed while still maintaining its pre-formed properties [60]. Commonly referred to as plastic deformation it is known that ductile materials are usually better suited for forming than brittle crystalline structures such as CF [17]. Since SBCF is discontinuous it acts as a pseudo-ductile material before cure so superior forming is a possibility. Little testing has been conducted to evaluate this behavior because of the of the recency of the material form and limited testing equipment. MSU has recently designed and implemented a forming fixture that subjects impregnated CF tows into a state of stress termed stretch bending in order to evaluate the load response of different CF formulations under a variety of geometrical and environmental conditions.

Data from the design of experiment (DOE) was collected and stored using a Mark-10 (Mark-10 Corp. Copiague, NY) universal test stand and Mark-10's companion software MESURGauge Plus. Raw data was then compiled into excel format with responses variables of load and displacement. Finally, the test data was compiled into MiniTab (Minitab LLC, State College, PA) software in order to conduct statistical analysis of independent and dependent variables and to create an ANOVA model for determining the effects of conditional variables on the outputs.

Materials

Material Properties

Mechanical properties for uncured CFRP tows are not widely known, primarily because for structural applications the final cured laminate is normally the form that is of most interest to designers. For meso-scale testing of formability at a tow level, mechanical characteristics of both the resin matrix and carbon fiber are important because they directly affect the yield force and yield strain of the CFRP which both contribute to formability. Strength of SBCF CFRPs have shown high dependance on temperature, so mechanical property data on uncured laminated tows is of limited use for characterizing formability in this test.

Characteristics of RDM2019-053

Huntsman RDM2019-053 is a proprietary resin system so many of the properties are not publicly available. For formability testing resin viscosity is important, the viscosity effects the shear strength of the resin and thus yield strength of the sample during stretch bending. Table 5.1 lists the resin viscosity values of RDM 2019-053 at relevant temperatures [70].

Table 5.1: Huntsman RDM 2019-053 resin viscosity at selected temperatures

Temperature (°C)	Viscosity (Pa·s) [72]
21 (70°F)	> 3500
57 (135°F)	791
82 (180°F)	168
107 (225°F)	25
121 (250°F)	11

The testing in this study is conducted between 21°C (70°F) and 82°C (180°F). From 21°C (70°F) to 82°C (180°F) the viscosity reduces almost 20 times. This reduction in viscosity implies that temperature will potentially influence the stretch bending strength of the CFRP tows.

Mechanical Properties of IM7 Carbon Fiber

All CFRPs used in this study are manufactured from a base feed stock of Hexcel produced IM7 CF. IM7 is a high-performance CF that is approved for military aerospace applications. The distinguishing factor between high-performance CF and standard grade CF is the manufacturing controls that are in place during the producing of the fiber. During the production of high-performance CF, environmental conditions are tightly monitored as well as the tooling condition. This results in a fiber that has less inherent flaws before it gets impregnated and cured into the final component [73]. It should be noted that at RT the mechanical properties of the individual CF filaments in a SBCF tow are of little importance because the fiber is mostly discontinuous past the break length of the fiber. The majority of the strength of SBCF tows at RT is derived from the interfacial properties of the filaments and the sizing treatment that is applied to the fiber [74]. In table 5.2 are the mechanical properties of Hexcel IM7 CF bundled in a 12,000 fiber (12K) tow.

Table 5.2: Mechanical properties of Hexcel 12K IM7 [42]

	IM7-12K
Tensile Strength (GPa)	5.7
Tensile Modulus (GPa)	275.8
Elongation at failure	1.8%
Density (g/cm^3)	1.8

Sizing Treatment on CF

Commonly a surface treatment termed “sizing” is applied on CF to improve various aspects of the CF tow. Sizing is known to increase the adhesive effect between the matrix and the CF as well as improving the handleability of the CF [75]. Handleability refers to the protection of the fiber during processing, alignment of the fiber filaments in the tow, and wettability of the fiber when it comes in contact with the resin system [76].

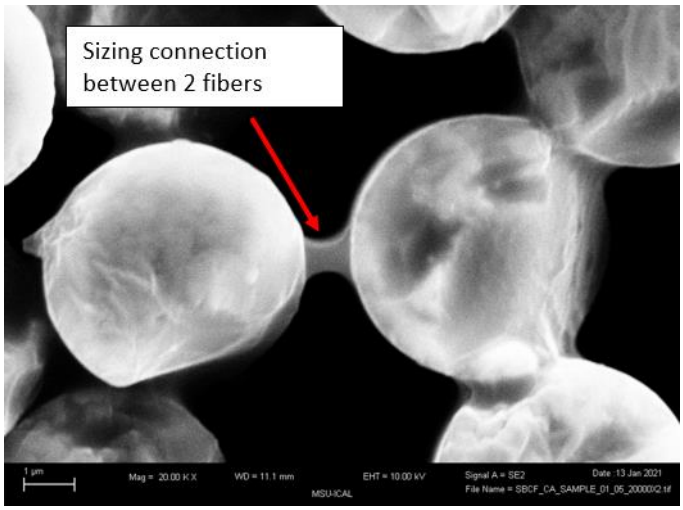


Figure 5.1: FE-SEM microscopy image of sizing bridge between carbon fiber filaments

Hexcel employed two sizing applications to the fibers used in this study. G and GP sizing applications are closely held proprietary formulations, but both are composed of an uncured epoxy oligomer with specifically chosen additives that improve adhesion and handleability [77]. GP is known to have comparable properties to G sized fiber but was produced to have less deleterious effects on the environment.

Fiber Volume Content of Impregnated Tow Samples

During the manufacturing process of CFRPs the "dry" CF tow is run through a lamination machine where resin film is compacted at elevated temperature and pressure in order to infuse the CF with the desired resin matrix. Using MSU lamination techniques this process was conducted on the three different fiber types using RDM2019-053 resin. An important factor in the commercial production of pre-impregnated CFRPs is the fiber to resin ratio, or simply fiber volume ratio, see equation 5.1.

$$V_f = \frac{v_f}{v_c} \qquad (5.1)$$

Where V_f is the fiber volume ratio, v_f is the volume of fiber and v_c is the volume of the composite. For commercial pre-pregs the industry standard for fiber volume is typically between 50% to 65% depending on application [78]. The solvent wash process was utilized by MSU to determine the fiber content. It consisted of washing the uncured pre-preg tow in a 50-50 bath of n-methyl-pyrrolidone (NMP) and acetone. The solvents are able to strip the resin away from the fiber after repeated cycles, leaving only the fiber which can be weighed to determine the final fiber volume.



Figure 5.2: Solvent washed CFRP samples

The process was repeated on 10 individual samples for each fiber type. Table 5.3 displays the solvent wash results of the MSU produced pre-preg tows.

Table 5.3: Fiber volume ratio of various uncured pre-preg tows

Fiber Type	Resin Type	Resin Volume (n = 10)	Fiber Volume (n = 10)
IM7-GP	RDM2019-053	50.1 %	49.9 %
Hexcel SBCF	RDM2019-053	53.6 %	46.4 %
MSU SBCF	RDM2019-053	67.2 %	32.8 %

The prepreg IM7-GP has the closest fiber volume ratio to what is found in commercial settings. The MSU SBCF shows a fiber volume about 17% lower than IM7-GP. Lower fiber volume could adversely affect the load bearing of the samples because the fiber carries the majority of the load when CFRPs are stressed.

Testing Methods and Design of Experiments

Sample Preparation

Three types of CF were used in the DOE; 12K Hexcel IM7-GP continuous, Hexcel SBCF, and MSU manufactured SBCF. Hexcel IM7-GP continuous was produced by Hexcel Corporation (Stamford, Connecticut). Hexcel SBCF was manufactured by Hexcel in small batch lots as late as 2011 [28]. Hexcel SBCF feed stock was Hexcel IM7 continuous fiber and sized with GP sizing. The specified break length of Hexcel SBCF is 50.8 mm (2 in), which was independently verified by MSU in a fiber pull out test [29]. From fiber pullout testing it has been observed that long corollary fibers up to ~228 mm (9 in) can be found which would suggest higher loads are possible and more variation could be seen throughout Hexcel SBCF. MSU SBCF was manufactured on a modified Hexcel SB2 machine using Hexcel IM7-G continuous fiber as feed stock. G sized fiber was used because the MSU processing team has found that the stretch-breaking process was more effective with G sizing instead of GP. The specified break-length of MSU SBCF is 35 mm (1.375 in) which is set from the break distance between the nip rollers on the machine. Each fiber tow was laminated with proprietary Huntsman (The Woodland, Texas) RDM2019-053 resin film using the Pro-Lam (Hamilton, MT) in the MSU composites lab. Laminated temperatures and procedures have been rigorously tested and optimized by the SBCF research group before tows were manufactured for the DOE.

Methods

The main method for testing the formability characteristics of CF in the DOE was based on using the MSU designed forming fixture. Details on material specifications and fixture design can be found in Chapter 4. The ends of CF tow samples were glued together with card

stock tabs and cyanoacrylate adhesive and clamped for a minimum of 30 minutes before testing. Samples were tested within 24 hours of preparation to reduce any out-time effects of the resin system. The gauge length for all samples was set at 203 mm (8 in) from inside of tab to inside of tab. Testing rate was set at 6.35 mm/min (0.25 in/min) for all tests. Testing rate was kept constant so that other factors can be investigated. Further design of experiments will be needed to study the effect of crosshead speed on forming. Radii of the corners of the forming blocks was kept constant at 6.35 mm (0.25 in). Temperature, plunger nose diameter, and gap width were identified as important factors that may influence the formability of the CFRP tow samples. For each independent factor the levels are:

(1) Plunger nose ⌀ and Gap Width Combined

[12.7,16],[12.7,28.6],[12.7, 54],[19, 28.6],[19, 54],[25, 28.6],[25, 54] mm

([0.5,0.625],[0.5,1.125],[0.5, 2.125],[0.75,1.125],[0.75, 2.125],[1.0,1.125],[1.0, 2.125]) in

(2) Plunger nose ⌀

12.7, 19, 25 mm

(0.5, 0.75, 1.00) in

(3) Gap Width

16, 28.6, 54 mm

(0.625, 1.125, 2.125) in

(4) Temperature

24 °C $\pm$ 1°C [RT], 82 °C $\pm$ 1°C

(75 $\pm$ 2.5 [RT]), 180 $\pm$ 2.5) °F

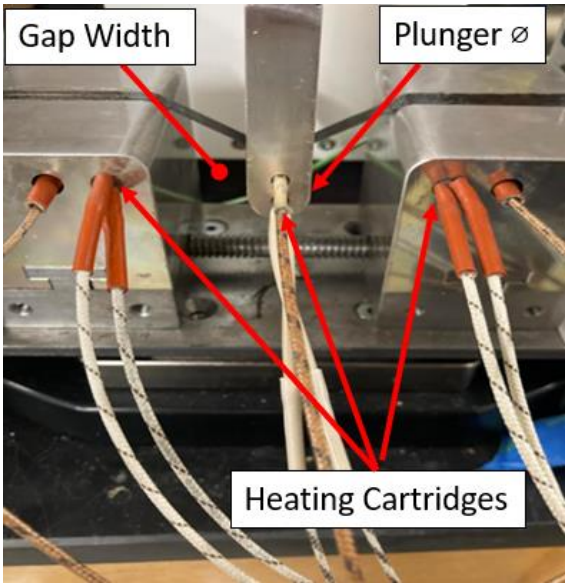


Figure 5.3: Overview of major forming fixture factors

It is hypothesized that the combination of plunger and gap width could have a contributing relationship. Therefore, it is important to study the combination of those factors. Results from the DOE testing was processed using the analysis of variance (ANOVA) statistical approach. This allows for identification of factors that influence formability in the stretch-bending test. The statistical significance of these factors provide information on which factors are most significant for formability.

Design of Experiment

The design of experiment is listed in table 5.4 shows the full scope of samples tested and factors that contribute to the outputs of force (F_{max}) and maximum yield displacement (Δ_{max}). F_{max} is calculated based on the average of 5 replicants. Δ_{max} refers to the maximum displacement that the samples undergo before the force output on the test gauge begins to diminish. To evaluate formability, the two dependent reaction variables (F_{max} and Δ_{max}) as well as visual

failure mode of the samples are recorded. For all tests at RT, except for MSU SBCF samples failed catastrophically indicating adverse formability.

Table 5.4: Design of experiment for CFRP single tow samples

	Temperature (°C)	Plunger ⌀ (mm)	Gap Width (mm)	Combined (mm)
1	RT	12.7	16	12.7, 16
2	RT	12.7	28.6	12.7, 28.6
3	RT	12.7	54	12.7, 54
4	RT	19	28.6	19, 28.6
5	RT	19	54	19, 54
6	RT	25	28.6	25, 28.6
7	RT	25	54	25, 54
8	82	12.7	16	12.7, 16
9	82	12.7	28.6	12.7, 28.6
10	82	12.7	54	12.7, 54
11	82	19	28.6	19, 28.6
12	82	19	54	19, 54
13	82	25	28.6	25, 28.6
14	82	25	54	25, 54

Results and Discussion

Response values for F_{max} and Δ_{max} for all fiber types; IM7-GP continuous, Hexcel SBCF, and MSU SBCF are displayed in Table 5.5. ANOVA is conducted at 95% confidence level for each reaction according to respective fiber type, see tables 5.6-5.11. A general linear model was

employed for the ANOVA with a Box-Cox transformation of $\lambda = 0$ [79]. Main effect plots are shown in figures 5.4 and 5.5 to illustrate the relative effective strength of each factor [80].

Table 5.5: Average max force (F_{max}), max yield displacement (Δ_{max}), for various CFRP tows

	IM7-GP Continuous		Hexcel SBCF		MSU SBCF	
	$F_{max\ (N)}$	$\Delta_{max\ (mm)}$	$F_{max\ (mm)}$	$\Delta_{max\ (N)}$	$F_{max\ (N)}$	$\Delta_{max\ (mm)}$
1	605.2	9.9	595.3	5.6	263.6	10.9
2	417.6	12.7	433.0	7.6	191.9	14.2
3	282.2	13.7	347.8	7.9	172.0	16.3
4	438.6	11.9	470.9	12.2	267.6	13.0
5	415.1	14.7	326.6	14.5	171.1	16.3
6	633.6	12.4	495.3	12.2	185.8	13.0
7	303.3	13.7	304.3	14.5	136.3	16.5
8	274.2	10.9	16.8	16.5	1.3	24.6
9	392.7	8.4	19.8	14.0	1.0	30.7
10	286.6	14.2	9.4	24.4	0.7	38.4
11	245.8	10.4	21.4	17.3	1.4	28.4
12	203.7	13.7	9.9	27.9	0.9	35.8
13	495.4	8.1	27.3	12.2	1.3	18.8
14	172.2	13.2	11.6	31.2	0.8	42.7

Table 5.6: Results of analysis of variance (ANOVA) for average max force (F_{max}) for IM7-GP

Source	DOF	Adj SS	Adj MS	F value	P value	Contribution (%)
Gap Width (mm)	2	3.35	1.68	27.78	0.00	38.35%
Plunger ⌀ (mm)	2	2.99	2.99	49.59	0.00	26.36%
Temperature (°C)	1	0.14	0.07	1.19	0.312	1.26%
Residual Error	64	3.86	0.06			
Total	69					

Table 5.7: Results of analysis of variance (ANOVA) for max yield displacement (Δ_{max}) for IM7-GP

Source	DOF	Adj SS	Adj MS	F value	P value	Contribution (%)
Gap Width (mm)	2	1.38	0.69	52.85	0	58.45%
Plunger ⌀ (mm)	2	0.03	0.02	1.27	0.29	1.13%
Temperature (°C)	1	0.35	0.35	26.84	0	11.94%
Residual Error	64	0.83	0.01			
Total	69					

Table 5.8: Results of analysis of variance (ANOVA) for average max force (F_{max}) for Hexcel SBCF

Source	DOF	Adj SS	Adj MS	F value	P value	Contribution (%)
Gap Width (mm)	2	5.98	2.99	41.7	0	3.23%
Plunger ⌀ (mm)	2	0	0	0.02	0.99	0.00%
Temperature (°C)	1	194.38	194.38	2709.85	0	94.54%
Residual Error	64	4.59	0.07			
Total	69					

Table 5.9: Results of analysis of variance (ANOVA) max yield displacement (Δ_{max}) for Hexcel SBCF

Source	DOF	Adj SS	Adj MS	F value	P value	Contribution (%)
Gap Width (mm)	2	2.71	1.36	35.73	0	30.22%
Plunger ⌀ (mm)	2	1.71	0.86	22.6	0	10.36%
Temperature (°C)	1	7.41	7.41	195.14	0	44.74%
Residual Error	64	2.43	0.04			
Total	69					

Table 5.10: Results of analysis of variance (ANOVA) for average max force (F_{max}) for MSU SBCF

Source	DOF	Adj SS	Adj MS	F value	P value	Contribution (%)
Gap Width (mm)	2	2.91	1.45	19.87	0	0.57%
Plunger ⌀ (mm)	2	0.47	0.24	3.23	0.05	0.10%
Temperature (°C)	1	476.08	476.08	6511.04	0	98.37%
Residual Error	64	4.68	0.073			
Total	69					

Table 5.11: Results of analysis of variance (ANOVA) max yield displacement (Δ_{max}) for MSU SBCF

Source	DOF	Adj SS	Adj MS	F value	P value	Contribution (%)
Gap Width (mm)	2	2.5	1.25	72.05	0	19.20%
Plunger ⌀ (mm)	2	0.03	0.02	0.93	0.4	0.23%
Temperature (°C)	1	10.04	10.04	579.09	0	72.55%
Residual Error	64	1.11	0.02			
Total	69					

It is clear from the contribution percentage that temperature has a dominant effect on the F_{max} of both the Hexcel SBCF and MSU SBCF, showing 98.37% and 94.54% respectively. For the Δ_{max} this effect of temperature is lessened, though still a significant factor in the response. IM7-GP indicates that it is less dependent on temperature showing a contribution percentage of 1.26% and 11.94% for F_{max} and Δ_{max} respectively. This response is expected since the IM7-GP fibers are continuous throughout the length of the sample despite temperature fluctuations, while the surrounding matrix continues to soften. Conversely SB fibers are permitted to move freely when subjected to elevated temperatures. The plunger and gap width effects on F_{max} values of SBCF are not statistically valid enough to show dependency, while the yield displacement values do demonstrate a slight contribution. Investigation on the combined contribution of the plunger and gap widths are required to determine any further effects. The gap width effect on IM7-GP does indicate relative high dependency on F_{max} of 38.35%. Gap width effect on Δ_{max} for IM7-GP shows a contribution dependency of 58.45%. Contribution dependency is the percentage that each factor contributes to the total sequential sums of squares, meaning a higher percentage shows the factor accounts for a more of a variation in the response variable. Mechanically the fiber is experiencing a higher stress contribution from the two directions as the gap width increases, σ_x and σ_z (see Chapter 4 for coordinate system of forming fixture), when the gap width

increases the force gauge registers lower forces because it records force only in the z-axis. Interaction plots in figure 5.4 serves to illustrate the effect of temperature on the SBCF materials while displaying the general insignificance the effect of temperature has on IM7-GP fibers.

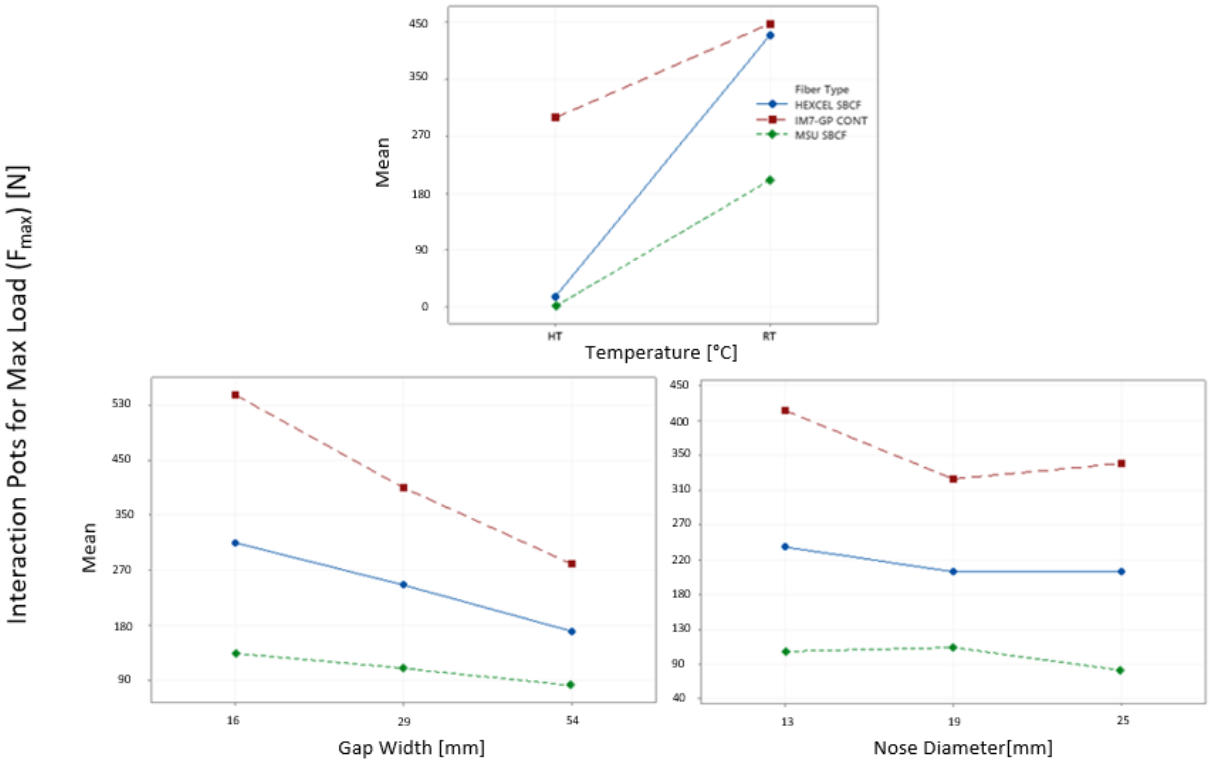


Figure 5.4: Interaction plots of max load (F_{max}) for different factors

P-values for temperature of IM7-GP are greater than 0.05 indicating low significance of effect while gap width and plunger diameter both show p-values less than 0.05. Hexcel SBCF has low p-values (<.05) for gap width and temperature giving confidence that both are significant, though gap width has a minority contribution of 3.23%, plunger diameter has a p-value of 0.99 pointing toward low significance. In addition, MSU SBCF has low p-values (<.05) for only temperature, while plunger diameter and gap width have p-values ≤ 0.5, though contribution is hardly significant. From the ANOVA model it can be concluded that in general

temperature has a significant effect on the F_{max} of SBCF materials while it has little effect on the IM7-GP. Alternatively, gap width and plunger diameter indicate an effect on F_{max} for IM7-GP, where the SBCF see little significant on the aforementioned factors.

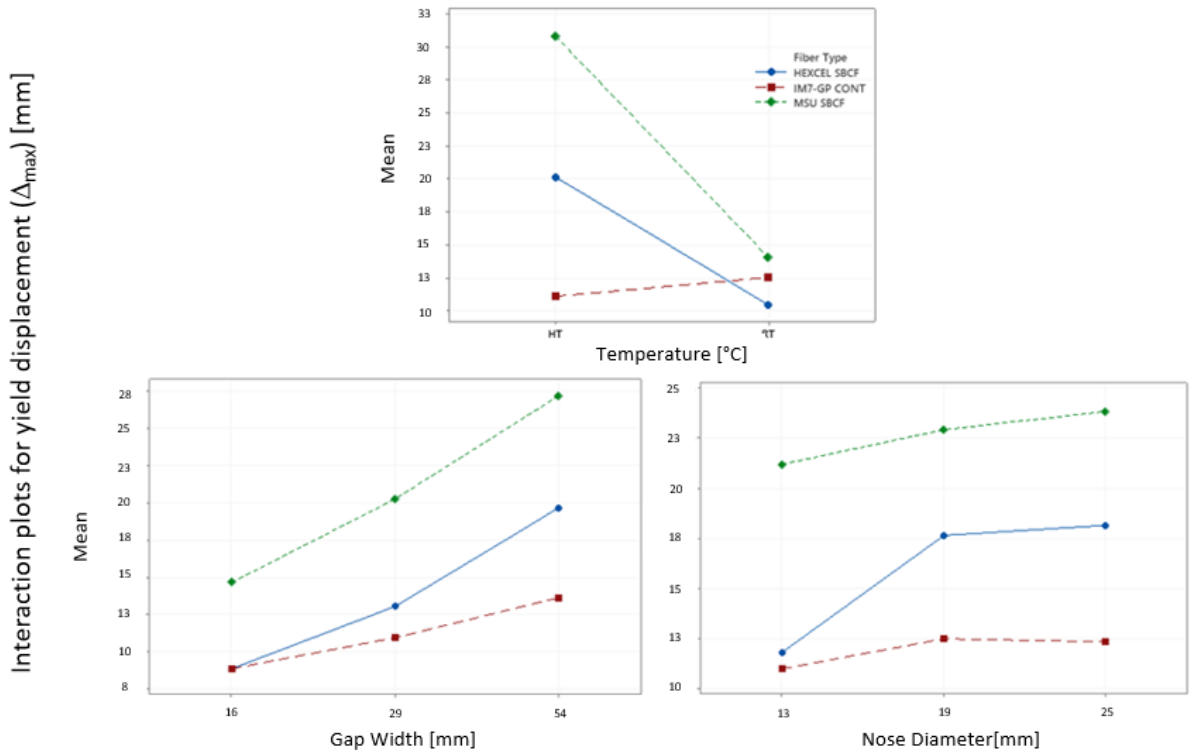


Figure 5.5: Interaction plots of yield displacement (Δ_{max}) for different factors

Similar to F_{max}, the ANOVA model indicates that temperature has little effect on the Δ_{max} of IM7-GP, but larger contribution to the Δ_{max} for both Hexcel SBCF and MSU SBCF. Unlike F_{max} though there is influence from the gap width to Δ_{max} on IM7-GP but little from the plunger nose diameter. For SBCF materials the contribution of plunger diameter and gap width are moderately significant, still slightly lower than then that of temperature.

Lastly, with the individual factors considered the combination of plunger diameter and gap width (interaction) must be investigated to determine if they effect the responses. Tables 5.12-5.17 display the ANOVA results for all fiber types.

Table 5.12: Results of analysis of variance (ANOVA) for average max force (F_{max}) for IM7-GP

Source	DOF	Adj SS	Adj MS	F value	P value	Contribution (%)
Plunger_gap combined (mm)	6	4.98	0.83	15.21	0	43.85%
Temperature (°C)	1	2.99	2.99	54.87	0	26.36%
Residual error	62	3.38	0.06			
Total	69					

Table 5.13: Results of analysis of variance (ANOVA) for max yield displacement (Δ_{max}) for IM7-GP

Source	DOF	Adj SS	Adj MS	F value	P value	Contribution (%)
Plunger_gap combined (mm)	2	1.82	0.30	24.6	0	62.01%
Temperature (°C)	1	0.35	0.35	28.43	0	11.94%
Residual error	62	0.76	0.01			
Total	69					

Table 5.14: Results of analysis of variance (ANOVA) for average max force (F_{max}) for Hexcel SBCF

Source	DOF	Adj SS	Adj MS	F value	P value	Contribution (%)
Plunger_gap combined (mm)	2	6.71	1.12	15.3	0	3.26%
Temperature (°C)	1	194.38	194.38	2660.97	0	94.54%
Residual error	62	4.53	0.07			
Total	69					

Table 5.15: Results of analysis of variance (ANOVA) for max yield displacement (Δ_{max}) for Hexcel SBCF

Source	DOF	Adj SS	Adj MS	F value	P value	Contribution (%)
Plunger_gap combined (mm)	2	6.75	1.12	29.04	0	40.75%
Temperature (°C)	1	7.41	7.41	191.29	0	44.74%
Residual error	62	2.40	0.04			
Total	69					

Table 5.16: Results of analysis of variance (ANOVA) for average max force (F_{max}) for MSU SBCF

Source	DOF	Adj SS	Adj MS	F value	P value	Contribution (%)
Plunger_gap combined (mm)	2	3.37	0.56	7.7	0	0.70%
Temperature (°C)	1	476.08	476.08	6516.37	0	98.37%
Residual error	62	4.53	0.07			
Total	69					

Table 5.17: Results of analysis of variance (ANOVA) for max yield displacement (Δ_{max}) for MSU SBCF

Source	DOF	Adj SS	Adj MS	F value	P value	Contribution (%)
Plunger_gap combined (mm)	2	2.79	0.47	28.69	0	20.18%
Temperature (°C)	1	10.04	10.04	618.72	0	72.55%
Residual error	62	1.00	0.02			
Total	69					

The results from tables 5.12 through 5.17 demonstrate that the plunger diameter and gap combinations does change the results of the ANOVA output. There was a return of near zero p-values for all sources indicating that no individual factor can be completely dismissed. For IM7-GP continuous fiber, the trend from the previous ANOVA is similar with still a greater contribution from the geometry rather than temperature. This effect is even greater when considering Δ_{max} showing a contribution of 62% from the plunger and gap width combined. The SB materials have large contributing percentages of the temperature effects on F_{max} of 94.54% for Hexcel SBCF and 98.37% for MSU SBCF. The contribution of the plunger gap combination on Δ_{max} was much closer leading to a conclusion that the geometry does affect the Δ_{max} of the SBCF during the testing. Figure 5.6 displays the interaction plots for the ANOVA analysis of plunger diameter and gap width combined for F_{max} and Δ_{max} respectively. It follows that in

general for continuous fiber the geometry has a dominant effect on the F_{max} while for SBCF the temperature is the greatest contributing factor.

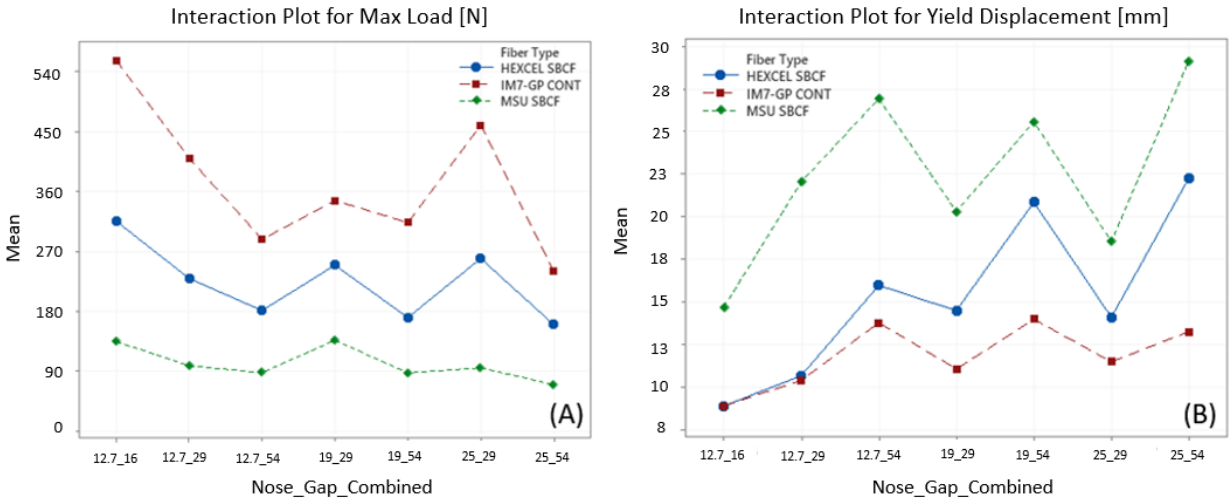


Figure 5.6: Interaction plot of F_{max} plunger nose & gap combined (A) Interaction plot of Δ_{max} plunger nose & gap combined

Recommendations for Complex Part Creation Using ANOVA

Usage of the general linear ANOVA model to determine how CFRPs will form into complex geometries is helpful for aerospace designers because often manufacturing limitations impede the ability for optimized shapes. Data analysis shows that SBCF requires less force to form into deep troughs and tight curvatures. In general, for long in-plane structures traditional continuous CFRPs would still be an acceptable choice but when bridging, resin pooling and other defects are of concern and SBCFs superior formability could potentially overcome production of these flaws. If geometry similar to the Forming Fixture is present then the force to form the CFRP in the tooling could be estimated, this would give manufacturing engineers the ability to determine if the production conditions are sufficient for curing the laminate. For

example, the force required to form a flat panel with a rib stiffened section running down the middle with a 19 mm wide and 38.1 mm deep trough could be estimated so that the best fiber type for formability could be selected. Table 5.18 and 5.19 show the regression equations with R-sq values and results for IM7-GP continuous CF, Hexcel SBCF, and MSU SBCF to predict the maximum forming load at elevated temperature based off the geometry described above. It is assumed that the fiber direction is perpendicular to the trough direction and the plunger width is modeled at the same width as the trough in order to imitate the distributed forces from a vacuum bag.

Table 5.18: Regression equations predicting maximum forming load at high temperature of continuous and stretch broken carbon fibers

Reg. Eqn. for IM7-GP (R-sq = 55.47%)	$Max\ Load\ [lbf] = 123.5 - 9.1 * \{Plunger\ \emptyset\ [in]\} - 34.09 * \{Gap\ Width\ [in]\}$	(5.2)
Reg. Eqn. for Hexcel SBCF (R-sq = 93.27%)	$Max\ Load\ [lbf] = 33.26 - 1.57 * \{Plunger\ \emptyset\ [in]\} - 19.17 * \{Gap\ Width\ [in]\}$	(5.3)
Reg. Eqn. for MSU SBCF (R-sq = 84.61%)	$Max\ Load\ [lbf] = 13.81 - 5.21 * \{Plunger\ \emptyset\ [in]\} - 6.64 * \{Gap\ Width\ [in]\}$	(5.4)

Table 5.19: Results for predicting maximum forming load at HT

Fiber Type	Plunger ∅ [mm]	Gap Width [mm]	Max Load [N]
IM7-GP	19	19	405.27
Hexcel SBCF	19	19	78.76
MSU SBCF	19	19	21.90

Results from the regressions equations show a predictive value for the maximum forming load that would be expected based on the conditions above. For complex forming applications that require low forming force the selection of MSU SBCF would be most appropriate.

Conclusion

This study investigated the formability aspects of different CFRP tows in a stretch bending forming fixture using statistics technique. The primary area of interest is the difference in forming load (F_{max}) between traditional continuous CF, Hexcel SBCF, and recently manufactured MSU SBCF. Yield displacement (Δ_{max}) was also considered since formability is defined by the magnitude a material can deform before it yields. A general linear ANOVA model was constructed to explore the effect of temperature and fixture geometry (gap width and plunger diameter) on the response variables F_{max} and Δ_{max}. For the IM7-GP continuous CFRP the ANOVA model gives a strong correlation between F_{max} and the geometry of the test fixture. Interaction plots illustrate that as the gap width increases F_{max} decreases and as the plunger diameter decreases F_{max} increases. Considering Δ_{max}, as gap width increases Δ_{max} increases and when plunger diameter decreases Δ_{max} decreases. Overall, with smaller plunger diameters and small gap width, F_{max} should be expected to be higher and Δ_{max} lower. For SBCF materials temperature was the dominant factor. When considering geometry of the combined plunger diameter and gap width there is slight correlation to response variable Δ_{max}. Several conclusions can be made from the data acquired in the ANOVA model.

(1) In continuous fiber CFRP tows forming, F_{max} and Δ_{max} is highly dependent on the plunger diameter and gap width.

(2) For continuous fiber CFRP tows forming, F_{max} and Δ_{max} does not show statistical significance based on temperature fluctuations from $24°C \pm 1°C$ to $82°C \pm 1°C$.

(3) In SBCF CFRP tows forming F_{max} and Δ_{max} is dominated by the temperature during testing in the range of $24°C \pm 1°C$ to $82°C \pm 1°C$.

(4) Geometry has low statistical influence on the F_{max} of SBCF CFRP tows. This indicates good formability in shapes consisting of tight radii and deep troughs

(5) MSU SBCF CFRP tows show less dependency than Hexcel SBCF on the geometry of the testing fixture for forming force. Contributions of geometry for Hexcel SBCF show 3.26 % and MSU SBCF show 0.70%. Lower dependance on tool geometry at higher temperature indicates possibly superior formability of MSU SBCF.

The results of this study give credence to the difference in formability of the traditional continuous CFRP's and newly developed SBCF CFRP's. Overall, it is shown that SBCF CFRP's have better formability by both measures of F_{max} and Δ_{max}, and the most recent iteration of MSU SBCF demonstrated the highest formability. Higher formability of the MSU SBCF may be a result of a better break length distribution when compared to Hexcel SBCF. It is known that Hexcel SBCF contains erroneous long fibers that may contribute to continuous fiber like behavior. Future work is recommended to substantiate these conclusions, including refining impregnation procedures, testing comparable tows at similar fiber volume ratios, rate of testing, and investigating thinning behavior in areas of interest (corners and plunger radii).

CHAPTER SIX

CONCLUSIONS AND RECOMMENDATIONS FOR FUTURE WORK

Results of research based on thesis objectives:

1. *Conduct gauge length study of CF tows to understand differences in continuous and stretch broken tensile behavior.*

   Tensile samples were made from IM7-G and Hexcel SBCF tow feedstocks. Testing was conducted using a universal testing machine over several gauge lengths and temperatures. A sample preparation procedure was devised to accurately calculate the cross-sectional area of CF at the unimpregnated tow level. Findings from the study include but are not limited to; the cross-section area of Hexcel SBCF is lower than that of 12K IM7-G even though the base number of fibers in each is 12,000 filaments. Hexcel SBCF is 8% weaker in tension than 12K IM7-G when normalized for cross-sectional area, fiber length distribution of SBCF is correlated to the gauge length of the tow which in turn is related to the tensile strength of the tow. Also, temperature has an increased effect on the tensile strength of the tow when gauge length is greater than the specified break length of the SBCF.

2. *Design and validate a stretch bending forming fixture for comparing the forming behavior of resin impregnated CF tows.*

   Several iterations of the Forming Fixture were designed to accurately test CFRP tows in the stretch-bending condition. Various modifications were required in the holding fixture to reduce slippage in high temperature CFRP tow samples. The heating control system was verified to operate under acceptable temperature ranges. A test matrix utilizing 12K IM7-GP

continuous fiber was completed as a verification of the Forming Fixture system to ensure future testing, reliability and repeatability.

3. *Apply statistical ANOVA modeling techniques to CFRP tow stretch-bending tests data to determine important factors that affect formability.*

   A DOE was constructed to study the factors influencing the formability of continuous fiber, Hexcel SBCF, and MSU SBCF on the Forming Fixture. Statistical tests using ANOVA were run to determine what independent variables influence the force and yield displacement values. It was found that continuous fibers have higher dependance on the Forming Fixture geometry while the SBCF has less dependance on geometry and more dependance on the temperature of the test. Furthermore, it was discovered that MSU SBCF was slightly more formable than Hexcel SBCF leading to the conclusion that this could be attributed to less variations in fiber length.

Recommendations for future work:

1. *Investigate rate dependency of forming force on SBCF CFRP tows in stretch bending tests*

   Further work in this space could investigate the rate dependency of the forming force when testing CFRP samples. The resin becomes less viscous as temperatures increase and the shear behavior of the resin may be related to the forming force required.

2. *Investigate forming force of various SBCF CFRP tows with known processing parameters and break lengths*

   In this paper two known SBCF's were tested to conduct the research. With more refinement of the SB process, it is expected that the break length of the tows will be more easily adjustable. Future work could include obtaining a multitude of SBCF tows at a variety of

break lengths. This will allow researchers to investigate which break length allows for the greatest formability while still maintaining its structure under RT conditions.

3. *Modeling of forming force based on FEA simulation and processing parameters*

   For manufacturing purposes modeling the forming force required for specific fiber type, resin, and model shape would be useful. Ideally SBCF would have material specifications that would allow it to be used in standard FEA software for modeling material movement and tuning manufacturing process like temperature and pressure to predict the load requirements to manufacture a desired part.

REFERENCES CITED

[1] L. Werfelman, "The Composite Evolution," *AeroSafety World,* pp. 17-21, March 2007.

[2] M. Mrazova, "Advanced composite materials of the future in," *Incas Bulletin,* vol. 5, no. 3, pp. 139-150, 2013.

[3] J. Cao and L. Chen, "Effect of thermal cycling on carbon fiber-reinforced PPS composites," in *SEM Annual Conference and Exposition on Experimental & Applied Mechanics,* Portland, 2005.

[4] Hexcel Corporation, *HexPly 8552,* 2021.

[5] K. Marlett, Y. Ng and J. Tomblin, "Hexcel 8552 IM7 Unidirectional Prepreg 190 gsm & 35% Qualification Material Property Data Report," National Institute For Aviation Research, Wichita, 2011.

[6] ASM Handbook Committee, Properties and Selection: Nonferrous Alloys and Special-Purpose Materials, 10 ed., vol. 2, ASM International, 1990.

[7] ASM Handbook Committee, ASM Handbook: Properties and Selection: Irons, Steels, and High-Performance Alloys, vol. 1, ASM International, 1990.

[8] A. Kelly and C. Zweben, Comprehensive Composite Materials, vol. 6, Pergamon, 2000.

[9] E. Kappel and R. Prussak, "On abnormal thermal-expansion properties of more orthotropic M21E/IMA carbon-fiber-epoxy laminates," *Composites Communications,* vol. 17, pp. 129-133, 2020.

[10] M. Saad, S. Miller and T. Marunda, "Thermal Characterization of IM7/8552-1 Carbon-Epoxy Composites," in *ASME International Mechanical Engineering Congress and Exposition, Proceedings (IMECE),* 2014.

[11] M. A. Pérez, X. Martínez, S. Oller, L. Gil, F. Rastellini and F. Flores, "Impact damage prediction in carbon fiber-reinforced laminated composite using the matrix-reinforced mixing theory," *Composite Structures,* vol. 104, pp. 239-248, 2013.

[12] D.-J. Kwon, N.-S.-R. Kim, Y.-J. Jang, S.-B. Yang, J.-H. Yeum, J.-H. Jung, S. Y. Nam, Y.-B. Park and W. Ji, "Investigation of impact resistance performance of carbon fiber reinforced polypropylene composites with different lamination to applicate fender parts," *Composites Part B: Engineering,* vol. 2015, 2021.

[13] M. Legault, "Composite vs. corrosion: Battling for marketshare," CompositesWorld, 1 October 2011. [Online]. Available: https://www.compositesworld.com/articles/composite-vs-corrosion-battling-for-marketshare. [Accessed 1 July 2021].

[14] A. Rudawska, "The Effect of the Salt Water Aging on the Mechanical Properties of Epoxy Adhesives Compounds," *Polymers,* vol. 12, no. 4, 2020.

[15] D. Cairns and C. Monfort, *Stretch Broken Fiber Material Forms for Primary Aerospace Structure,* Bozeman, MT, 2018.

[16] G. Jacobsen, "Process And Performance Characterization Of Stretch Broken Carbon Fiber Material," Baltimore, 2007.

[17] S. Park, Carbon Fibers, Springer, 2015.

[18] K. Shirvanimoghaddam, S. U. Hamim, M. K. Akbari, S. M. Fakhrhoseini, H. Khayyam, A. H. Pakseresht, E. Ghasali, M. Zabet, K. S. Munir, S. Jia, J. P. Davim and M. Naebe, "Carbon fiber reinforced metal matrix composites: Fabrication processes and properties," *Composites Part A: Applied Science and Manufacturing,* vol. 92, pp. 70-96, 2017.

[19] D. D. Chung, Carbon Fiber Composites, Butterworth-Heinemann, 1994.

[20] J. Hitchon and D. Phillips, "The dependence of the strength of carbon fibres on length," *Fibre Science and Technolog,* vol. 12, no. 3, pp. 217-233, 1979.

[21] E. Stoner, E. D.D and S. Durham, "An end-effect model for the single-filament tensile test," *Journal of Materials Science,* vol. 29, p. 6561–6574, 1994.

[22] E. Parra-Venegas, K. Campos-Venegas, R. Martinez-Sanchez, J. Herrera-Ramirez and A. Rodriguez-Miranda, "The Tensile Behavior of E-glass fibers," *Journal Microscopy and Microanalysis,* vol. 18, no. S2, pp. 784-785, 2012.

[23] T. Langston, "The Tensile Behavior of High-Strength Carbon Fibers," *Microscopy and Microanalysis,* vol. 22, no. 4, pp. 841-844, 2016.

[24] Z. Peng, X. Wang and Z. Wu, "A bundle-based shear-lag model for tensile failure prediction of unidirectional fiber-reinforced polymer composites," *Jounral of Materials & Design,* vol. 196, 2020.

[25] D. Heider, J. Tierney, M. Henchir, V. Gargitter, S. Yarlagadda, J. Gillespie Jr, J. Sun, J. Sietins and D. Knorr, "Microstructural Evaluation of Aligned, Short Fiber TUFF Material," in *SAMPE 2019,* Charlotte, 2019.

[26] P. Scallan, Process Planning, Butterworth-Heinemann, 2003.

[27] R. Okine, D. Edison and N. Little, "Properties and Formability of an Aligned Discontinuous Fiber Thermoplastic Composite Sheet," *Journal of Reinforced Plastics and Composites,* vol. 9, no. 1, pp. 70-90, 1990.

[28] G. Jacobsen and W. Schimpf, "Process development and characterization of stretch broken carbon fibre materials," in *SAMPE*, Baltimore, 2009.

[29] A. D5103-07, "Standard Test Method for Length and Length Distribution of Manufactured Staple Fibers (Single-Fiber Test)," *ASTM International,* 2018.

[30] C. Red, "777X: Bigger-than-Expected Carbon Fiber Impact," 30 August 2016. [Online]. Available: www.compositesworld.com/articles/777x-bigger-than-expected-carbon-fiber-impact. [Accessed 15 July 2020].

[31] A. McIlhagger, E. Archer and R. McIlhadder, Polymer composites in the aerospace industry, Woodhead Publishing, 2014.

[32] C. Hueber, G. Fischer, N. Schwingshandl and R. Schledjewski, "Production planning optimisation for composite aerospace manufacturing," *International Journal of Production Research,* vol. 57, no. 18, pp. 5857-5873, 2019.

[33] P. Wang, N. Hamila, P. Boisse, P. Chaudet and D. Lesueur, "Thermo-mechanical behavior of stretch-broken carbon fiber and thermoplastic resin composites during manufacturing," *Polymer Composites,* vol. 36, pp. 694-703, 2015.

[34] G. Dillon and D. Stiver, "Development of enabling automated forming technology for Stretch Broken Carbon Fiber (SBCF) materials," in *SAMPE '09 Spring Symposium: Changing Times. New Opportunities. Are You Prepared?*, Baltimore, 2009.

[35] C. Scoutis, "Carbon fiber reinforced plastics in aircraft construction," *Materials Science and Engineering: A,* vol. 412, no. 1-2, pp. 171-176, 2005.

[36] S. Shi, Z. Sun, M. Ren, H. Chen and X. Hu, "Buckling resistance of grid-stiffened carbon-fiber thin-shell structures," *Composites Part B: Engineering,* vol. 45, no. 1, pp. 888-896, 2013.

[37] G. Jacobsen, "Characterization of stretch broken fiber composites – IM7 fiber 8552 resin – stretch at prepreg level," in *SAMPE*, Long Beach, 2011.

[38] Aijun, G., G. Yizhuo, W. Qing, Y. Chao, L. Min and Z. Zuoguang, "Influence of processing temperature on interfacial behavior of HKT800 carbon fiber with BMI and epoxy matrices," *Chinese Journal of Aeronautics,* vol. 28, no. 4, pp. 1255-1262, 2015.

[39] Hexcel Corporation, *HexTow IM7 Carbon Fiber Product Data Sheet,* Stamford, CT, 2020.

[40] C. Wanigasekara , E. Oromiehie, S. Akshya, B. Prusty and N. Kiong, "Machine Learning Based Predictive Model for AFP-Based Unidirectional Composite Laminates," *IEEE Transactions on Industrial Informatics,* pp. 2315-2324, 2020.

[41] K. Naito, J. Yang, Y. Tanaka and Y. Kagawa, "The effect of gauge length on tensile strength and Weibull modulus of polyacrylonitrile (PAN)- and pitch-based carbon fibers," *Journal of Materials Science,* vol. 47, pp. 632-642, 2012.

[42] S. Constantinos, "Carbon fiber reinforced plastics in aircraft construction.," *Journal of Materials Science and Engineering: Part A,* vol. 412, no. 1, pp. 171-176, 2005.

[43] M. Such, C. Ward and K. Potter, "Aligned Discontinuous Fibre Composites: A Short History," *Journal of Multifunctional Composites,* vol. II, no. 2, pp. 155-168, 2014.

[44] C. Bathias, "An engineering point of view about fatigue of plymer matrix composite materials," *International Jounral of Fatigue,* vol. 28, no. 10, pp. 1094-1099, 2006.

[45] S. Bruschi, T. Altan, D. Banabic, P. Bariani, A. Brosius, J. Cao, A. Ghiotti, M. Khraisheh, M. Merklein and A. Tekkaya, "Testing and modelling of material behaviour and formability in sheet metal forming," *CIRP Journal of Manufacturing Science and Technology,* vol. 63, pp. 727-749, 2014.

[46] A. E643, *Standard Test Method for Ball Punch Deformation of Metallic Sheet Material,* 2009.

[47] T. Kikuma and K. Makazima, "Effects of the Deformation Conditions and Mechanical Properties on the Stretch Forming of Steel Sheets," in *Transactions of the Iron and Steel Institute of Japan,* 1971.

[48] Z. Marciniak, K. Kuczynski and T. Pokota, "Influence of the Plastic Properties of a Material on the Forming Limit Diagram for Sheet Metal in Tension," *International Journal of Mechanical Science,* vol. 15, pp. 789-805, 1973.

[49] J. Lee, B. Kim and D. Ko, "“Development of vacuum-assisted prepreg compression molding for production of automotive roof panels," *Jounral of Composite Structures,* vol. 213, pp. 144-153, 2019.

[50] L. Mosse, P. Compston, W. Cantwell, M. Cardew-Hall and S. Kalyanasundaram, "Stampforming of polypropylene based fibre–metal laminates: The effect of process variables on formability," *Journal of Material Process Technology,* vol. 172, no. 2, pp. 163-168, 2006.

[51] S. Suresh and V. S. Kumar, "Investigation on influence of stamp forming parameters on formability of thermoplastic composite," *Polímeros,* vol. 28, no. 5, pp. 422-432, 2018.

[52] G. McGuinness and C. Ó'Brádaigh, "Effect of preform shape on buckling of quasi-isotropic thermoplastic composite laminates during sheet forming," *Journal of Composite Manufacturing,* vol. 6, pp. 269-280, 1995.

[53] M. R. N. Fazita, K. Jayaraman and D. Bhattacharyya, "Formability Analysis of Bamboo Fabric Reinforced Poly (Lactic) Acid Composites," *Materials,* vol. 9, p. 539, 2016.

[54] G. Sun, W. Zhang, Z. Wang, H. Win, G. Zheng and Q. Li, "A novel specimen design to establish the forming limit diagram (FLD) for GFRP through stamping test," *Composites: Part A,* vol. 130, no. https://doi.org/10.1016/j.compositesa.2019.105737, 2020.

[55] S. Venkatesan and S. Kalyanasundaram, "Finite element analysis and optimization of process parameters during stamp forming of composite materials," *Materials Science and Engineering,* vol. 10, no. 1, 2010.

[56] Y. Uriya and J. Yanagimoto, "Erichsen cupping test on thermosetting CFRP sheets," *International Journal of Material Forming,* vol. 10, pp. 527-534, 2017.

[57] A. Nishino and T. Oya, "Multiscale analysis of the formability of CFRP sheets subjected to warm forming with a temperature-dependent epoxy model," *International Journal of Material Forming,* vol. 12, pp. 793-800, 2019.

[58] T. Oya and A. Nishino, "Formability mechanism of CFRP sheets using multiscale model based on microscopic characteristics of thermosetting resin," *Multiscale and Multidisciplinary Modeling, Experiments and Design,* vol. 4, pp. 65-76, 2021.

[59] Y. Uriya and J. Yanagimoto, "Suitable structure of thermosetting CFRP sheet for cold/warm forming," *International Journal of Material Forming,* vol. 9, pp. 243-252, 2016.

[60] P. Bussetta and N. Correia, "Numerical forming of continuous fibre reinforced composite material: A Review," *Composites: Part A,* vol. 113, pp. 12-31, 2018.

[61] J. Llorca, C. Gonzales, J. Molina-Aldareguia and C. Lopes, "Multiscale Modeling of Composites: Toward Virtual Testing … and Beyond," *The Journal of The Minerals, Metals & Materials Society,* vol. 65, pp. 215-225, 2012.

[62] K. Matouš, M. Geers, V. Kouznetsova and A. Gillman, "A review of predictive nonlinear theories for multiscale modeling of heterogeneous materials," *Jounral of Composite Physics,* vol. 330, pp. 192-220, 2017.

[63] J. Belnoue and S. Hallett, "A rapid multi-scale design tool for the prediction of wrinkle defect formation in composite components," *Jounral of Materials & Design,* vol. 187, 2020.

[64] M. Ameen, R. Peerlings and M. Geers, "A quantitative assessment of the scale separation limits of classical and higher-order asymptotic homogenization," *European Journal of Mechanics - A/Solids,* vol. 71, pp. 89-100, 2018.

[65] M. R. N. Fazita, K. Jayaraman and D. Bhattacharyya, "Formability Analysis of Bamboo Fabric Reinforced Poly (Lactic) Acid Composites," *Materials,* vol. 9, no. 7, 2016.

[66] R. Theriault, T. Osswald and J. Castro, "A numerical model of the viscosity of an epoxy prepreg resin system.," *Journal of Polymer Composites,* vol. 20, no. 5, pp. 628-633, 2004.

[67] K. Gornicki, R. Winiczenko and A. Kaleta, "Estimation of the Biot Number Using Genetic Algorithms: Application for the Drying Process.," *Jounral of Energies,* vol. 12, no. 14, 2019.

[68] X. Zhang, S. Fujiwara and M. Fujii, "Measurements of thermal conductivity and electrical conductivity of a single carbon fiber.," *International Journal of Thermophysics,* vol. 21, pp. 965-980, 2000.

[69] D. Kim, S. Fujiwara and S. Nutt, "In-situ cure monitoring of an out-of-autoclave prepreg: Effects of out-time on viscosity, gelation and vitrification," *Jounral of Composite Science and Technology,* vol. 102, pp. 132-138, 2014.

[70] Hunstman Corporation, *RDM 2019-053 Data Sheet,* The Woodlands, TX, 2020.

[71] L. Herbeck, H. Wilmes, B. Kolesnikov and M. Kleineberg, "Technology and design development for a CFRP fuselage," in *SAMPE Europe Conference,* Paris, 2003.

[72] D. Kim, T. Centea and S. Nutt, "In-situ cure monitoring of an out-of-autoclave prepreg: Effects of out-time on viscosity, gelation and vitrification," *Composites Science and Technology,* vol. 102, pp. 132-138, 2014.

[73] D. D. Edie and J. J. McHugh, "High Performance Carbon Fibers," in *Carbon Materials for Advanced Technologies,* Elsevier Science Ltd, 1999, pp. 119-138.

[74] J. Janicki, D. Bajwa, D. Cairns, R. Amendola, C. Ryan and A. Dynkin, "Gauge length and temperature influence on the tensile properties of stretch broken carbon fiber tow," *Composites Part A: Applied Science and Manufacturing,* vol. 146, 2021.

[75] W. Nie and J. Li, "Effects of plasma and nitric acid treatment of carbon fibers on the mechanical properties of thermoplastic polymer composites," *Mechanics of Composite Materials,* vol. 46, no. 3, pp. 251-256, 2010.

[76] Z. Dai, F. Shi, B. Zhang, M. Li and Z. Zhang, "Effect of sizing on carbon fiber surface properties and fibers/epoxy interfacial adhesion," *Applied Surface Science,* vol. 257, no. 15, pp. 6980-6985, 2011.

[77] N. Broyles, N. Verghese, R. Davis, J. Lesko and J. Riffle, "Pultruded Carbon Fiber/Vinyl Ester Composites Processed with Different Fiber Sizing Agents. Part I: Processing and Static Mechanical Performance," *Journal of Materials in Civil Engineering,* vol. 17, no. 3, 2005.

[78] R. Gibson, Principles of Composite Material Mechanics, 2nd ed., Boca Raton, FL: CRC Press, 2007.

[79] H. L. Nelson and C. Granger, "Experience with using the Box-Cox transformation when forecasting economic time series," *Journal of Econometrics,* vol. 10, no. 1, pp. 57-69, 1979.

[80] J. Antony, Design of Experiments for Engineers and Scientists, Elsevier, 2014.

[81] R. Christensen, "Properties of carbon fibers," *Journal of the Mechanics and Physics of Solids,* vol. IV, no. 42, pp. 681-695, 1994.

[82] F. Shieu and W. Lee, "Measurement of the mechanical properties of a fibre-reinforced composite on the submicrometre scale," *Journal of Materials Science,* vol. 32, p. 6533–6538, 1997.

[83] A. B. Strong, Fundamentals of composite manufacturing: Materials, methods and application, Dearborn, Michigan: Society of Manufacturing Engineer, 2008.

[84] Q. E. Incorporated, "Composites 101," Quartus Engineering Incorporated, [Online]. Available: https://www.quartus.com/composites-101. [Accessed 15 July 2021].

[85] I. Jiménez-Fortunato, D. J. Bull, O. T. Thomsen and J. M. Dulieu-Barton, "On the source of the thermoelastic response from orthotropic fibre reinforced composite laminates," *Composites Part A: Applied Science and Manufacturing*, vol. 149, no. 3, 2021.

APPENDICES

APPENDIX A

RESIDUAL PLOTS FROM ANOVA ANALYSIS

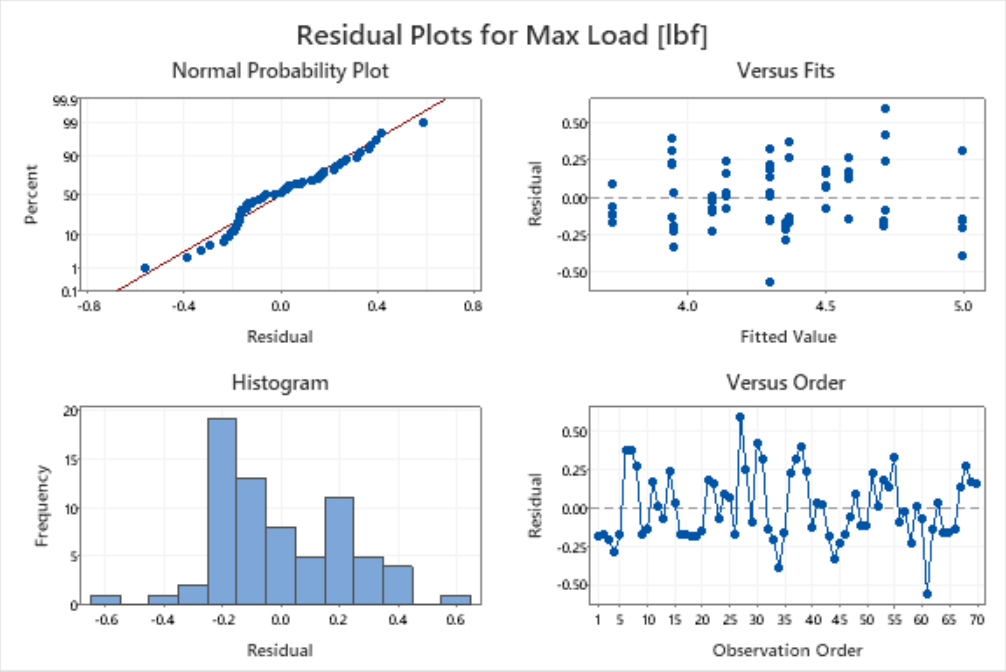


Figure A.1: Residual plots for IM7-GP ANOVA for max load (F_{max})

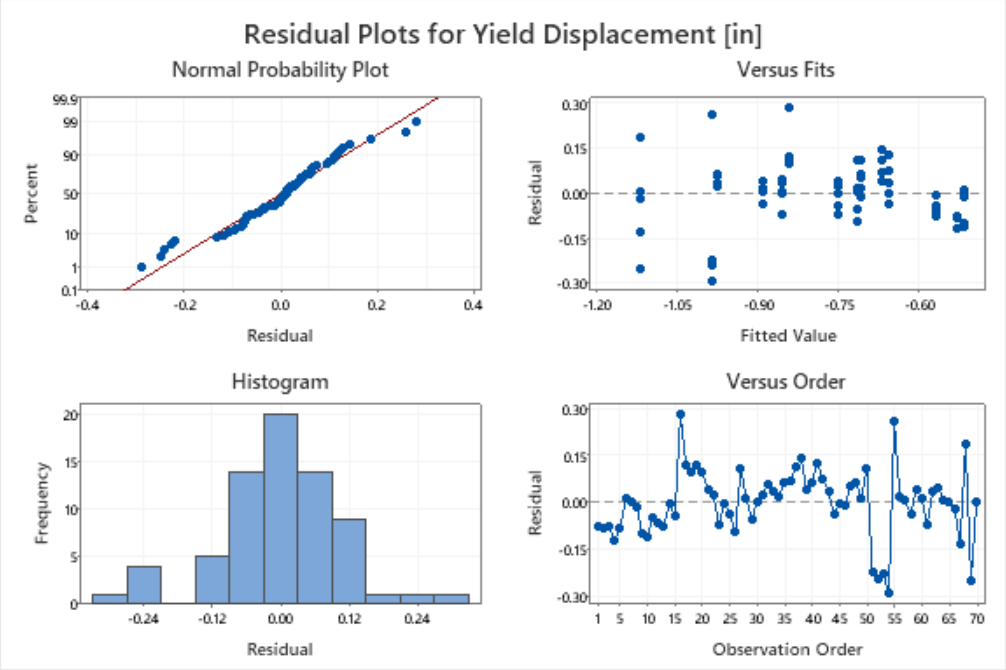


Figure A.2: Residual plots for IM7-GP ANOVA for max yield displacement (Δ_{max})

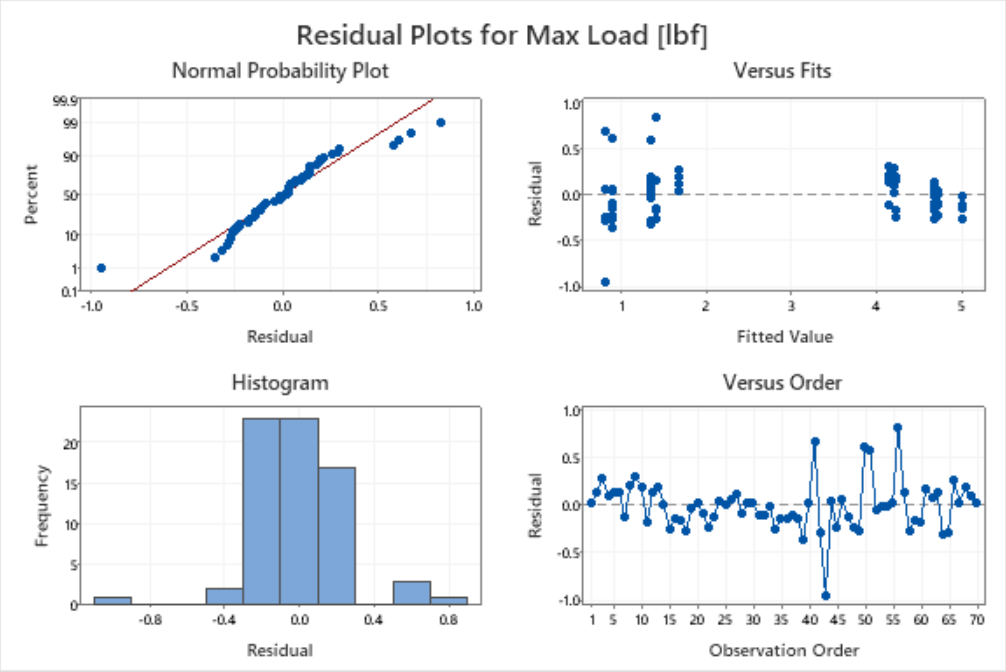


Figure A.3: Residual plots for Hexcel SBCF ANOVA for max load (F_{max})

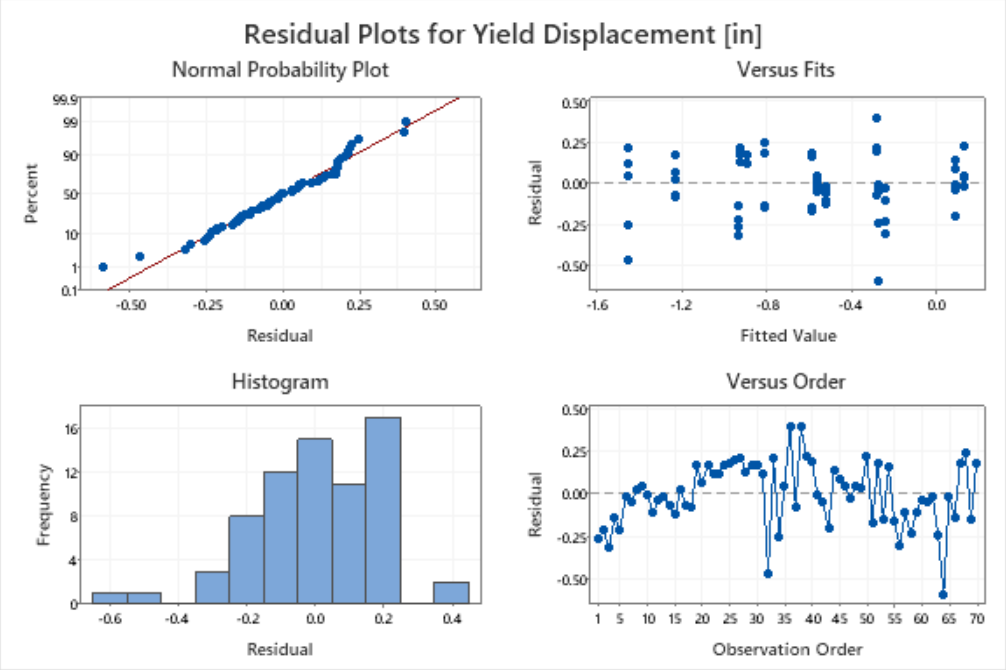


Figure A.4: Residual plots for Hexcel SBCF ANOVA for max yield displacement (Δ_{max})

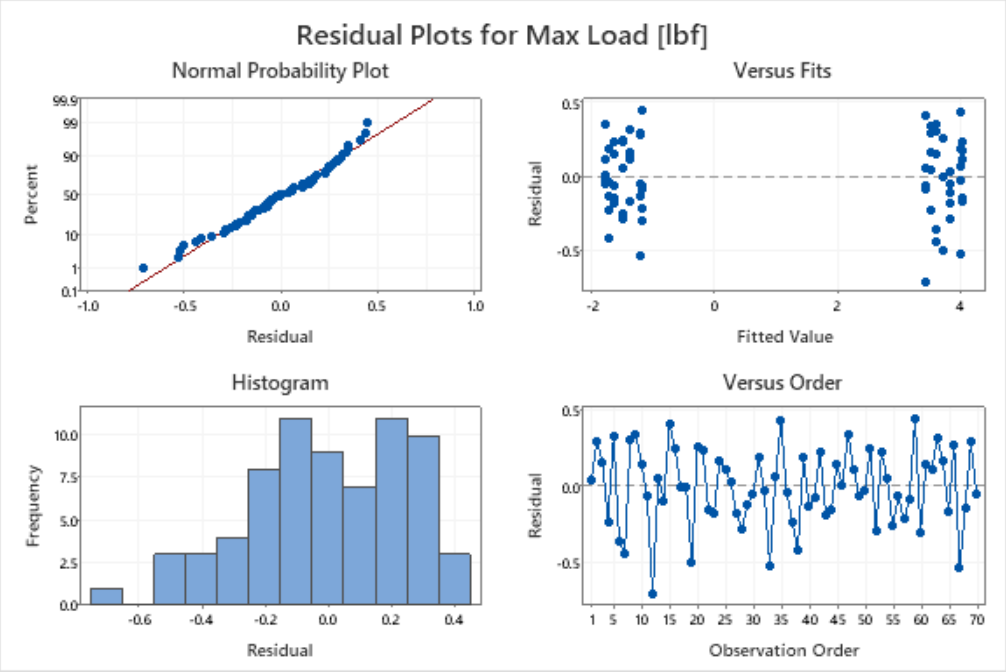


Figure A.5: Residual plots for MSU SBCF ANOVA for max load (F_{max})

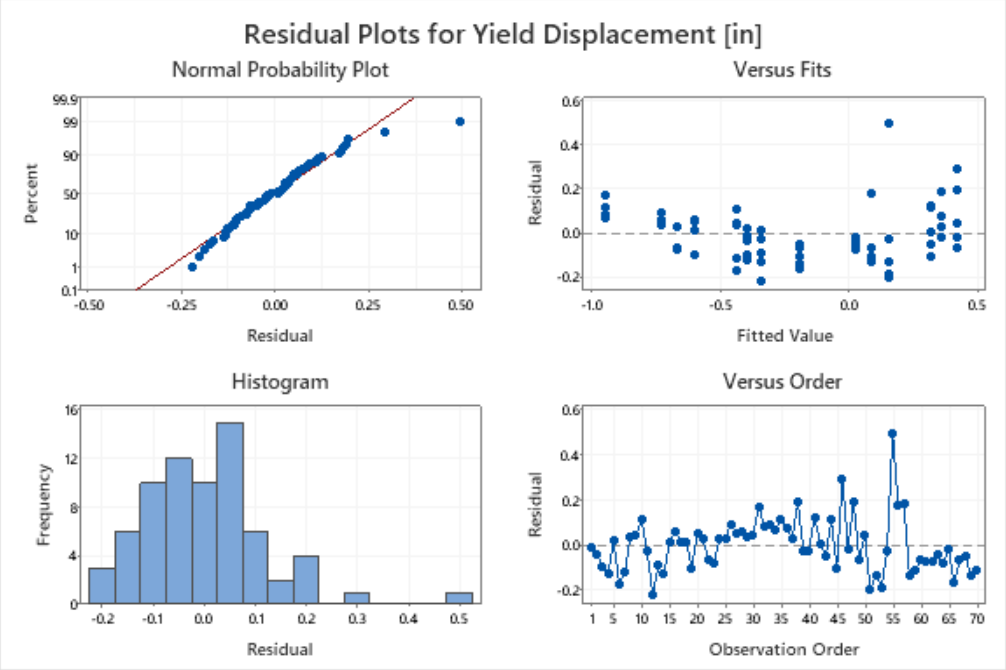


Figure A.6: Residual plots for MSU SBCF ANOVA for max yield displacement (Δ_{max})